UCSF
UC San Francisco Electronic Theses and Dissertations

Title
Inhibitory neuron transplantation: Insights into the developmental cell death and ocular dominance plasticity of the cerebral cortex

Permalink
https://escholarship.org/uc/item/3611x619

Author
Southwell, Derek

Publication Date
2009

Peer reviewed|Thesis/dissertation

eScholarship.org Powered by the California Digital Library
University of California

Inhibitory neuron transplantation: Insights into the developmental cell death and ocular dominance plasticity of the cerebral cortex

by

Derek Gardner Southwell

DISSERTATION

Submitted in partial satisfaction of the requirements for the degree of

DOCTOR OF PHILOSOPHY

in

Neuroscience

in the

GRADUATE DIVISION

Copyright 2009
by
Derek Gardner Southwell

To my parents, Gayle and James Southwell

Acknowledgements

I give my most sincere gratitude to Arturo Alvarez Buylla for the opportunity to learn science in his laboratory. More than anything, Arturo taught me that discoveries are made by scientists who are undaunted by technical obstacles. Arturo expects his students to develop and master difficult techniques that are rarely practiced in other labs. Without question, it can be humbling and frustrating to be stuck working out an experimental method. Yet through persistence, one eventually gains the technical skills that offer unique and revealing perspectives of nature. From those vantage points, valuable discoveries can be made. I am deeply appreciative of Arturo's high technical standards, and his patience in allowing me to learn the inhibitory neuron transplantation technique I have used here. Moreover, I have been inspired by Arturo's curiosity and his openness to all scientific discoveries. Arturo has taught me that science should never be approached as a means for confirming our conceptions of nature. Rather, the thrill of science comes when we approach nature with an open mind, when we see nature for the first time, and when we realize that nature works in ways we ever could have expected.

I must also thank other members of the Alvarez Buylla lab, past and present, particularly Hirohide Takebayashi, Cynthia Yaschine, Ricardo Romero, Florian Merkle, Minoree Kohwi, Zaman Mirzadeh, Dan Lim, Young-Goo Han, Rebecca Ihrie, and Rui Galvao. Hirohide was an especially patient and gracious mentor to me when I first joined the lab. Cynthia and Ricardo offered exceptional

administrative and technical support, while Florian, Minoree and Zaman offered useful experimental insights and taught me various aspects of the cell transplantation procedure. Likewise, I thank Dan, Young-Goo, Rebecca and Rui for their encouragement and excellent scientific perspectives. With great diligence and care, Rui also quantified the cell death of endogenous inhibitory neurons (Chapter 3).

I have also benefited from the generosity of many other scientists outside our laboratory. I thank Yuchio Yanagawa for sharing the GAD67-GFP mice with us. Also, I thank Patrick McQuillen for his encouragement and guidance, and for teaching me the stereology technique. Thanks as well to Greg Stratmann and Linda Noble for allowing me to use their stereology systems. I also thank John Rubenstein, Scott Baraban and Arnold Kriegstein for the opportunity to take part in our collaborative studies of inhibitory neuron transplantation in epilepsy models. Jose Manuel Garcia Verdugo contributed ultrastructural electron micrographic studies to this work, and taught me the methods of electron microscopy. Finally, I have also benefitted from the guidance of my thesis committee, which included John Rubenstein, Jeremy Reiter, and Sam Pleasure.

Many of my fondest memories of graduate school were shared with my dear friend, Sunil Gandhi. Sunil and I have worked collaboratively to study the effects of transplanted inhibitory neurons on recipient ocular dominance plasticity (Chapter 4). In particular, Sunil performed all monocular deprivation, intrinsic signal imaging, and data analysis of the physiology results. I could not be happier with the way we have worked together. It seems like good times and

scientific productivity are often at odds with each other, but when Sunil is part of either, I am always willing to let go of one for the other.

I also give my great thanks to Sunil's advisor, Michael Stryker, and the rest of the Stryker lab, for supporting our collaborative project. It has been very exciting to share our labs' unique interests, and to learn a new field of neuroscience from absolute experts.

I also thank my previous mentor, Joan Bechtold, for nurturing my early interests in science. Joan offered me the opportunity to work in her lab when I was a just sixteen. She helped me to understand the value of clinically relevant research, one that undoubtedly guides my scientific and clinical interests to this day. Joanie has always been my role model for a scientist and mentor. Without question, my life's trajectory changed when I entered her lab.

Finally, I am most indebted to my mother and father, Gayle and James Southwell. You have always made me feel like anything is possible. My greatest challenge is to become the type of parent you have both been for me.

This research has been funded by the National Institutes of Health, the California Institute for Regenerative Medicine, and the Medical Scientist Training Program of the University of California, San Francisco.

Abstract

Inhibitory neuron transplantation: Insights into the developmental cell death and ocular dominance plasticity of the cerebral cortex

By

Derek Gardner Southwell

Neocortical inhibitory neurons originate primarily in the ventral telencephalon and migrate tangentially into the dorsal telencephalon. In the postnatal neocortex, inhibitory neurons sculpt information processing and regulate critical periods for experience-dependent cortical plasticity. Remarkably, when transplanted, embryonic inhibitory neurons disperse, survive, and modulate inhibition in the recipient neocortex. Inhibitory neuron transplantation may thus offer a means for modifying neural circuits in the diseased brain. At present, however, little is understood about how these cells develop postnatally, both during normal development and in transplantation scenarios. My dissertation has thus examined the developmental cell death of inhibitory neurons, and the functional contributions of transplanted inhibitory neurons to recipient cortical plasticity. My results define a postnatal period of *Bax*-dependent developmental cell death, through which 40% of this population is eliminated from the neocortex. When embryonic inhibitory neuron precursors were transplanted during the period of normal recipient cell death, they died when they reached a cell-intrinsic age equivalent to that of endogenous cells during the period of endogenous cell death. Surprisingly, over a range of transplant sizes, the rate of transplant cell

death also remained fixed and equal to that of normal endogenous cell death. It thus appears that the timing and extent of inhibitory neuron cell death are intrinsically determined, and free from competitive influences. This feature allows the neocortical inhibitory population to be significantly expanded by transplantation. In collaboration with Sunil Gandhi and Michael Stryker, I examined whether transplanted inhibitory neurons alter cortical plasticity in the recipient neocortex. Remarkably, transplanted inhibitory neurons induced cortical plasticity during a brief period, again when they reached a cell-intrinsic age equivalent to that of endogenous inhibitory neurons at the peak of the normal critical period. Thus, it appears that both inhibitory neuron developmental cell death, and the critical period, could reflect the execution of cell intrinsic developmental programs in inhibitory neurons. Surprisingly, transplanted inhibitory neurons retain and execute these developmental programs in the recipient brain. These findings provide fundamental insights into the nature of inhibitory neuron development and transplantation, ones that will guide the development and therapeutic application of inhibitory neuron transplantation strategies.

Table of Contents

Title i
Copyright ii
Dedication iii
Acknowledgements iv
Abstract vii
Table of Contents ix
List of Tables xiii
List of Figures xiv
List of Abbreviations xvi

Chapter 1 Introduction 1

Section 1: Overview 2

Section 2: The mammalian neocortex 5

Section 3: Neocortical inhibitory neurons 7

Basic features and diversity 7
Embryonic origins of diverse neocortical inhibitory neurons 10
Migration of inhibitory neurons into the developing neocortex 13
Functional roles of inhibitory neurons during development and adulthood 15
Inhibitory neuron precursor transplantation 17

Section 4: Developmental cell death in the nervous system 19

Basic features of developmental cell death 19
Molecular mechanisms of programmed cell death 21
Regulation of developmental cell death in the nervous system 25

Section 5: Ocular dominance plasticity in the visual cortex 28

Ocular dominance plasticity and the critical period 28
Regulation of ocular dominance plasticity by GABAergic signaling 29
Induction of ocular dominance plasticity after the critical period 30

Chapter 2 Materials and Methods 44

Section 1: Surgical devices 45
Head molds 45
Glass injection needles for cell transplantation 45

Section 2: Animals and genotyping 46

Epifluorescence genotyping of GAD67-GFP, GFP and DsRed mice 47
Polymerase Chain Reaction genotyping of Bax and TrkB mice 48
Breeding of mice 48

Section 3: Transplantation of inhibitory neuron precursors 49

Tissue dissection 49
Cell injection procedure 50

Section 4: Optical imaging of intrinsic signals 52

Monocular deprivation 52
Surgical procedures for repeated transcranial optical imaging 53
Optical imaging of eye-specific responses to visual stimulation 54
Analysis of optical imaging data 55

Section 5: Preparation of histological specimens 56

Transcardial perfusion for immunohistochemistry and electron microscopy 56
Preparation of brain sections 56
Diaminobenzidine immunostaining 57
Immunostaining and tissue processing for electron microscopy 58
Fluorescence immunostaining 59

Section 6: Imaging and quantification of histological specimens 61

Characterization of cleaved caspase-3 expression 61
Characterization of inhibitory neuron marker expression 62
Measurements of inhibitory neuron population sizes 64
Imaging of specimens by electron microscopy 66
Production of digital images 66

Section 7: Statistical analyses 67

Chapter 3 Intrinsically determined developmental cell death of neocortical inhibitory neurons 68

Section 1: Introduction 69

Section 2: Results 71

Temporal features of cleaved caspase-3 expression in the developing postnatal neocortex 71
Spatial distribution of cleaved caspase-3 expression in the Developing postnatal neocortex 73
Over forty percent of developing inhibitory neurons are eliminated from the neocortex during the period of early postnatal cell death 74
The developmental cell death of native neocortical inhibitory neurons requires the pro-apoptotic function of Bax 75
Bax-dependent developmental cell death occurs uniformly across neurochemically defined populations of neocortical inhibitory neurons 76
The timing of inhibitory neuron cell death is determined by the intrinsic age of the developing cells, not the developmental state of the brain 77
Survival time-course of transplanted inhibitory neuron precursors 80
The survival of transplanted inhibitory neurons is affected by the cell autonomous function of Bax 81
TrkB signaling does not affect the migration or survival of transplanted inhibitory neurons 82
Transplanted inhibitory neuron cell death remains constant in magnitude over a range of transplant sizes 84
The neocortex can support remarkable numbers of additional inhibitory neurons, with no effect on the endogenous population size 85

Section 3: Discussion 86

Chapter 4 Cortical plasticity induced by inhibitory neuron transplantation 117

Section 1: Introduction 118

Section 2: Results 120

Optical imaging of intrinsic signals in untreated GAD67-GFP mice at the peak of the critical period 120
Transplanted cells from the medial ganglionic eminence induce ocular dominance plasticity 33-35 days after transplantation 122

to P9-P11 recipients
Transplanted cells from the medial ganglionic eminence do not induce ocular dominance plasticity 43-46 days after transplantation to P0-P2 recipients 123
Transplanted cells from the medial ganglionic eminence do not alter ocular dominance plasticity during the critical period 124
Transplantation induces cortical plasticity that is 77% as strong as that observed during the normal critical period 125
Transplanted cells from the medial ganglionic eminence populate the recipient visual cortex and develop into mature inhibitory neurons 126

Section 3: Discussion 128

Chapter 5 Conclusions 147

Chapter 6 References 156

UCSF Library Release 174

List of Tables

Chapter 2 Materials and Methods

Table 1.	Mouse strains and descriptions	46
Table 2.	Antibodies	60

List of Figures

Chapter 1 Introduction

Figure 1. Neurons of the mammalian neocortex. 32
Figure 2. Distinct origins of neocortical excitatory and inhibitory neurons. 34
Figure 3. Migratory patterns of embryonic neocortical inhibitory neurons 35
Figure 4. Morphological features and basic mechanisms of necrosis and apoptosis. 37
Figure 5. intrinsic pathway of apoptosis. 38
Figure 6. The extrinsic pathway of apoptosis. 40
Figure 7. Trophic signaling regulates the apoptosis of developing neurons. 41
Figure 8. Ocular dominance plasticity and the critical period. 42

Chapter 3 Intrinsically determined developmental cell death of cortical inhibitory neurons

Figure 1. Quantification of cleaved caspase-3^+ cells in the postnatal neocortex. 96
Figure 2. Spatial distribution of GAD67-GFP^+/cleaved caspase-3^+ cells in the postnatal neocortex. 98
Figure 3. Spatial distribution of total (GAD67-GFP^+ and GAD67-GFP^-) cleaved caspase-3^+ cells in the postnatal neocortex. 99
Figure 4. The neocortical GAD67-GFP population size decreases by 40% during early postnatal life. 100
Figure 5. *Bax* is required for the developmental cell death of Neocortical inhibitory neurons. 101
Figure 6. *Bax*-dependent developmental cell death is not restricted to a particular neurochemically defined sub-type of inhibitory neurons. 102
Figure 7. Heterochronically transplanted inhibitory neuron precursors disperse throughout the recipient neocortex and develop morphological characteristics of mature inhibitory neurons. 104
Figure 8. Transplanted inhibitory neurons establish synaptic contacts with host neurons by 15 days after transplantation. 106
Figure 9. Quantification of cleaved caspase-3^+ transplanted inhibitory neurons. 108
Figure 10. Nearly equal fractions of transplanted and endogenous inhibitory neurons undergo developmental cell death in the neocortex, at timepoints defined by their intrinsic cellular ages. 110

Figure 11. The developmental cell death of transplanted inhibitory neurons is regulated by the cell autonomous function of *Bax* 111
Figure 12. The developmental cell death of transplanted inhibitory neurons is not regulated by neurotrophin signaling through the TrkB receptor 112
Figure 13. Transplanted inhibitory neuron cell death remains contant in magnitude over a range of transplant sizes. 114
Figure 14. The neocortex can support 35% additional inhibitory neurons, with no effect on the endogenous inhibitory neuron population size. 115

Chapter 4 Cortical plasticity induced by inhibitory neuron transplantation

Figure 1. Experimental design: Inhibitory neuron precursor transplantation and optical measurements of visual responses. 135
Figure 2. Untreated GAD67-GFP mice exhibit normal ocular dominance plasticity during the critical period. 137
Figure 3. Transplanted MGE cells induce ocular dominance plasticity 33-35 days after transplantation to P0-P2 and P9-11 recipients, when they reach a cellular age equivalent to that of endogenous inhibitory neurons at the peak of the normal critical period. 138
Figure 4. The absolute magnitudes of cortical responses are similar in MGE cell transplant recipients and dead-cell control recipients. 141
Figure 5. Ocular dominance plasticity is equally affected in wild type and GAD67-GFP mice at 33-35 days after transplantation. 142
Figure 6. MGE cell transplantation does not alter ocular dominance plasticity during the critical period. 143
Figure 7. At 33-35 days after transplantation to P9-P11 recipients, ocular dominance plasticity is 77% the magnitude of that observed in untreated animals during the critical period. 144
Figure 8. Transplanted MGE cells populate the recipient visual cortex and develop into mature inhibitory neurons. 145

Chapter 5 Conclusions

Figure 1. Intrinsic developmental programs govern the cell death of inhibitory neurons and the critical period for ocular dominance plasticity. 155

List of Abbreviations

AIF	apoptosis inducing factor
Apaf-1	apoptosis protease activating factor
Arx	aristaless homeobox
Bak	Bcl-2-homologous antagonist/killer
Bax	Bcl-2-associated X protein
Bcl	B-cell lymphoma
BDNF	brain-derived neurotrophic factor
Bid	BH3-interacting domain death agonist
BSA	bovine serum albumin
CaBP	calcium-binding protein
CAD	caspase-activated deoxyribonucleotidase
Caspase	cysteine-requiring aspartate protease
CB	calbindin
CR	calretinin
PV	parvalbumin
NPY	neuropeptide y
CCK	cholecystokinin
SOM	somatostatin
VIP	vasoactive intestinal peptide
CGE	caudal ganglionic eminence
CNTF	ciliary neurotrophic factor
Dlx	distalless homeobox
DNA	deoxyribonucleic acid
DR	death receptor
DsRed	discosoma red
ERK	extracellular signal-regulated protein kinase
FasL	fas-ligand
FS	fast spiking
GABA	gamma-aminobutyric acid
GAD65	glutamic acid decarboxylase, isoform of 65 kilodaltons
GAD67	glutamic acid decarboxylase, isoform of 67 kiloldaltons
GDNF	glial cell line-derived neurotrophic factor
GFP	green fluorescent protein
HGF	hepatocyte growth factor
IZ	intermediate zone
JNK	c-Jun n-terminal kinase
MAPK	mitogen-activated protein kinase
MD	monocular deprivation
MGE	medial ganglionic eminence
MZ	marginal zone
NGF	nerve growth factor
NgR	nogo receptor
NT-4	neurotrophin 4

ODI	ocular dominance index
ODS	ocular dominance shift
Otx2	orthodentical homeobox 2
p75-NTR	p75 neurotrophin receptor
PBS	phosphate buffered saline
PFA	paraformaldehyde
SDF	stromal cell-derived factor
Smac	second mitochondrial activator of caspase
SSRI	selective serotonin reuptake inhibitor
SVZ	subventricular zone
TNFR	tumor necrosis factor receptor
TRAIL	tumor necrosis factor-related apoptosis-inducing ligand
Trk	tropopmyosin related kinase
VZ	ventricular zone

Chapter 1

Introduction

Section 1: Overview

The brain is an organ of enormous complexity and scale. In humans, it contains billions of neurons and glia, all arranged into a network of trillions of synapses. Despite its vastness, however, the brain originates from a simple neuroepithelium. Through a remarkable process of division, migration, differentiation, and death, embryonic brain cells multiply and arrange themselves into the exquisite neural circuits that generate our movements, emotions, thoughts and language. Developmental neurobiologists share the great privilege of witnessing this amazing transformation. Our challenge, in turn, is to understand the brain's complexity by studying its cellular components, each one of daunting intricacy in its own right.

Throughout life, the brain continuously undergoes progressive and regressive processes, through which young cells and neural connections are rapidly produced and eliminated. These processes, which construct and refine neural circuits, are most prevalent in early postnatal periods. As a result, the brain is uniquely able to undergo change early in life.

Neurological disorders, including epilepsy, Huntington's disease, Alzheimer's disease, and Parkinson's disease, directly affect neural circuits. At present, disorders such as these are treated pharmacologically with agents that grossly alter the brain circuitry, both diseased and healthy. Current pharmacological treatments cannot regenerate new cellular populations, for example, or mediate the formation of new neuronal connections. There is thus

great interest in developing cellular therapies that can generate new neural circuits.

Nearly a decade ago, our laboratory discovered a cellular population with a unique potential to migrate and survive in the brain after transplantation. Transplanted inhibitory neuron precursors from the medial ganglionic eminence disperse widely and persist in multiple regions of the recipient brain (Wichterle et al., 1999). Additionally, transplanted inhibitory neurons alter GABAergic inhibitory signaling events in host brain circuits (Alvarez-Dolado et al., 2006). As such, there is much excitement that transplanted inhibitory neurons could one day be used as therapeutic agents. Still, very little is known about how transplanted inhibitory neurons, or endogenous inhibitory neurons, for that matter, develop in the postnatal brain.

My thesis research has used cell transplantation to study the development of neocortical GABAergic inhibitory neurons. In particular, I have focused on two features of postnatal brain development - developmental cell death and experience-dependent neural circuit refinement – and examined how transplanted inhibitory neurons participate in these phenomena. Together, my experiments describe 1) how cell death regulates the incorporation of endogenous and transplanted inhibitory neurons into the neocortex, and 2) how transplanted inhibitory neurons induce profound circuit refinements in the recipient brain.

In Chapter 3, I describe experiments that focused on the developmental cell death of native and transplanted inhibitory neurons. To date, the

developmental cell death of neocortical inhibitory neurons has not been described (Oppenheim, 1991; Buss et al., 2006), although there has been evidence for the cell death of inhibitory neurons in mature brain circuits (Petreanu et al., 2002). My findings indicate that cell death is a prominent feature of the normal development of inhibitory neurons, and that it also occurs prominently in transplanted populations as well. Surprisingly, endogenous cell death and transplanted cell death do not appear to interact; rather, transplanted and endogenous cell deaths occur discretely through an intrinsically defined process that is conserved in the two populations. Because transplanted inhibitory neurons die at a fixed fraction during a characteristic cell-intrinsic age, transplantation can be used to load the brain with large numbers of exogenous inhibitory neurons.

In Chapter 4 I focus on how these transplanted inhibitory neurons alter the neural circuitry of the recipient neocortex. These studies have been conducted collaboratively with Sunil Gandhi and Michael Stryker, two experts in the physiology of the visual cortex. The Stryker laboratory originally elucidated the role of inhibitory signaling in the regulation of cortical plasticity in the visual system. Together we have examined whether transplanted inhibitory neurons induce ocular dominance plasticity in the recipient visual cortex. Our experiments demonstrate that transplanted inhibitory neurons induce ocular dominance plasticity after the critical period, and that inhibitory neurons – both endogenous and transplanted – separately affect plasticity during a cell-intrinsically defined developmental age.

In the remainder of this chapter I briefly review the organization, development, and cellular components of the neocortex, the brain region I have studied. Additionally, in another section I describe the developmental and mature properties of neocortical inhibitory neurons, and their development. Finally, this chapter concludes with a review of developmental cell death in the nervous system, and a review of ocular dominance plasticity in the developing visual cortex.

Section 2: The mammalian neocortex

Across vertebrates, the brain is organized into seven fundamentally similar structures. They are: the cerebral hemispheres, thalamus, hypothalamus, midbrain, cerebellum, pons, and medulla. Each of these structures is composed of various sub-structures, and each demonstrates characteristic cell populations, architecture, connectivity, and function.

My thesis research has focused on the postnatal development of the neocortex, the outer-most layer of the cerebral hemispheres. In rodents, the neocortex is lissencephalic, or smooth in shape, while in primates and other larger animals the neocortex is folded, or gyreencephalic (Figure 1A). Despite these gross anatomical differences, the neocortex shares a basic cellular organization across mammals. The mammalian neocortex is organized into six layers, each distinguished by its composition of neurons and its internal and external connectivity (Nieuwenhys, 1994). The neocortex contains the neural substrates for sensory perception, motor commands, cognition, and language.

The neurons of the neocortex are broadly classified by their neurotransmitter phenotypes and cellular morphologies (Figure 1B). Excitatory neurons, which comprise approximately 70-80% of neocortical neurons, release the excitatory neurotransmitter, glutamate. Inhibitory neurons, which comprise approximately 20-30% of neocortical neurons, release the inhibitory neurotransmitter, γ-aminobutyric acid (GABA; Markram et al., 2004). Morphologically, excitatory neurons have large, pyramidal cell bodies that extend distant projections across and outside the neocortex (thus, they are often called "pyramidal neurons" or "projection neurons"). By contrast, neocortical inhibitory neurons exhibit small, round and ovoid cell bodies, and a great diversity of cellular morphologies (Figure 1B). Inhibitory neurons make dense local projections, and thus are often referred to as "local circuit neurons" or "interneurons." These distinct cellular morphologies of excitatory and inhibitory neurons reflect their unique functions. Excitatory neurons produce the principal outputs by which the neocortex communicates with rest of the nervous system, while inhibitory neurons play an essential role in sculpting the patterns of excitatory neuron activity and cortical output (Buzsaki et al., 2004).

Excitatory and inhibitory neurons are also distinguished by their origins in the embryo. Neocortical excitatory neurons are produced by the division of radial glial cells in the ventricular- and subventricular zones (VZ and SVZ, respectively) of the dorsal embryonic telencephalon (Figure 2A; Parnavelas, 2000; Noctor, 2004). Newborn excitatory neurons then migrate radially along the fibers of radial glia, populating the cortical laminae in an inside-to-out fashion (Kriegstein

and Noctor, 2004). Neocortical inhibitory neurons, on the other hand, are produced primarily in the ganglionic eminences of the ventral telencephalon (Figure 2B; Anderson et al., 1997; Parnavelas, 2000; Wichterle et al., 2001; Nery et al., 2002). From this distant origin, newborn inhibitory neurons undergo a dramatic process of long-distance, tangential migration into the overlying, dorsal telencephalon (Figure 3; Marin and Rubenstein, 2003). In the section that follows, I will focus on the classification, origin, migration, function and transplantation of this uniquely migratory cell type.

Section 3: Neocortical inhibitory neurons

Basic features and diversity

Neocortical inhibitory neurons, despite their remarkable diversity, share several common features that distinguish them from excitatory neurons (Markram et al., 2004). First, the dendrites of inhibitory neurons are aspiny. Second, the somata of inhibitory neurons can receive both excitatory and inhibitory inputs. Third, the axons of inhibitory neurons project densely within local cortical areas, and across cortical columns, but they do not project outside the neocortex. Fourth, different subtypes of inhibitory neurons preferentially target different subcellular regions of post-synaptic neurons.

Inhibitory neurons have been classified by their cellular morphologies, neurochemical marker expression, and electrophysiological properties. While a morphologically defined subtype of inhibitory neuron may, for example, tend to express a particular molecular marker, the presence of one feature (morphology,

marker expression, or electrophysiological phenotype) does not necessarily predict another (Markram et al., 2004). Thus, a great diversity of interneuron subtypes exists, each marked by a variety of overlapping and non-overlapping features. Here I will briefly focus on the morphological, neurochemical, and electrophysiological properties that most clearly differentiate rodent inhibitory neuron subtypes.

Morphologically, inhibitory neurons are reliably classified by the sub-cellular targeting of their axons (Buzsaki et al., 2004; Markram et al., 2004). As mentioned, inhibitory neurons project axons to particular sub-cellular regions of their post-synaptic targets (Figure 1B). Basket cells, which comprise nearly half of inhibitory neurons, target the somata and proximal dendrites of target neurons. This specificity of targeting allows basket cells to alter the electrical gain at target cell bodies, where dendritic responses are integrated and transduced to axonal outputs. Basket cells tend to project extensively within and outside their cortical column. Chandelier cells, by contrast target the axon initial segment with vertically branched fibers that terminate in patterns resembling candlesticks on a chandelier. By targeting axons, chandelier cells are uniquely poised to modify the final outputs of their target neurons. Dendrite-targeting inhibitory neurons include the Martinotti, bi-tufted, double bouquet, bipolar, and neurogliaform cells (Figure 1B). With the exception neurogliaform cells, these inhibitory neurons form vertically oriented processes that extend through several cortical layers. The axons of Martinotti and bi-tufted cells also project laterally across the cortex. Dendrite-targeting inhibitory neurons modify the excitability of target neurons

where neural signals are received, which allows them to fine-tune the spatial and temporal features of excitatory inputs.

Neurochemically, inhibitory neurons are distinguished from excitatory neurons by the expression of GABA, and its biosynthetic enzymes, glutamic acid de-carboxylase- 65 and 67 (GAD65 and GAD67, respectively; Gonchar et al., 2008). GABAergic inhibitory neuron subtypes can be further classified by the expression of calcium binding proteins (CaBPs) and neuropeptides (NPs). These include the CaBPs, calbindin (CB), calretinin (CR), and parvalbumin (PV); and the NPs, cholecystokinin (CCK), neuropeptide-y (NPY), somatostatin (SOM), and vaso-active intestinal peptide (VIP).

In the rat neocortex, three distinct inhibitory neuron subtypes have been identified by their non-overlapping expression of CR, PV, and SOM (Kawaguchi and Kubota, 1997). In the mouse, a similar organization exists, although there appears to be a partial overlap of the CR- and SOM-expressing populations (Gonchar et al., 2008). Calretinin is expressed primarily by bi-tufted, double bouquet, and bipolar cells; PV is expressed by basket and chandelier cells; and SOM is expressed by Martinotti and bi-tufted cells, although again, some overlap exists (Markram et al., 2004).

Electrophysiologically, the great majority of inhibitory neurons were long considered to be fast spiking (FS) cells, owing to their broad tendency to initially fire high frequency discharges in response to depolarizing currents. More recently, the electrophysiological classification of inhibitory neurons has been expanded to consider their prolonged steady-state responses to depolarization

(Markram et al., 2004): the initial high frequency responses of inhibitory neurons may remain constant throughout prolonged depolarization, or they may decline in frequency through a process known as “spike frequency adaptation.” Non-accomodating subtypes of inhibitory neurons display little or no spike frequency adaptation, while accommodating inhibitory neurons do. Stuttering cells discharge high frequency spikes at irregular intervals, while intermediate spiking cells discharge single spikes at irregular intervals. Finally, burst spiking inhibitory neurons gradually depolarize to a threshold and then fire brief clusters of three to five spikes, after which they display a prolonged after hyperpolarization (Markram et al., 2004).

Embryonic origins of diverse neocortical inhibitory neurons

Neocortical inhibitory neurons, like excitatory neurons, are produced almost entirely during mid- to late gestational periods (Parnavelas, 2000; Wonders and Anderson, 2006). In the mouse, the vast majority of neocortical inhibitory neurons are born during embryonic days 12 to 16 (E12-16; Wonders and Anderson, 2006; Wonders et al., 2008), although a relatively small number of CR- and CCK-expressing cells are also produced during postnatal periods (Dayer et al., 2005; Dragos et al., 2008). Neocortical inhibitory neurons, unlike excitatory neurons, appear to derive entirely from two ventral telencephalic structures, the medial- and caudal ganglionic eminences (MGE and CGE, respectively; Anderson et al., 1997; Lavdas et al., 1999; Wichterle et al., 2001; Nery et al., 2002; Valcanis and Tan, 2003). While there is evidence that rodent

neocortical inhibitory neurons are not derived from the dorsal telencephalon (Anderson et al., 1997; Gorski et al., 2002), some human neocortical inhibitory neurons may arise dorsally (Letinic et al., 2002).

The ventral origin of neocortical inhibitory neurons has been elucidated through a combination of *in vitro* slice- and cell culture experiments, the analysis of genetic mutants, genetic lineage tracing, and in utero fate mapping. Just over ten years ago, slice culture experiments provided strong evidence for the ventral origin of neocortical inhibitory neurons by demonstrating the migration of dye-labeled GABA- and CB-positive neurons from the ventral telencephalon into the dorsal telencephalon (Anderson et al., 1997). Notably, mice defective in the distalless homeobox transcription factors, DLX-1 and DLX-2, which are expressed in the proliferative zones of the ventral telencephalon, demonstrated a drastic reduction of young inhibitory neurons in the developing neocortex (Anderson et al., 1997).

The MGE was identified as a specific origin of neocortical inhibitory neurons just a few years later, when the neocortical phenotype of *Nkx2.1* mutant mice was examined (Sussel et al., 1999). The disruption of *Nkx2.1*, which encodes another homeobox-containing transcription factor, resulted in the dorsalization of the MGE to an identity similar to that of the lateral ganglionic eminence (LGE). Notably, *Nkx2.1* mutant mice exhibited a dramatic, but not complete, reduction of neocortical inhibitory neurons at birth (Sussel et al., 1999). These findings were later complemented by *in vitro* slice experiments (Lavdas et al., 1999; Wichterle et al., 2003; Xu et al., 2004) and homochronic in utero

transplantation experiments (Wichterle et al., 2001), which demonstrated the migration of MGE-derived cells into the developing neocortex, where they eventually differentiated into neurons that expressed a diversity of morphological features and molecular markers (GABA, PV and SOM) characteristic of inhibitory neurons.

The CGE, which is marked by expression of some transcription factors expressed in the MGE and LGE, was later also identified as a source of neocortical inhibitory neurons, particularly, CR-expressing cells (Nery et al., 2002; Xu et al., 2004; Butt et al., 2005). *In vitro* cell culture experiments demonstrated that CGE explants gave rise to large numbers of CR cells and smaller numbers of SOM and PV cells, while MGE explants produced large numbers of SOM and PV cells, but few CR cells (Xu et al., 2004). These findings were corroborated by *in utero* fate mapping experiments in which CGE-derived cells migrated into the developing neocortex and differentiated into CR-expressing inhibitory neurons, among others (Nery et al., 2002, Butt et al., 2005).

In recent years, we have learned more about the temporal and spatial origins of neocortical inhibitory neurons (Butt et al., 2005; Fogarty et al., 2007; Miyoshi et al., 2007; Wonders et al., 2008). Based largely on heterotopic and heterochronic transplantation experiments, it has been determined that the migratory, laminar, molecular, and electrophysiological phenotypes of inhibitory neurons are largely specified at their origins in the ventral telencephalon (Valcanis et al., 2003; Butt et al., 2005; Wonders et al., 2008). With respect to the temporal sequence of inhibitory neuron subtype production, it appears that

CR cells are produced during slightly later gestational stages (E13 to E16; Xu et al., 2004; Butt et al., 2005), while SOM cells are produced slightly earlier (E10 to E14) and PV cells are produced relatively consistently (E10 to E16; Xu et al., 2004; Butt et al., 2005; Miyoshi et al., 2007). In terms of the spatial organization of inhibitory neuron progenitor domains, a dorsal-ventral organization exists in the MGE: the dorsal MGE primarily generates SOM-expressing cells, while the ventral MGE primarily generates PV-expressing cells (Fogarty et al., 2007; Wonders et al., 2008). The signaling pathways and transcriptional events that parcellate these neurogenic domains have yet to be elucidated (Cobos et al., 2006; Du et al., 2008; Wonders et al., 2008).

Migration of inhibitory neurons into the developing neocortex

Newborn inhibitory neurons undergo a remarkable process of migration from their ventral origins to their final positions in the neocortex (Figure 3A; Marin and Rubenstein, 2003). This process can be broken into three general stages: their traversal from the ventral telencephalon through the striatal primordia, their passage around the dorsal-ventral border of the telencephalon into the developing cortex, and their invasion into the cortical plate (Figure 3B). These events, and the motility factors, chemo-repellents and chemo-attractants, and cell-cell interactions that guide them, are described below.

Newborn inhibitory neurons are guided out of the ventral telencephalon by a variety of secreted molecules. The migratory activity of newborn inhibitory neurons is stimulated by motogenic factors such as hepatocyte growth factor

(HGF; Powell et al., 2001), brain-derived neurotrophic factor (BDNF), neurotrophin-4 (NT-4; Polleux et al., 2001), and glial cell line-derived neurotrophic factor (GDNF; Pozas and Ibanez et al., 2005). With respect to the directionality of inhibitory neuron migration, the secretion of chemorepulsive molecules, such as Slits and Semaphorins, appears to direct neocortical inhibitory neurons away from the ventral telencephalon (Marin et al., 2001; Wichterle et al., 2003, Marin and Rubenstein, 2003; Nobrega-Pereira et al., 2008).

As migrating inhibitory neurons course away from the ganglionic eminences, they are exposed to attractant forces that guide them away from other areas of the ventral telencephalon, and into the dorsal telencephalon. Migrating inhibitory neurons enter and disperse through the dorsal telencephalon through superficial and deep routes (in the marginal- and intermediate zones (MZ and IZ, respectively; Figure 3B; Nakajima, 2007). Corticofugal axons, expressing an attractant surface molecule, TAG-1, may act as a substrate for the migration of young inhibitory neurons into the marginal and intermediate zones (Parnavelas, 2000; Denaxa et al., 2001; Denaxa et al., 2005; Metin et al., 2006). Additionally, soluble chemoattractant molecules, such as neuregulin-1 (Flames et al., 2004), GDNF (Pozas and Ibanez, 2005), and stromal-derived factor 1 (SDF-1; Stumm et al., 2003; Tiveron et al., 2006) also direct migrating inhibitory neurons through the dorsal telencephalon.

Neocortical inhibitory neurons attain their final laminar positions in the dorsal telencephalon through radially directed migration (Marin and Rubenstein,

2003; Ang et al., 2004). Curiously, migratory cells in deeper layers (SVZ and IZ) may first enter the ventricular zone before reversing direction and moving into the cortical plate (Figure 3B; Nadarajah et al., 2002). In the marginal zone, young inhibitory neurons proceed through a "random-walk" pattern of migration before entering the cortical plate (Figure 3B; Tanaka et al., 2009). Notably, young inhibitory neurons may invade the cortical plate upon losing responsiveness to chemo-attractants present in their dorsal migratory routes. For example, young inhibitory neurons exit the MZ and enter the cortical plate after down-regulating the chemokine receptor 4, a receptor for the chemo-attractant, SDF-1 (Li et al., 2008).

Much remains to be discovered about the remarkable migration of neocortical inhibitory neurons precursors from their ventral origins into the distant neocortex. While I have summarized what is known about the mechanisms of inhibitory neuron migration, it is still a great mystery why inhibitory neurons originate far outside the neocortex, and then enter into it. Moreover it is amazing how these cells, which arise from concentrated progenitors clustered in the ventral telencephalon, can disperse so evenly over the dorsal telencephalon, tiling the neocortex in a beautifully organized and remarkably even distribution. It will be fascinating to learn how this distribution is attained.

Functional roles of inhibitory neurons during development and adulthood

GABAergic signaling plays a critical role in the development and ultimate function of the neocortex. During embryonic and early postnatal life, GABA

regulates several of the developmental processes that form the neocortex, including cellular proliferation, migration, and differentiation (Owens and Kriegstein, 2002). Through paracrine GABA signaling, migratory inhibitory neurons may alter the proliferation of excitatory neuronal progenitors (LoTurco et al., 1995; Owens and Kriegstein, 2002). Additionally, GABA also alters the migratory behavior of both excitatory and inhibitory neuronal precursors (Behar et al., 2000; Lopez-Bendito et al., 2003; Cuzon et al., 2005), and GABA is required for the morphological maturation of excitatory and inhibitory neurons (Maric et al., 2001; Cancedda et al., 2007; Chattopadhyaya et al., 2007). During postnatal periods, the maturation and function of inhibitory neurons is also essential to the refinement of cortical circuits (Hensch et al., 1998; Huang et al., 1999; Fagiolini et al., 2000).

Inhibitory neurons also play a vital role in the function of the mature neocortex. At the cellular level, inhibitory neurons modulate synaptic integration and alter the probability and timing of action potential firing by pyramidal neurons (Buzsaki et al., 2007; Huang et al., 2007). Computationally, distinct inhibitory neurons may differentially contribute to sensory processing and memory functions across neural ensembles. For example, the stimulus tuning of excitatory neurons is thought to reflect concerted inhibition by soma-targeting inhibitory neurons and the localized disinhibition of excitatory neurons by inhibitory neuron-targeting inhibitory neurons (Wang and Tegner et al, 2004). Also, neocortical inhibitory neurons form extensive gap junction-mediated

electrical networks, through which they sculpt oscillatory patterns across large brain volumes (Freund, 2003; Cardin et al., 2009; Sohal et al., 2009).

Neocortical inhibitory neurons are also involved in the pathogenesis of neurological and psychiatric disorders. In rodent models, seizure phenotypes have been associated with the disruption of genes such as flathead (Sarkisian et al., 2001), aristaless (*Arx*; Kitamura et al., 2002), and *Dlx-1* (Cobos et al., 2005), all of which are crucial to inhibitory neuron development. Moreover, familial mutations in the human orthologue of *Arx* have been identified in X-linked lissencephaly with abnormal genitalia, a disorder marked by seizures and a variety of other phenotypes (Kitamura et al., 2002; Kato and Dobyns, 2005). Additionally, mouse models and human studies have implicated inhibitory neuron dysfunction in schizophrenia (Vawter, 2000; Kamnassaran et al., 2003; Erbel-Sieler et al., 2004; Lewis et al., 2005).

Inhibitory neuron precursor transplantation

Neocortical inhibitory neurons have a remarkable capacity to integrate into the postnatal brain following heterochronic transplantation. This surprising discovery came nearly a decade ago, when Hynek Wichterle dissected tissue explants from three sites in the embryonic telencephalon (MGE, LGE and dorsal telencephalon) and individually transplanted them into the adult mouse striatum, thalamus, and neocortex (Wichterle et al., 1999). While cell transplants from the LGE and dorsal telencepahlon remained largely clustered at the injection sites, transplanted cells from the MGE dispersed widely. Through

immunohistochemistry and electron miscroscopy, many of these transplanted migratory MGE cells were identified as GABAergic neurons.

Additional evidence for the integration of transplanted inhibitory neurons followed in 2006, when a detailed anatomical and electrophysiological characterization was performed after MGE cell transplantation to the neonatal neocortex and hippocampus (Alvarez-Dolado et al., 2006). As before, transplanted MGE cells dispersed widely throughout the recipient brain, and also developed features characteristic of various neocortical inhibitory neurons. In particular, the morphological, neurochemical, and electrophysiological phenotypes of the transplanted cells were consistent with those of MGE-derived inhibitory neurons. These finding suggested that: 1) the fates of transplanted inhibitory neurons were largely determined in their ventral origins, and, 2) that when heterochronically transplanted, inhibitory neuron precursors remain able to express this fate in the recipient brain.

Transplanted MGE cells also modify inhibitory signaling in the recipient brain (Alvarez-Dolado et al., 2006). Endogenous excitatory neurons in the recipient brain demonstrated an increased frequency and amplitude of spontaneous inhibitory events after inhibitory neuron transplantation. It is not yet clear, however, whether this increase in inhibition is mediated by new transplant-to-host synapses, or if transplantation somehow induces the modification of existing host synapses. Regardless, these findings have raised the possibility that inhibitory neuron transplantation could be used modify neural circuits in the diseased brain.

Section 4: Developmental cell death in the nervous system

Basic features of developmental cell death

Cell death is a widespread phenomenon throughout the development of many tissues and organs. Across species, cell death serves a variety of developmental purposes, including, the elimination of transient tissues that once served a function in the organism ("metamorphic" cell death), the elimination of vestigial ancestral features ("phylogenetic" cell death), and the formation of morphological and structural patterns ("morphogenetic" cell death; Oppenheim, 1991).

In the nervous system, massive numbers of neurons and glia are eliminated by developmental cell death during embryonic and postnatal periods. With respect to neurons, developmental cell death typically claims anywhere from 20 to 80% of a given cellular population, often during late maturational stages after the population has expressed phenotypic markers and formed afferent and efferent connections. (Cowan et al., 1984).

Neuronal cell death occurs through one of three processes, each distinguished by its basic mechanism and accompanying morphological features (Schweichel and Merker, 1973). In type-III cell death, or necrosis, cellular energy production is disrupted, most typically as the result of pathologic conditions or injury. Consequently, necrotic cells become unable to maintain osmotic homeostasis, a condition that leads to the rupture of cellular organelles and eventual autolysis. Necrotic cells develop a swollen appearance before bursting

open and releasing their cellular contents into the extracellular space (Figure 3A). By contrast, type-II cell death, or autophagy, is a self-contained process by which cellular degradation is mediated by lysosomes. Morphologically, autophagic cells are marked by the dramatic accumulation of intracellular lysosomal bodies, and occasionally, the condensation of nuclear chromatin. While dying neurons do sometimes express morphological characteristics of autophagy, it remains somewhat controversial whether autophagy directly mediates cellular suicide, or if it instead reflects a self-clearance process secondary to another type of cell death (Yuan 2003).

Type-I cell death, or apoptosis, is a well-described and prominent mechanism of cell death during nervous system development (Sanes). Compared to type-III cell death, apoptosis is remarkably active, ordered, and contained. Through mechanisms that require protein synthesis, apoptotic cells initiate the degradation of their nuclear contents and cell-structure components, and form membrane-bound apoptotic bodies, which are quickly phagocytosed by neighboring cells (Figure 3B). Morphologically, apoptotic cells develop a reduced cellular volume, and highly condensed, circumferentially displaced nuclear chromatin, which is termed “pyknosis.” Given that type-I cell death is by far the most prominent form of cell death during nervous system development (Yuan et al., 2003), the remainder of this section will focus on the molecular mechanisms by which it occurs.

Molecular mechanisms of programmed cell death

Programmed cell death, or apoptosis, is a process of protease-mediated cellular disassembly. It culminates in the proteolytic fragmentation of cellular DNA; the degradation of DNA repair elements, DNA replication machinery, and RNA splicing enzymes; and the cleavage of cytoskeletal and membrane proteins (Sanes et al., 2006). During apoptosis, DNA fragmentation and membrane degradation are mediated in part by reactive oxygen species, but the most prominent effectors of cell death are members of the cysteine-requiring aspartate protease (caspase) family. Caspase activation is a central feature in both the extrinsic and extrinsic pathways of apoptosis, which are described sequentially below.

Caspases reside intracellularly as inactive zymogens. Upon proteolytic activation by autocatalysis or other caspases, they directly proteolyze intracellular substrates, including proteins that maintain the integrity of the genetic material and cellular structure. Additionally, caspases activate a host of other effector proteins that mediate cellular breakdown. The cleaved forms of caspase-3 and caspase-9 are highly specific molecular markers of apoptotic cells, and they are critical mediators of cell death in the nervous system (Sanes et al., 2006). The genetic elimination of caspase-3 or caspase-9 causes relatively few gross phenotypes outside the brain. However, in the caspase-3 (Kuida et al., 1996) and caspase-9 deficient brains (Kuida et al., 1998 and Hakem et al., 1998), cell death is markedly diminished, resulting in the accumulations of post-mitotic neurons and cellular hyperplasias.

In contrast to the extrinsic pathway of apoptosis, which is mediated by extracellular signaling, the intrinsic pathway of apoptosis involves intracellular signals from mitochondria (Figure 5). In the intrinsic pathway, caspase-3 and caspase-9 are activated by the mitochondrial release of cytochrome-c and Smac (the second mitochondrial activator of caspase; Du et al., 2000). Mitochondria also release apoptosis inducing factor (AIF), which can directly translocate to the nucleus and fragment DNA without the involvement of caspases (Joza et al., 2001).

The release of mitochondrial proteins is a critical tipping point in the intrinsic pathway of apoptosis. Therefore, the permeability of the mitochondria is tightly regulated by an expansive family of pro- and anti-apoptotic genes, in particular, members of the B-cell lymphoma-2 (Bcl-2) family (Reed, 2000). Pro-apoptotic members of the Bcl-2 family, such as Bax (Bcl-2-associated X protein), Bak (Bcl-2-homologous antagonist/killer), and Bid (BH3-interacting domain death agonist) interact with ion channels to form pore complexes in the mitochondrial membrane, through which cytochrome-c is released (Shimizu et al., 1999). Notably, the expression of Bax peaks perinatally in the nervous system (Krajewska et al., 2002), and then rapidly declines during early postnatal life (Vekrellis et al., 1997 and Krajewska et al., 2002). The genetic disruption of Bax enhances the survival of various neuronal populations, including developing sympathetic and dorsal root ganglia neurons, motor neurons (Knudson et al., 1995; Sun et al., 2003), and adult-generated hippocampal and olfactory bulb neurons (Sun et al., 2004; Kim et al., 2007).

Once released from the mitochondrion, cytochrome-c binds to apoptosis protease activating factor-1 (Apaf-1) and initiates the formation of an apoptosome, which recruits and activates caspase-9 (Li et al., 1997). Additionally, Smac also contributes to caspase-9 activation via its antagonism of the inhibitor of apoptosis proteins (Iaps; Verhagen et al., 2002). Activated caspase-9 in turn cleaves the pro-form of caspase-3, which then frees caspase-activated deoxyribonucleotidase (CAD) from its inhibitor (ICAD; Enari et al., 1998). Once activated, CAD translocates to the nucleus and mediates DNA fragmentation.

As mentioned, some Bcl-2 family members serve anti-apoptotic roles by preventing mitochondrial cytochrome-c release and the subsequent activation of Apaf-1. Bcl-2 maintains the mitochondrial sequestration of cytochrome-c (Kluck et al., 1997, Yang et al., 1997), while (DEFINITION) Bcl-x_L inhibits the activity of Apaf-1 (Boise et al., 1993; Hu et al., 1998). Conversely, Bcl-2 and Bcl-x_L are antagonized by dimerization with pro-apoptotic Bcl-2 family members such as Bad, Bax, Bim, and Bid (Gross et al., 1999). The expression of Bcl-2 (Abe-Dohmae et al., 1993; Krajewska et al., 2002) and Bcl-x_L (Krajewska et al., 2002) begins around neural tube formation, and peaks during the period of neurogenesis. Bcl-x_L remains expressed in post-mitotic adult neurons (Vekrelis et al., 1997) while Bcl-2 expression rapidly declines after birth (Krajewska et al., 2002). The genetic disruption of Bcl-x_L dramatically increases apoptosis in the embryonic nervous system (Motoyama et al., 1995), while the disruption of Bcl-2 does not profoundly affect embryonic nervous system development (Veis et al.,

1993), but does reduce the survival of motor neurons, sympathetic neurons and sensory neurons in postnatal life (Michaelidis et al., 1996). Conversely, Bcl-2 over-expression dramatically increases the survival of retinal ganglion cells and facial motor neurons in the brainstem (Martinou et al., 1994).

The extrinsic pathway of apoptosis is mediated by the activation of cell surface receptors belonging to the tumor necrosis factor receptor (TNFR) family, such as TNFR-1, Fas/CD95, p75 neurotrophin receptor (p75-NTR), death receptors (DRs) and the tumor necrosis factor-related apoptosis-inducing ligand receptors (TRAIL receptors; Haase et al., 2008). These receptors are activated by a variety of ligands, including Fas-ligand (FasL), TRAIL and others (Nagata, 1997). Upon activation, these death receptors recruit the adaptor protein Fas-associated death domain (FADD; Chinnaiyan et al., 1995), which proteolytically activates caspase-8 (Muzio et al., 1996). Caspase-8 then directly activates effector caspases (such as caspase-3 and caspase-9), leading to apoptosis through the downstream mechanisms described above (Scaffidi et al., 1998).

Additionally, the extrinsic pathway can be amplified through the recruitment of intrinsic pathway components (Scaffidi et al., 1998). In this scenario, caspase-8 cleaves the pro-apoptotic Bcl-2 family member, Bid, which in turn activates Bax and Bak, and subsequent events of the intrinsic pathway (cytochrome-c and Smac release), as described above (Luo et al., 1998; Deng et al., 2002).

It remains unclear whether the extrinsic pathway of apoptosis plays a prominent role in the developmental cell death of the brain (Haase et al., 2008).

Fas/CD95 and caspase-8 expression are quite low in the embryonic nervous system, implying that the extrinsic pathway of apoptosis may not be activated during developmental neuronal cell death (French et al., 1996). On the other hand, it does appear that the *in vitro* neuronal cell death may be triggered by Fas activation (Raoul et al., 1999). *In vivo*, *Fas* mutants exhibit decreased axotomy-induced cell death (Zuliani et al., 2005). Mice lacking downstream Fas effectors, including FADD and caspase-8, die during mid- to late embryonic stages, but the embryonic lethality appears to arise from defective cardiac development (Varfolomeev 1998; Yeh et al., 1998). Neither gross abnormalities nor hypercellularities of the brain were described in Fadd (Yeh et al., 1998) and caspase-8 mutant mice (Varfolomeev et al., 1998), although neural tube defects were observed in caspase-8 mutants (Sakamaki et al., 2002, Kang et al., 2004). Recently, an autocrine mechanism of DR6 activation has been implicated axonal degeneration and cell death in developing motor neurons (Nikolaev, et al., 2009).

Regulation of developmental cell death in the nervous system

For several decades it has been known that soluble molecules promote the survival of developing neurons (Levi-Montalcini and Cohen, 1956; Cohen and Levi Montalcini, 1956). A large number of these trophic factors have been identified, particularly those that promote motor neuron survival, such as ciliary neurotrophic factor (CNTF; Bonni et al., 1993), GDNF (Lin et al., 1993; Airaksinen and Saarma, 2002), and HGF (Ebens et al., 1996; Yamamoto et al., 1997). Perhaps the best-known neurotrophic molecules are those of the

neurotrophin family, including nerve growth factor (NGF), neurotrohpin-3 (NT-3), BDNF, and neurotrophin 4/5 (NT-4/5).

All neurotrophins bind to the low-affinity NGF receptor, p75, a member of the death-promoting TNF receptor family (Johnson et al., 1986). Neurotrophin family members also bind with higher affinity and greater specificity to the tropopmyosin related kinase (Trk) family of receptors (Kaplan et al., 1991; Barbacid, 1994). Trk signaling plays a well-defined role in developmental neuronal cell death. Below I briefly describe Trk signaling as a model pathway for the regulation of developmental cell death.

As mentioned earlier, a balance of pro- and anti-apoptotic protein activity determines whether the mitochondrion releases cytochrome-c and activates downstream caspases. Neurotrophins, like a variety of other trophic signals, maintain this balance in favor of neuronal survival by regulating the gene expression and biochemical activity of pro- and anti-apoptotic molecules. Pro-survival signaling by Trk receptors is mediated by protein kinases, such as Akt and mitogen-activated protein kinase (MAPK; Yuan and Yankner, 2000). For example, Trk signaling leads to the phosphorylation of Akt kinase and mitogen-MAPK, among others, which activate the transcription of anti-apoptotic genes, such as Bcl-2 (Riccio et al., 1999). Additionally, phosphorylation by kinases inhibits pro-apoptotic molecules, such as Bad (Zha et al., 1996; Datta et al., 2001) and caspase-9 (Cardone et al., 1998), while suppressing the expression of Bim (Yuan and Yankner, 2000; Putcha et al., 2001).

In the developing nervous system, trophic signaling may block a neuronal default program to undergo apoptosis (Raff et al., 1994; Sanes et al., 2006). Trophic signals are derived from features in the cellular environment, including other neurons, glia, extracellular matrix, the vasculature, and non-neural tissues. A series of well-known studies demonstrated that when the levels of trophic signals are manipulated by expanding or reducing post-synaptic targets, then the survival of pre-synaptic neurons was increased or decreased, respectively (Hamburger and Levi-Montalcini, 1949). From these experiments the neurotrophin hypothesis emerged, which postulates that trophic signals are produced in limited quantities by neuronal targets, and that an over-abundance of developing neurons competes for these limited survival signals. It is thought that neurons that successfully innervate their targets can receive adequate trophic signals, and thus survive, while those that are unsuccessful die because they do not obtain sufficient trophic support. This competitive process is thought to ensure that neuronal populations are adequately scaled to their post-synaptic targets (Buss et al., 2006).

Target tissues are not the only source of trophic signals for developing neurons, however. For example, neuronal cell death in the developing brainstem has been increased by the experimental ablation of afferent sensory inputs, indicating that afferents may also provide trophic support to developing neurons (Levi-Montalcini, 1949, Parks, 1979; Born and Rubel, 1985; Trune, 1982a; Trune, 1982b). Additionally, there is evidence that molecules presented by glia (Johnson et al., 1988) and extracellular matrix (Hamburger et al., 1981) may also

promote the survival of developing neurons (Oppenheim et al., 1991). Finally, distant endocrine tissues, such as the thyroid and gonads, may also produce trophic signals that influence cellular survival in the developing nervous system (Lewis et al., 1976; Nordeen et al., 1985).

Section 5: Ocular dominance plasticity in the visual cortex

Ocular dominance plasticity and the critical period

Perhaps more than any other organ, the brain has an amazing ability to be modified by experience. This property, plasticity, has been widely considered the basic mechanistic substrate for learning. While learning occurs throughout life, it is hard to deny that the ability to learn is greatest during youth. In the past decades, neuroscientists have identified so called critical periods, during which the brain is highly plastic and able to undergo functional rearrangements (Hensch, 2004). Across a variety of species, including mouse, rat, ferret, cat, and birds, these critical periods tend to occur during early postnatal life, or shortly after neural circuit formation.

Critical period plasticity has been extensively studied in the mammalian primary visual cortex, the region where inputs from the two eyes first converge (Wiesel and Hubel, 1963). In the mouse, single-cell electrode recordings have shown that neurons in the primary visual cortex respond to stimulation of either eye, although with a bias in responsiveness to the contralateral eye. This property, ocular dominance, (Figure 7A, Drager, 1975) is in turn altered by monocular visual deprivation (MD). Monocular deprivation shifts neuronal

responses away from the visually deprived, contralateral eye, and towards the non-deprived, ipsilateral eye (Figure 7A, Drager, 1978). In the mouse, ocular dominance plasticity is greatest during a critical period that spans the fourth and fifth postnatal weeks of life (Gordon and Stryker, 1996). Peak ocular dominance plasticity is observed between P25 and P30 in the mouse, although more subtle and distinct forms of ocular dominance plasticity are observed in adulthood (Figure 7B; Sato, 2008; Lehmann et al., 2008).

Regulation of ocular dominance plasticity by GABAergic signaling

Pharmacological, genetic, and behavioral manipulations have defined the essential role of inhibitory GABAergic signaling in establishing the critical period for ocular dominance plasticity (Figure 7B; Hensch et al., 1998; Huang et al., 1999; Fagiolini and Hensch, 2000; Morales et al., 2002). Most notably, *Gad65* mutant mice, which show reduced GABA release yet relatively normal visual processing, do not exhibit ocular dominance plasticity (Hensch et al., 1998). However, the local infusion of GABA-receptor agonists (benzodiazepines; BDZs) can restore ocular dominance plasticity in *Gad65* mutants even after the critical period, suggesting that GABAergic inhibition is required for the establishment of ocular dominance plasticity (Fagiolini and Hensch, 2000).

There is also compelling evidence that the timing of the critical period is determined by the maturation of inhibitory signaling. Over-expression of BDNF or the orthodenticle homeobox transcription factor, Otx2, accelerates the juvenile morphological maturation of soma-targeting, PV-expressing inhibitory neurons,

and increases the strength of neocortical inhibitory signaling (Huang et al., 1999; Sugiyama et al., 2008). Additionally, BDNF over-expression also produces a precocious critical period, suggesting that the maturation of inhibitory neurons may regulate the onset of ocular dominance plasticity (Huang et al., 1999, Hanover et al., 1999). The intracortical infusion of benzodiazepines prior to the critical period elicits precocious ocular dominance plasticity in mice (Fagiolini and Hensch, 2000). This feature has been exploited to dissect the contributions of specific sub-cellular GABA-receptors to ocular dominance plasticity (Fagiolini et al., 2004). Remarkably, ocular dominance plasticity is regulated by a subset of GABA receptors, in particular, those located at the soma of post-synaptic neurons (Huang et al., 1999; Fagiolini et al., 2004). Together, these studies indicate that a specific sub-population of soma-targeting inhibitory neurons could be directly involved in establishing the critical period of ocular dominance plasticity.

Induction of ocular dominance plasticity after the critical period

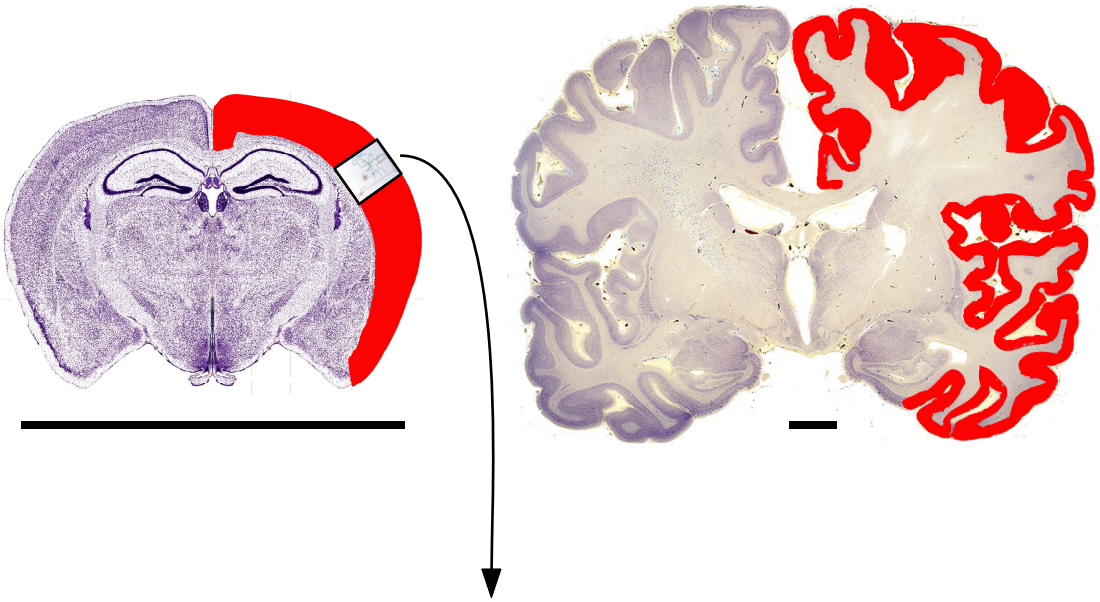
To date, a small handful of manipulations have restored ocular dominance plasticity outside of the critical period. Two of these manipulations targeted molecules that govern neuronal structural plasticity (Pizzorusso et al., 2002 McGee et al., 2005). The infusion of chondroitinase, which proteolytically degrades extracellular matrix components, reactivated strong ocular dominance plasticity in adult rats (Pizzorusso et al., 2002). Also, Nogo-receptor (NgR) mutant mice exhibit extended ocular dominance plasticity that continues past the

end of the critical period, indicating that NgR-myelin interactions may restrict ocular dominance plasticity at the end of the critical period (McGee et al., 2005). Finally, chronic administration of a selective serotonin reuptake inhibitor (SSRI), fluoxetine, activated ocular dominance plasticity in adult rats, although the mechanistic basis for this observation is less defined (Vetencourt et al., 2008).

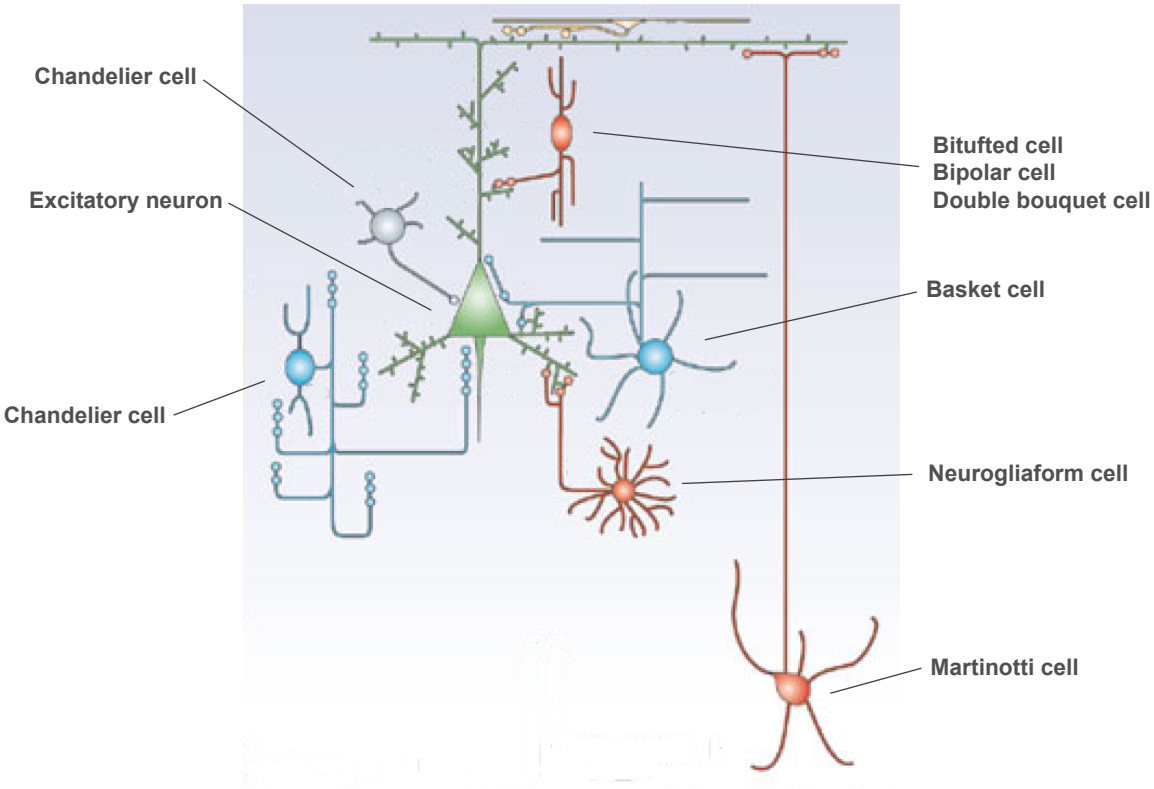
Figure 1. Neurons of the mammalian neocortex.

(**A**) Coronal sections of adult mouse (left) and human (right) brains. The neocortices of the left hemispheres are highlighted in red. Inset on left image depicts the orientation of (**B**). Scale bars, 10 mm. Left image from Allen Reference Atlas, <http://mouse.brain-map.org/atlas/index.html>, right image from Comparative Mammalian Brain Collection, <http://brainmuseum.org> (**B**) Neocortical neurons can be broadly classified by their neurotransmitter phenotypes. Excitatory neurons (green) release the neurotrasmitter, glutamate, and tend to form distant projections within and outside of the neocortex. Inhibitory neurons (grey, blue, and red) release GABA and form dense local projections within the neocortex. Inhibitory neurons exhibit a great diversity of morphologies and target different sub-cellular regions of post-synaptic neurons. Image adapted from Hensch, 2005.

A



B


Chandelier cell
Excitatory neuron
Chandelier cell
Bitufted cell
Bipolar cell
Double bouquet cell
Basket cell
Neurogliaform cell
Martinotti cell

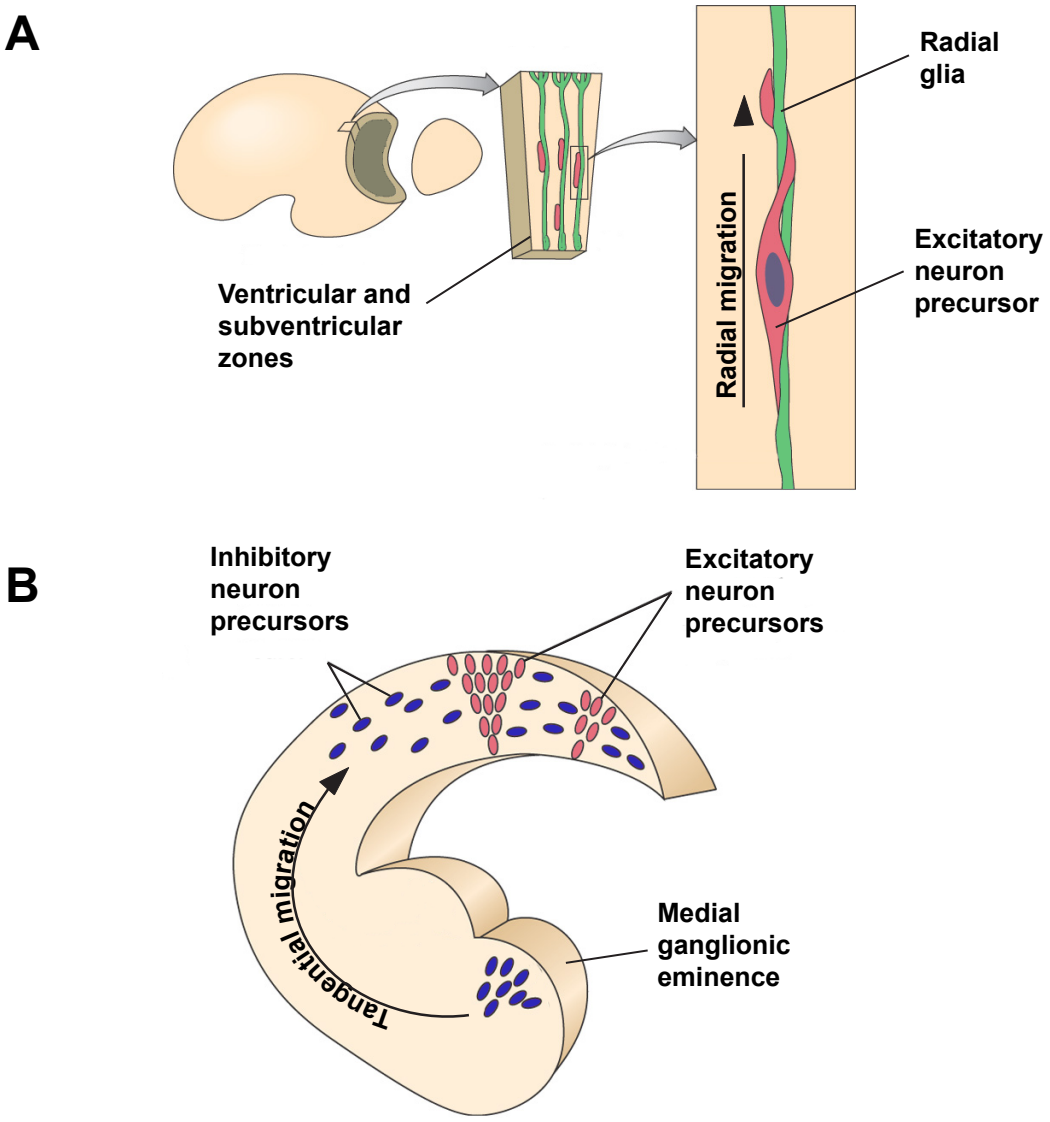


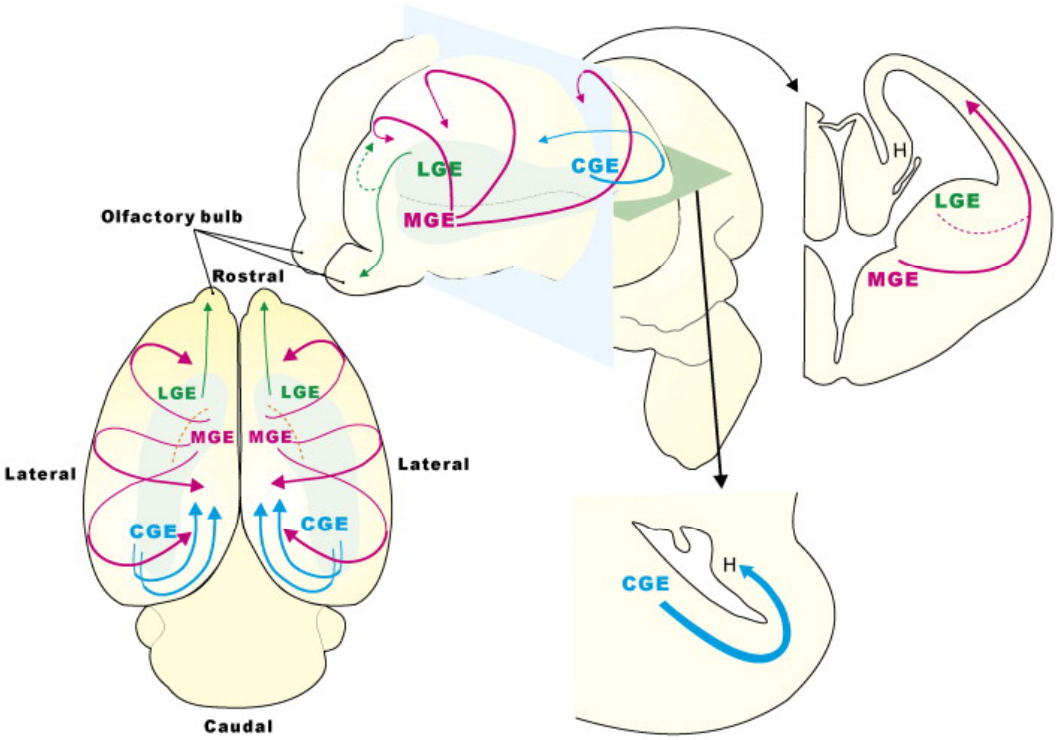
Figure 2. Distinct origins of neocortical excitatory and inhibitory neurons.

(**A**) Neocortical excitatory neurons are produced by radial glia in the ventricular- and subventricular zones of the embryonic dorsal telencephalon. Excitatory neuron precursors migrate radially into the developing neocortex, along the processes of their radial glial progenitors. (B) Neocortical inhibitory neurons are produced in ventricular- and subventricular zones of the ventral telencephalon, and migrate tangentially into the dorsal telencephalon. Images adapted from Sanes et al, 2006.

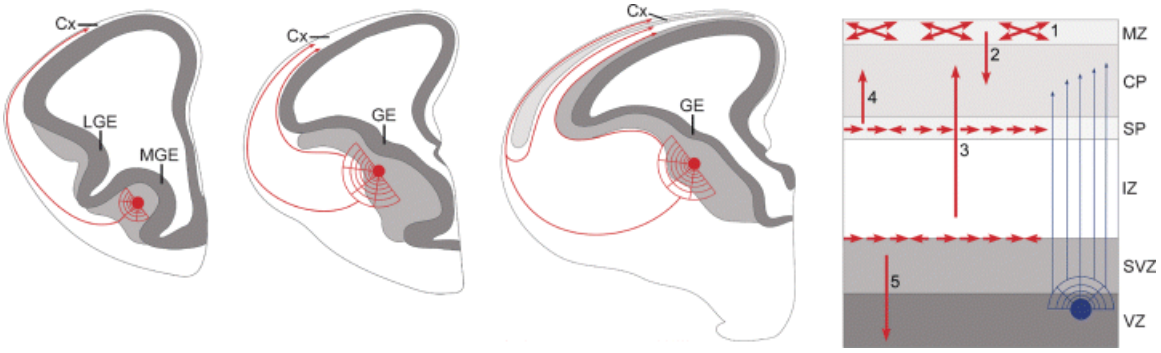
Figure 3. Migratory patterns of embryonic neocortical inhibitory neurons.

(**A**) Neocortical inhibitory neuron precursors originate in medial- and caudal ganglionic eminences (MGE and CGE, respectively) of the ventral telencephalon and migrate tangentially into the dorsal telencephalon. Image from Nakajima, 2007. (**B**) Coronal views of the embryonic telencephalon. During early developmental stages (embryonic day 12.5, E12.5), tangentially migrating inhibitory neuron precursors course through the marginal zone (MZ) of the dorsal telencephalon (red; far left). Around E14.5, migrating inhibitory neuron precursors also migrate through the intermediate zone (IZ) and subventricular zone (SVZ; second from left), while at later stages (E14.5 to E16.5) they may also migrate through the subplate (SP; second from right). Some migrating inhibitory neuron precursors exit the MZ and enter the cortical plate (CP) dorsal telencephalon after undergoing a random-walk pattern of migration in the MZ (1; far right). Additionally, migratory neurons in the IZ and SVZ may enter the ventricular zone (VZ) of the dorsal telencephalon (5; far right) before reversing direction and entering the CP (3). Image from Metin et al., 2006.

A


Olfactory bulb
Rostral
LGE
MGE
CGE
Lateral
Lateral
Caudal
H

B


Cx
LGE
MGE
GE
MZ
CP
SP
IZ
SVZ
VZ
1
2
3
4
5

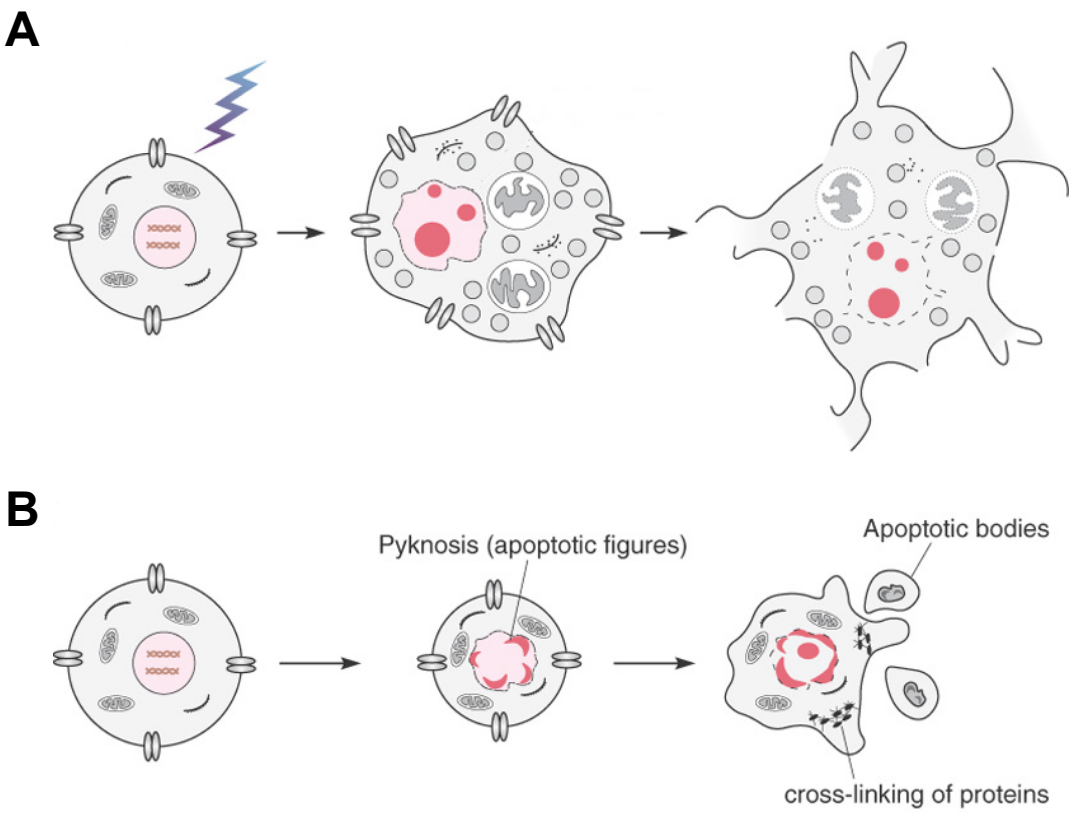
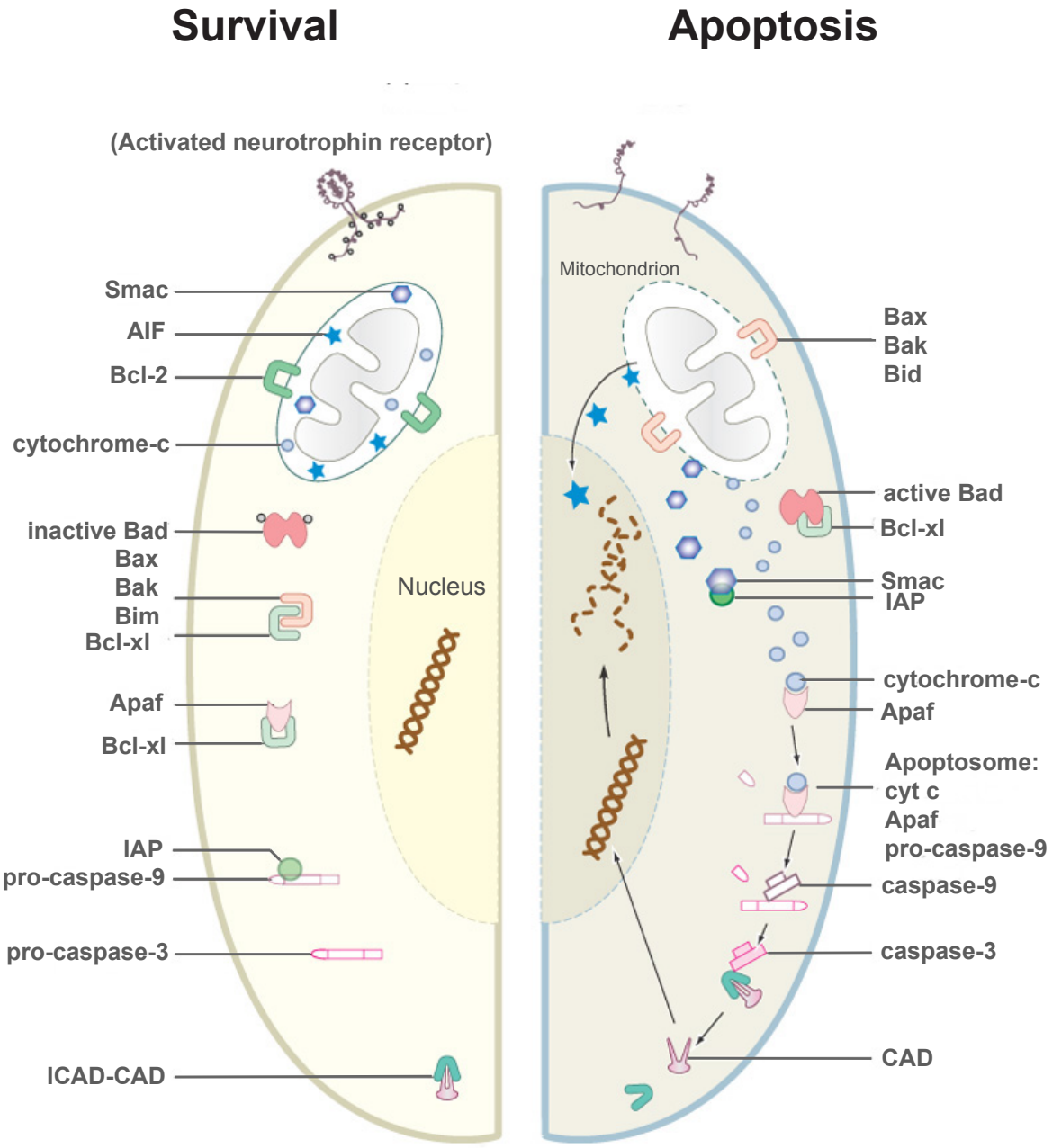


Figure 4. Morphological features and basic mechanisms of necrosis and apoptosis.

(**A**) Severe cellular damage initiates necrosis. Due to decreased mitochondrial energy production, necrotic cells cannot maintain an osmotic balance, which leads to the rupture of organelles and autolysis. Necrotic cells become swollen and eventually burst open, releasing their cytoplasmic contents into the extracellular space. (**B**) Developmental cell death occurs largely through apoptosis, which is marked by a contraction of cell morphology, condensation of the nuclear genetic material (pyknosis), and protein cross-linking. Portions of apoptotic cells are encapsulated in plasma membrane and released as apoptotic bodies, which become cleared from the extracellular space by phagocytes. Image adapted from Sanes et al., 2006.

Figure 5. The intrinsic pathway of apoptosis.

The intrinsic pathway of apoptosis directly involves mitochondria. The balance of pro- and anti-apoptotic regulators of the Bcl-2 family determines whether cytochrome-c is released from the mitochondrion. Anti-apoptotic member of the Bcl-2 family, such as Bcl-X_L and Bcl-2, reduce mitochondrial permeability and antagonize pro-apoptotic Bcl-2 family members, such as Bax, Bak and Bim. Up-regulation of pro-apoptotic Bcl-2 activity results in the increased permeability of the mitochondrial membrane, allowing the release of apoptosis initiating factor (AIF), second mitochondrial activator of apoptosis (Smac), and cytochrome-c. AIF translocates to the nucleus and initiates DNA cleavage, while Smac antagonizes the inhibitor of apoptosis molecule (IAP). Cytochrome-c activates apoptosis activating factor (Apaf), which assembles into an apoptosome with pro-caspase-9. Caspase-9 is activated by cleavage in the apoptosome, and goes on to activate caspase-3. Caspase-3 activates CAD (caspase-activated deoxyribonucleotidase), which cleaves DNA, while caspase-3 also degrades molecules that maintain the nuclear and cellular structure. Image adapted from Sanes et al., 2006.


Survival
Apoptosis
(Activated neurotrophin receptor)
Smac
AIF
Bcl-2
cytochrome-c
inactive Bad
Bax
Bak
Bim
Bcl-xl
Apaf
Bcl-xl
IAP
pro-caspase-9
pro-caspase-3
ICAD-CAD
Nucleus
Mitochondrion
Bax
Bak
Bid
active Bad
Bcl-xl
Smac
IAP
cytochrome-c
Apaf
Apoptosome:
cyt c
Apaf
pro-caspase-9
caspase-9
caspase-3
CAD

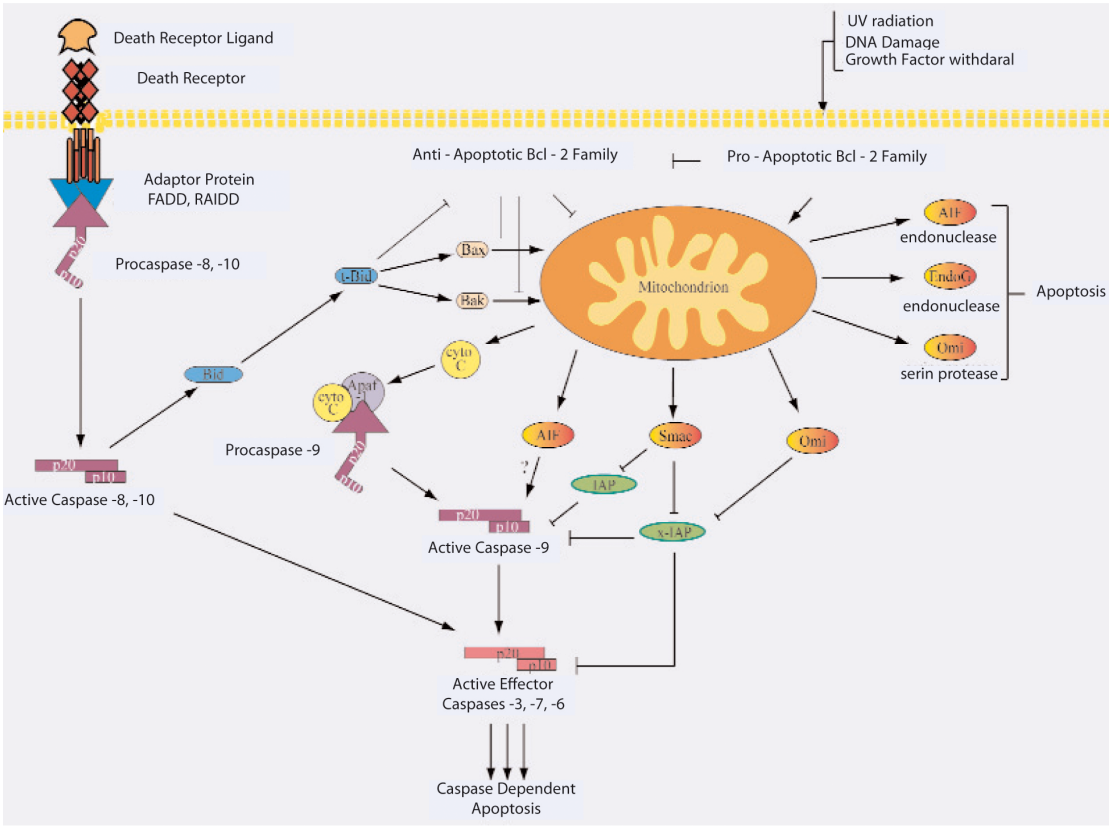


Figure 6. The extrinsic pathway of apoptosis.

The extrinsic pathway of apoptosis is mediated by extracellular signaling through surface receptors of the tumor necrosis factor receptor (TNFR) family. Activated TNFRs recruit the adapter protein, Fas-associated death domain (FADD), which proteolytically activates caspase-8. Caspase-8 can activate caspase-3 and caspase-9, leading to apoptosis through the mechanisms described in Figure 5. Additionally, the extrinsic pathway can activate mechanisms the intrinsic pathway through the recruitment of Bid, which mediates cytochrome-c by activating other pro-apoptotic Bcl-2 family members. Image adapted from Sanes et al., 2006.

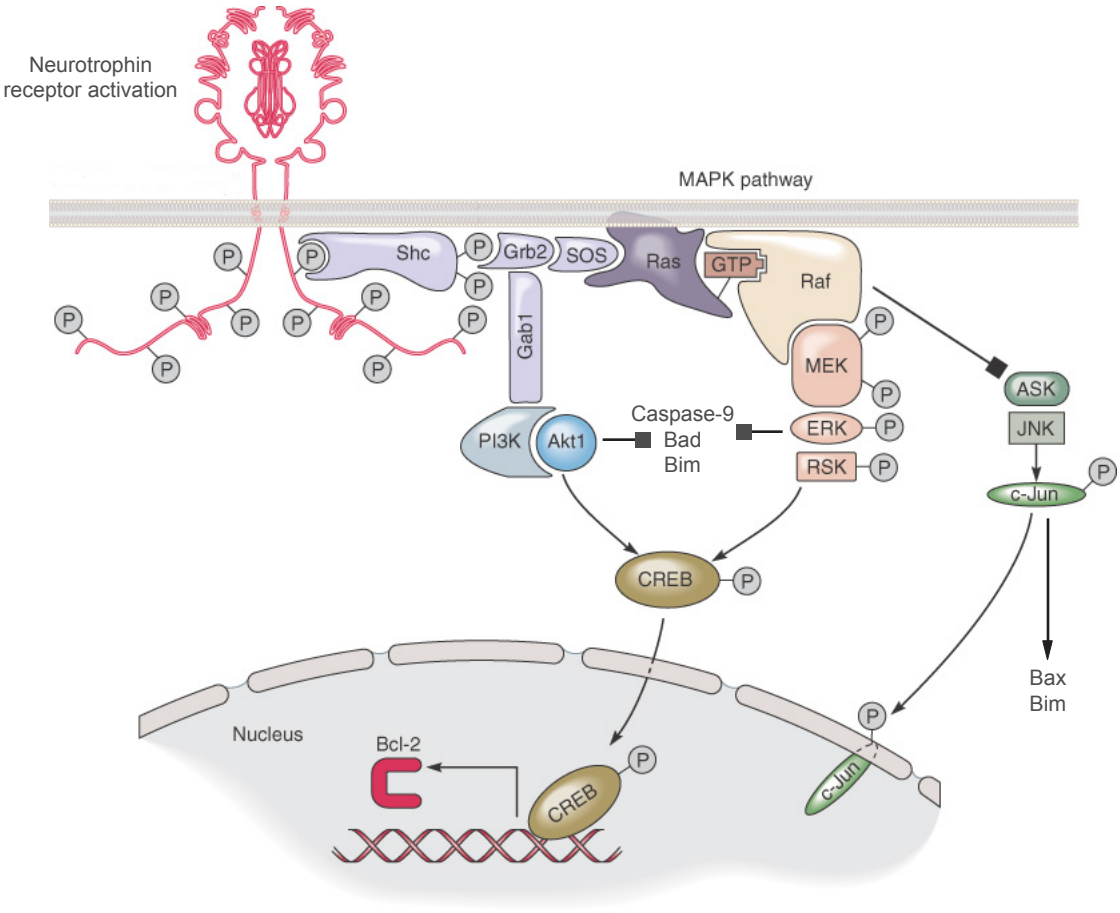
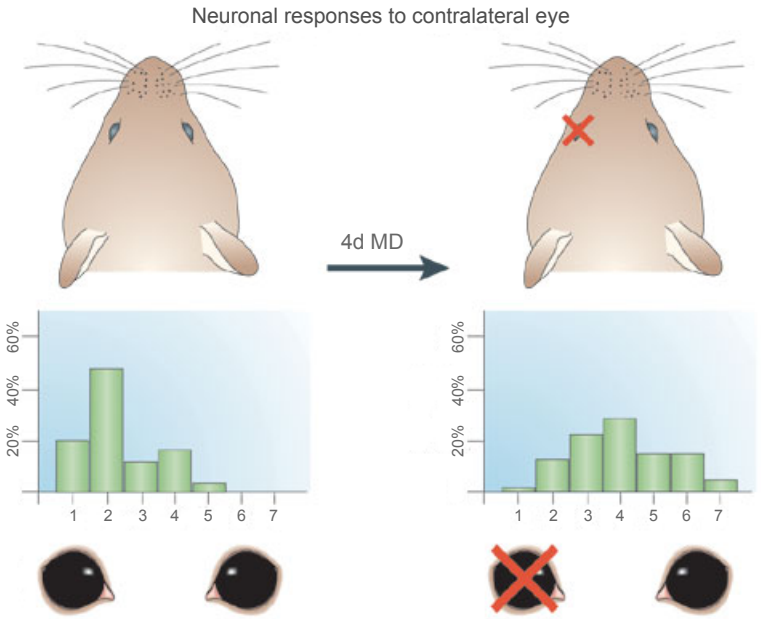


Figure 7. Trophic signaling regulates the apoptosis of developing neurons. Neurotrophin receptor activation promotes signaling by Akt kinase and the mitogen-activated protein kinase (MAPK), ERK (extracellular signal-regulated protein kinase). Akt and ERK activate cyclic-AMP response element binding protein (CREB). Activated CREB translocates to the nucleus and promotes the production of the anti-apoptotic, Bcl-2. Additionally, Akt and ERK phosphorylate and inhibit pro-apoptotic molecules, such as Bad, caspase-9, and Bim. Activated neurotrophin receptors also promote the inhibition of c-Jun N-terminal kinase (JNK), an activator of pro-apoptotic signals. Image adapted from Sanes et al., 2006.

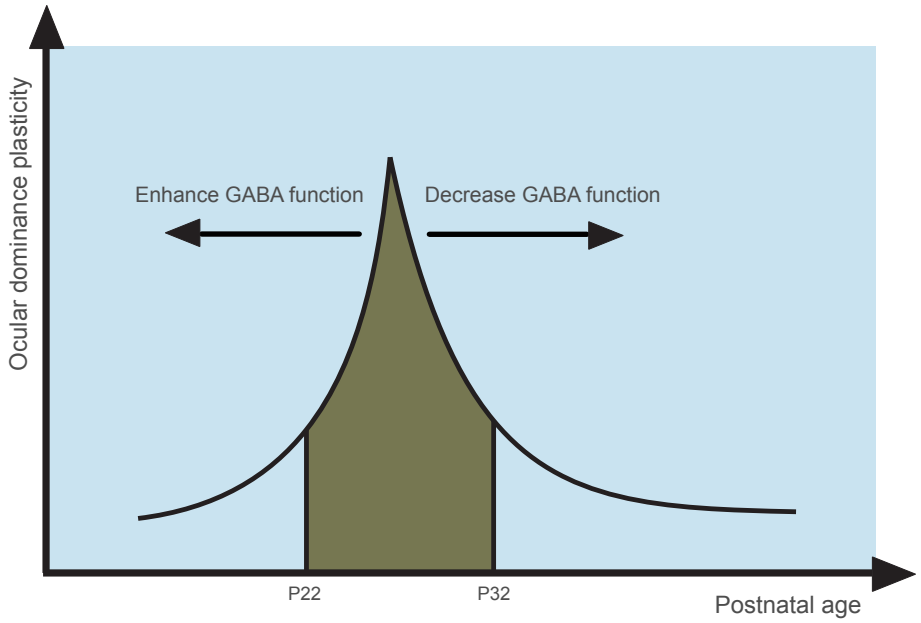
Figure 8. Ocular dominance plasticity and the critical period.

(**A**) Neurons in the primary visual cortex exhibit a bias in responsiveness to the contralateral eye. Monocular deprivation (MD) of the contralateral eye elicits ocular dominance plasticity, whereby the eye-specific neuronal responses shift away from the deprived eye and towards the non-deprived, ipsilateral eye. (**B**) Monocular deprivation elicits strong ocular dominance plasticity during a critical period of juvenile development. In the mouse, the critical period for ocular dominance plasticity occurs approximately from postnatal days 22 to 32 (P22 to P32), with peak of ocular dominance plasticity occurring around P28. Ocular dominance plasticity is regulated by local GABAergic signaling in the visual cortex. Manipulations that enhance the maturation of GABAergic signaling elicit precocious ocular dominance plasticity, while those that disrupt GABAergic signaling prevent ocular dominance plasticity. Images adapted from Hensch, 2005.

A


Neuronal responses to contralateral eye
4d MD
60%
40%
20%
1 2 3 4 5 6 7
60%
40%
20%
1 2 3 4 5 6 7

B


Ocular dominance plasticity
Enhance GABA function
Decrease GABA function
P22
P32
Postnatal age

Chapter 2

Materials and Methods

Section 1: Surgical devices

Head molds

A head mold was used to stabilize recipient mice during the cell transplantation procedure. Dental acrylic casts of neonatal mice were made and then pressed onto oven-bake clay (Sculpey, Polyform Products Company) to create contoured impressions of the head and neck of the mouse. The mold was baked and then surrounded with modeling clay to create a surface for attaching the mold to a stereotaxic injection device.

Glass injection needles for cell transplantation

Glass capillary tubes (5 μl size, Drummond WIRETROL) were pulled using a vertical pipette puller (David Kopf Instruments) to create fine injection needles for cell transplantation. The heating element and solenoid of the puller were adjusted and calibrated empirically with each use to create injection needles of the desired shape. The capillary tubes were pulled to create needles that tapered over a distance of 6 mm from their shoulder to tip. After the pipette was pulled, the tip was then beveled on a rotating polishing disc made of diamond dust abrasive. In order to prevent the accumulation of debris inside the tip, compressed air was blown through the tip during the beveling procedure. Tips were beveled to an angle of 35-45° and an outer diameter of 60-80 μm.

Section 2: Animals and genotyping

All experiments were performed on mice, which were housed and treated in accordance with the guidelines established by the Laboratory Animal Care and Use Committee of the University of California, San Francisco. Mouse strains are described in Table 1.

Table 1. Mouse strains and descriptions.

Strain	Full name	Description	Source	Reference
GAD67-GFP	GAD67-GFP (Δneo)	Contain an EGFP sequence knocked-in to the first exon of the GAD67 allele. GFP labels essentially all GABAergic cells. Maintained as heterozygotes by breeding to C57Bl/6 mice.	Yuchio Yanagawa	Tamamaki *et al*., 2003
Bax	B6.129X1-*Bax*^{tm1Sjk}/J	Bax function is eliminated in all cells by the substitution of exons 2 through 5 of the BAX sequence with a PGK-Neo cassette. Maintained as homozygotes by breeding to C57Bl/6 mice.	Jackson Labs	Knudson *et al*., 1995
GFP	STOCK Tg(CAG-EGFP) B5Nagy/J	Transgenic mice in which EGFP is constitutively expressed by all cells. Bred for several generations to CD-1 and maintained as homozygotes on CD-1 background.	Jackson Labs	Hadjantonakis *et al*., 1998

TrkB	ß-actin: Cre;$TrkB^{lox/lox}$	Knock-out mice originally produced by breeding $TrkB^{flox/flox}$ mice and ß-actin: Cre mice. The TrkB allele is disrupted in all cell types. Maintained as heterozygotes by breeding to CD-1 mice.	Rui Galvao	Galvao *et al*., 2008
DsRed	B6.Cg-Tg(CAG-DsRed*MST) 1Nagy/J	Transgenic mice in which DsRed is constitutively expressed by all cells. Bred for several generations to CD-1 and maintained on CD-1 background. Maintained as heterozygotes.	Jackson Labs	Vintersten *et al*., 2004
C57Bl/6	C57Bl/6NCrl	Outbred wild-type strain used for breeding and as recipients for cell transplantation. Purchased from Charles River Labs.	Charles River Labs	(none)
CD-1	Crl:CD1(ICR)	Outbred wild-type stain used for breeding, and for matings to produce embryonic donor tissue for cell transplantation. Purchased from Charles River Labs.	Charles River Labs	(none)

Epifluorescence genotyping of GAD67-GFP, GFP, and DsRed mice

GAD67-GFP, green fluorescent protein (GFP), and discosoma red (DsRed) mice were genotyped by visual examination under a fluorescence

dissection microscope (Leica). GAD67-GFP epifluorescence could be detected up until approximately P5 by examining the brain through the intact skull and scalp up. The ubiquitous expression of GFP and DsRed could were observed by epifluorescence at all stages past E13.5.

Polymerase Chain Reaction genotyping of Bax and TrkB mice

Genomic DNA samples were obtained from 1-2 mm tail tissue samples using a DNeasy Blood & Tissue Kit (Qiagen). Polymerase chain reaction solutions (20 µl total volume) contained 1.5 µl DNA sample, 2 µl 10X buffer, 2.7 µl 25 mM $MgCl_2$, 0.4 µ l 200 µ M dNTP solution, 4 µ l Q solution, 0.1 Taq polymerase (5U/µl), primers, and autoclaved ddH_2O (Qiagen). Reactions were run on a thermal cycler (MJ Research). The cycle number, primer design, and annealing and polymerase extension temperatures for the PCR reactions have been described elsewhere (Knudson et al., 1995; Galvao et al., 2008).

Breeding of mice

To produce GAD67-GFP mice for the characterization of developmental cell death, heterozygous GAD67-GFP mice were bred to wild type C57Bl/6 mice. To produce *Bax*$^{-/-}$;GAD67-GFP mice for the characterization of cell death in the *Bax*$^{-/-}$ background, *Bax*$^{+/-}$ mice were bred to heterozygous GAD67-GFP mice to produce *Bax*$^{+/-}$;GAD67-GFP mice. *Bax*$^{+/-}$;GAD67-GFP mice were then maintained and bred to *Bax*$^{+/-}$ mice to produce *Bax*$^{-/-}$;GAD67-GFP and wild type GAD67-GFP littermates.

To produce GFP or DsRed embryonic donor tissue for cell transplantation, homozygous GFP or homozygous DsRed male mice were bred to wild type female CD-1 mice. Each morning, the female mice were examined for an intra-vaginal sperm plug. When a sperm plug was detected, the resultant embryonic mice were considered to be at stage E0.5. To produce *Bax*;GFP donor tissue for cell transplantation, $Bax^{+/-}$ mice and homozygous GFP mice were bred to produce $Bax^{+/-}$;GFP mice. $Bax^{+/-}$;GFP mice were then crossed together to produce *Bax*;GFP donor tissue for cell transplantation. Likewise, To produce *TrkB*;GFP donor tissue for cell transplantation, $TrkB^{+/-}$ mice and homozygous GFP mice were bred to produce $TrkB^{+/-}$;GFP mice. $TrkB^{+/-}$;GFP mice were then crossed together to produce *TrkB*;GFP donor tissue for cell transplantation.

Section 3: Transplantation of inhibitory neuron precursors

Tissue dissection

The ventricular and subventricular layers of the MGE were dissected from E13.5 to E14.5 donor embryos under a dissection microscope (Leica). Embryonic MGE explants were dissected in Liebovitz L-15 medium containing DNaseI (100 µg/ml). Care was taken to dissect the entire dorsal-ventral axis of the MGE, and to dissect MGE explants of equal size. For the transplantation of *Bax*;GFP and *TrkB*;GFP donor tissue, single MGE explants were directly loaded into glass capillary needles for injection. To identify the genotype of the donor embryo, extra tissue was harvested and processed for PCR genotyping as described above.

All other donor cell types were further dissociated from MGE explants into single cell suspensions. Briefly, MGE explants were pooled in 500 µl microentrifuge tubes (Eppendorf) and mechanically dissociated by repeated pipetting (approximately 20-30 times) through a 200 µl pipet tip. The dissociated cells were then concentrated by centrifugation (3 minutes, 1000 x g). The entire volume of L-15 supernatant was removed the microcentrifuge tube, and the tube was then covered in foil and placed on ice.

Cell injection procedure

Single MGE explants (for *Bax*;GFP and *TrkB*;GFP transplants) or concentrated cell suspensions (for transplants of all other cell types) were loaded into beveled glass capillary needles. Injection needles were positioned at an angle of 10-45 degrees from vertical in a stereotactic injection apparatus (Lois and Alvarez-Buylla, 1994), such that the axis of the needle was positioned normal to the surface of the recipient mouse's skull at each injection site. The densities of the concentrated cell suspensions were measured prior to the injection procedure, to determine the cellular density of the injected cell suspension (cell densities ranged from approximately 800-1150 cells/nl).

Recipient mice were anesthetized by hypothermia until pedal reflex was abolished and then positioned in a head mold. Cells were then injected into the neocortex at a depth of 650-700 µm (P0-P3 recipients) or 800-850 µm (P9-11 recipients) from the surface of the scalp. The surface coordinates of the needle tracks are listed below. Cell transplants for the transplant survival time-course

experiments were made into a single site in P0-P3 recipients: angle of needle = 40º; coordinates from the surface of the scalp directly above the bifurcation of the sagittal sinus = 2.0 mm lateral (L), 2.0 mm rostral (R), 0.5 mm deep (D; along axis of the angled needle)). For transplantation of cells into multiple sites in P0-P3 recipients, the injection coordinates were, using reference frame as above: site 1, angle of needle 30º; 0.9 mm L, 1.0 mm R, 0.6 mm D; site 2, angle 30º; 0.5 mm L, 2.5 mm R, 0.5 mm D; site 3, angle 30º; 0.3 mm L, 3.9 mm R, 1.2 mm D; site 4, angle 40º; 0.8 mm L, 2.5 mm R, 0.2 mm D; site 5, angle 40º; 2.0 L, 2.0 mm R, 0.5 mm D; site 6, angle 40º; 1.7 mm L, 3.0 mm R, 0.8 mm D; site 7, angle 45º; 3.1 mm L, 1.0 mm R, 0.6 mm D; site 8, angle 45º; 3.0 mm L, 2.3 mm R, 0.2 mm D. For transplantation of cells into the visual cortex of P0-P2 recipients, the injection coordinates were, using reference frame as above: site 1, angle of needle 20º; 0.9 mm L, 1.0 mm R, 0.7 mm D; site 2, angle of needle 40º; 0.9 mm L, 2.6 mm R, 0.2 mm D. For transplantation of cells into the visual cortex of P9-P11 recipients, the reference frame was set with respect to the center of the eye, because the sagittal sinus could not be visualized through the scalp. The surface coordinates of the injection tracks in P9-P11 recipients were: site 1, angle of needle 10º; 4.0 mm medial (M); 7.2 mm caudal (C); 5.0 mm deep (D); site 2, angle of needle 25º; 3.6 mm M, 7.0 mm C, 4.8 mm D.

Whole, single explants of *Bax*;GFP and *TrkB*;GFP MGE were injected in 80-200 nl volumes of Liebovitz's L-15 medium. For all other cell transplantation experiments, except for the injection of cells into the visual cortex (Chapter 4), injection volumes were adjusted according to the density of the loaded cell

suspension, and injected into a single site, or injected into eight sites (with equal volumes injected at each site). Injections into the recipient visual cortex were made by transplanting 100 nl of cell suspension to each site. Through the course of the transplantation procedure, recipient animals were examined for pedal reflex. If an animal exhibited a pedal reflex then it was anesthetized by hypothermia again, until the pedal reflex was abolished, then the transplantation procedure was resumed. Typically each recipient animal underwent one, or at most, two, rounds of anesthesia.

For some experiments in Chapter 3, a control, vehicle injection of L-15 + DNase was injected into the contralateral hemisphere. For control transplants into the visual cortex (Chapter 4) freeze-thawed dead cells were used. Briefly, freeze-thawed dead cells were prepared by placing concentrated MGE cell suspensions (prepared as described above) at -80º C for 10 minutes and rapidly thawing them at 40º C in a water bath. This process of freeze-thawing was repeated 4 times before the dead cells were loaded into the glass capillary needle.

After the injections were completed, transplant recipients were placed on a warm surface until they became active. The mice were then returned to their mothers until they were perfused or weaned.

Section 4: Optical imaging of intrinsic signals

Monocular deprivation

Monocular visual deprivation was produced by suturing shut the right eyelid, contralateral to the transplanted or control-treated visual cortex, according to procedures described previously (Gordon and Stryker, 1996). Mice were checked daily to make sure that the eyelids remained sealed for 4 days. Mice whose eyelids opened prematurely or whose corneas showed signs of damage were removed from the study. The MD procedure was performed on recipient and control animals at 17, 33-35 and 43-46 days after transplantation (Chapter 4, Figure 3A).

Surgical procedures for repeated transcranial optical imaging

The surgical preparation for repeated optical imaging of intrinsic signals closely followed procedures that are described in great detail elsewhere (Kalatsky and Stryker, 2003). Briefly, mice were anesthetized with 2-3% Isoflurane and a single intraperitoneal injection of Chlorprothixene (1 mg/kg), and then placed in a stereotaxic frame. Subcutaneous injections of Atropine (0.3 mg/kg) and Carprofan (5 mg/kg) were delivered to reduce airway secretions and to provide post-operative analgesia, respectively. The animal's temperature was maintained at 37.5°C using a heating pad under feedback control from a rectal thermoprobe. The skull over the left occipital cortex was exposed and covered with agarose and a coverslip. The eyes were protected with a thin coat of silicon oil.

Optical imaging was performed while a stable plane of anesthesia was maintained with 0.7-0.9% Isoflurane. The concentration of Isoflurane was

continually monitored using an Ohmeda 5250 respiratory gas monitor (Datex-Ohmeda).

At the conclusion of the first optical imaging session, the MD procedure was performed. Mice were returned to their home cages once they recovered normal awake behavior, no more than 2-3 hours after Isoflurane was discontinued. Four days later, the sutured eyelid was opened and the skull was exposed at the same location for the subsequent recording session. For some experiments, recordings were performed using the acute, transcranial preparation. At the end of the final imaging session, the rostro-caudal and medio-lateral boundaries of binocular primary visual cortex were marked with penetrations of fine tungsten wire coated in the dye DiI (Invitrogen). The dye penetrations were made based on the optical imaging maps of binocular visual cortex.

Optical imaging of eye-specific responses to visual stimulation

Optical images of the visual cortex were acquired directly through the skull, as previously described (Kalatsky and Stryker, 2003). Briefly, a Dalsa 1M30 CCD Camera (Dalsa), equipped with a 135 X 50 mm tandem lens (Nikon), gathered images of 610 nm light reflected by the visual cortex at 7.5 Hz and 512 x 512 resolution. The focal plane of the optics was positioned 550-650 μm beneath the surface of the brain. During the recording sessions, the visual stimulus consisted of a contrast-modulated stochastic noise movie (Niell and Stryker, 2008; Gandhi *et al*., 2008). The temporal spectrum of the movie was flat

with a sharp low-pass cutoff of 4 Hz. A smooth spatial low-pass cutoff was applied at 0.05 cyc/deg. The noise stimulus was displayed so that it fell within the limits of the mouse binocular visual field (- 5 to +15 deg azimuth). Finally, the noise movie was multiplied by a sinusoidally varying contrast (frequency = 0.1 Hz) and presented on a high refresh rate monitor that sat 25 cm from the animal's eyes. The movie was presented alternately to each eye in 5 min epochs; cumulatively, responses were recorded for 20-30 min for each eye.

Analysis of optical imaging data

A map of visual responses was extracted from the optical imaging data using Fourier analysis. For each pixel, the Fourier component corresponding to the frequency of contrast modulation in the visual stimulus (0.1 Hz) was computed as described before (Kalatsky and Stryker, 2003). The resultant response map was then smoothed with a 5 X 5 pixel uniform filter and cropped to isolate the region of the map corresponding to the visual cortex. The maximum amplitude in the smoothed, cropped region was taken to represent the overall strength of the response. The ocular dominance index (ODI) was then computed as (C-I)/(C+I), where C represents the response strength to contralateral eye stimulation and I represents the response strength to ipsilateral eye stimulation.

An ocular dominance shift was quantified for each animal as the difference between the ODI value measured before and the ODI value measured after MD. Fourier analysis was performed using custom written software (Kalatsky and

Stryker, 2003) and map amplitude calculations in custom-written Matlab routines (Mathworks).

Section 5: Preparation of histological specimens

Transcardial perfusion for immunohistochemistry and electron microscopy

Neonatal mice (P0-P5) were deeply anesthetized by hypothermia, while juvenile and adult mice were deeply anesthetized with tribromoethanol (Avertin). Once the pedal reflex was absent, mice were placed on a surgical tray and the abdominal and thoracic cavities were opened to expose the heart. The right atrium of the heart was cut and a perfusion needle was inserted into the left ventricle. Neonatal mice were perfused sequentially with 5 ml of saline and 5 ml of 4% paraformaldehyde (PFA) using a perfusion pump (Watson Marlow). All juvenile and adult mice, except for those that were later examined by electron microscopy, were perfused sequentially with 20 ml of saline and 20 ml of PFA. For electron microscopy, mice were perfused with 20 ml of saline and 20 ml of 4% PFA and 0.5% glutaraldehyde. Brains were removed from the skull and placed in a post-fixing solution of 4% PFA for 12-18 hours at 4º C. After post-fixing the brains were then transferred to a cryo-protectant solution of phosphate buffered saline (PBS), 25% sucrose, and 0.1% sodium azide; and stored at 4º C.

Preparation of brain sections

Brains were sectioned coronally using a sliding microtome (Microm). Cryo-protected brains were first blocked coronally between the cerebral

hemispheres and the cerebellum using a razor blade. The blocked brains were then placed on a cooling stage and completely frozen in PBS. Floating sections were then cut serially and collected in cell culture plates (Corning) containing PBS and 0.1% sodium azide, and stored at 4º C. Depending on the experiment, sections were cut at different thicknesses. For diaminobenzidine (DAB) immunostaining, sections were cut at a thickness of 80 µm. For fluorescence immunostaining of samples later analyzed by design-based stereology, sections were cut at 60 µm. All other sections were cut at a thickness of 50 µm.

Diaminobenzidine immunostaining

To measure the endogenous neocortical GAD67-GFP population size in GAD67-GFP and Bax;GAD67-GFP mice, brains were cut into 80 µm coronal sections and processed for DAB immunostaining. Coronal sections were collected and placed on an orbital shaker in a solution of PBS, 3% hydrogen peroxide, and 5% methanol for fifteen minutes at room temperature, to quench endogenous peroxidase activity. Sections were washed briefly in PBS and incubated on an orbital shaker in a blocking solution consisting of PBS, 2% bovine serum albumin, 8% normal goat serum, and 2% triton for 1 hour at 4º C. Sections were then transferred to a primary antibody solution containing blocking solution and chicken anti-GFP antibody (antibodies, and their dilutions for immunostaining are listed below in Table 2), and incubated on an orbital shaker overnight at 4º C. After incubation in primary antibody, the sections were washed in PBS and transferred to a secondary antibody solution containing

blocking solution and peroxidase-conjugated goat anti-chicken antibody. Sections were incubated in secondary antibody solution for 1.5 hours at room temperature and then washed in PBS. After the secondary antibody was washed off the sections, they were placed in a solution of 0.1 M phosphate buffer (PB) and 0.3% DAB. Sections were incubated in DAB solution for 20 minutes, after which 1% hydrogen peroxide (diluted in water) was added to the DAB solution to reach a concentration of 0.01%. The DAB signal was allowed to develop for approximately 5-30 minutes, until strong signal intensity was observed under an inverted microcscope (Leica). While the sections were being incubated in DAB solution and developed for DAB signal, they were kept protected from light. The DAB/hydrogen peroxide solution was washed from the sections in 0.1 M PB. Sections were then immediately mounted onto frosted glass microscope slides (Fisher), and cover-slipped in Aqua-Poly/Mount (Polysciences, Inc.) with a glass coverslip (Fisher). The sections were mounted as quickly as possible to prevent them from drying as they were mounted.

Immunostaining and tissue processing for electron microscopy

Fifty μm floating sections were freeze-thawed three times in methyl butane on dry ice. Sections were then washed in PB, blocked for 1 hour at room temperature in PB and 0.3% bovine serum albumin (BSA; Aurion), then transferred to a primary antibody solution of PB and chicken anti-GFP antibody. Sections were incubated in primary antibody solution on an orbital shaker for 72 hours at 4º C. Sections were then washed in PB and blocked in PB, 0.5% BSA,

and 0.1% fish gelatin (Aurion) for 1 hour at room temperature, then incubated for 24 hours at 4º C in blocking solution and 1:50 colloidal gold-conjugated anti-chicken secondary antibody (Aurion). Sections were next washed in PB containing 2% sodium acetate at room temperature. Silver enhancement was performed according to the manufacturer's instructions (Aurion), and sections were again washed in 2% sodium acetate. To stabilize the silver particles, the sections were immersed in 0.05% gold chlorine for 10 minutes at 4ºC and washed in sodium thiosulfate. Sections were then post-fixed in 2% glutaraldehyde for 30 minutes at room temperature. Sections were contrast enhanced in 1% osmium and 7% glucose then embedded in araldite for ultra-thin sectioning.

Fluorescence immunostaining

Fluorescence immunostaining was performed on 50 µ m and 60 µm sections. All fluorescence immunostains, except for cleaved caspase-3 immunostaining (which is described below), were performed as follows: Sections were incubated on an orbital shaker for 1 hour at room temperature in blocking solution, which contained PBS, 8% BSA, 2% normal goat serum, and 0.5% triton. Sections were then transferred to primary antibody solutions, which contained blocking solution and various antibodies that are described in Table 2. Primary antibody incubations were conducted overnight at 4º C on an orbital shaker. The sections were then washed in PBS and incubated in secondary antibody solution, containing PBS and the corresponding secondary antibodies (described in Table

2) for 1-2 hours at 37º C. Sections were washed in PBS, then immediately mounted onto frosted glass microscope slides (Fisher), and cover-slipped in Aqua-Poly/Mount (Polysciences, Inc.) with a glass coverslip (Fisher). The sections were mounted as quickly as possible to prevent them from drying as they were mounted.

Immunostaining for cleaved caspase-3 was performed using solutions identical to those described above. However, when double fluorescence immunostaining was performed for cleaved caspase-3 and GFP, the immunostaining procedure was modified as follows: The primary antibody incubation against cleaved caspase-3 was conducted overnight, as described. Then, the sections were washed in PBS. For 2 hours the sections were then incubated in a primary antibody solution against GFP, at 4º C. The anti-GFP primary antibody was washed off in PBS, then the sections were incubated in a solution that contained both secondary antibodies, as described above.

Table 2. Antibodies.

Antigen	Host	Dilution	Source
calbindin (CB)	rabbit	1:3000	SWANT
calretinin (CR)	rabbit	1:750	SWANT
cleaved caspase-3 (Csp3)	rabbit	1:500	Cell Signaling Technologies
discosoma red (DsRed)	rabbit	1:500	Clontech
green fluorescent protein (GFP)	chicken	1:500	Aves Labs
neuropeptide y (NPY)	rabbit	1:1250	ImmunoStar
parvalbumin (PV)	mouse	1:4000	Sigma
somatostatin-14 (SOM)	rabbit	1:300	Bachem
anti-chicken (peroxidase-conjugated)	goat	1:80	Sigma

anti-chicken (Alexa fluor 488-conjugated)	goat	1:500	Molecular Probes
anti-mouse (Alexa fluor 594-conjugated)	donkey	1:500	Molecular Probes
anti-rabbit (Alexa fluor 594-conjugated)	donkey	1:500	Molecular Probes

Section 6:

Imaging and quantification of histological specimens

Characterization of cleaved caspase-3 expression

The expression of cleaved caspase-3 in endogenous and transplanted cells was examined under a 20x objective (Olympus AX70 microscope). Unless otherwise noted, cleaved caspase-3 expression in endogenous cells (Chapter 3, Figures 1B, 1C, 5A, and 5B) was measured in every sixth coronal section from a series that spanned the entire rostro-caudal axis of the neocortex. The phenotypes of endogenous cells (GAD67-GFP$^+$ or GAD67-GFP$^-$) were recorded. Cells were examined at all medio-lateral levels and depths of the neocortex. Once raw cell counts were obtained, the total cell counts were calculated by scaling the raw counts by a factor of 6 (to account for the section sampling frequency). In order to compare total cleaved caspase-3 expression between wild type and GAD67-GFP animals (Chapter 3, Figure 1D) three coronal sections from similar rostro-caudal levels were examined at each postnatal age. The resultant raw cell counts were not scaled.

In order to characterize the spatial patterns of cleaved caspase-3 expression (Chapter 3, Figures 2 and 3), the neocortex was divided along three axes, and the spatial positions of cleaved caspase-3-labeled cells (counted as

described above) were noted. The neocortex was separated into three regions rostro-caudally, each of equal size along the rostro-caudal axis. Likewise, the neocortex was separated into thirds along the depth of the neocortex, with each third being of equal size along the superficial-deep axis. Also, the neocortex was separated into halves of equal area along the medio-lateral axis, such that the medial half contained dorso-medial cortex and the lateral half contained ventro-lateral cortex.

Cleaved caspse-3 expression was characterized in transplanted cells and endogenous cells of the recipient neocortex (Chapter 3, Figures 9B and 9C) by examining every second coronal section from a series that spanned the entire rostro-caudal axis of the neocortex. Again, cleaved caspase-3 expression was characterized across the entire extents of all three axes of the neocortex, and the raw cell counts were scaled by a factor of 2 to account for the section sampling frequency. As previously described (Alvarez-Dolado et al., 2006), essentially all transplanted MGE cells develop morphologies typical of migratory and mature inhibitory neurons; only those transplanted cells with neuronal morphologies were examined for cleaved caspase-3 expression, while all endogenous cells of the recipient neocortex were examined for cleaved caspase-3 expression.

Characterization of inhibitory neuron marker expression

The expression of inhibitory neuron markers in endogenous and transplanted cells was also examined under a 20x objective (Olympus AX70 microscope). Inhibitory neuron marker expression in endogenous GAD67-GFP

cells of P120 *Bax*$^{-/-}$;GAD67-GFP mice (Chapter 3, Figure 6B) was examined by studying every 24th coronal section (60 µm sections) from a series that spanned the entire rostro-caudal axis of the neocortex. In each section, GAD67-GFP cells were examined in a ~600 µm-wide strip that spanned all layers of neocortex. In each coronal section, this region of interest was positioned at the middle of the dorso-ventral axis of the neocortex. For each marker, a total of approximately 900 to 1200 GAD67-GFP cells were examined per group.

The expression of inhibitory neuron markers in cells transplanted from TrkB donors (Chapter 3, Figure 12C) was examined in every 6th 50 µm coronal section from a series that spanned the entire rostro-caudal axis of the neocortex. Only transplanted GFP^{+} cells with morphologies characteristic of inhibitory neurons were studied; as mentioned above, these cells comprised essentially all transplanted cells. Again, transplanted cells were examined in a ~600 µm-wide strip that spanned all layers of neocortex. In each coronal section, this region of interest was positioned at the middle of the dorso-ventral axis of the neocortex. For each marker, a total of approximately 1200 to 1500 GAD67-GFP cells were examined per group.

Finally, in transplant recipient mice studied for ocular dominance plasticity, inhibitory neuron marker expression in transplanted cells was examined within and immediately adjacent to the DiI-labeled boundaries of primary visual cortex. For each marker, three or four sections (Chapter 4, Figure 8D) at an interval of 600 µm between sections) were used for quantification. Two of the sampled sections included the binocular visual cortex, as indicated by the DiI injections,

while the remainder of the sections were immediately rostral or caudal to binocular visual cortex. A total of approximately 700-1000 transplanted cells were examined for each marker.

Measurements of inhibitory neuron population sizes

Depending on the relative size of the cellular population to be counted, one of two counting methods was applied. The choice of counting method was made to maximize the accuracy and efficiency of cell counting. Generally, design-based stereology was used to measure populations that contained approximately 4 x 10^4 cells or more. Cellular populations of smaller size were directly counted without using random systematic sampling.

All stereological measurements (Chapter 3, Figures 4, 5A, 11, 13, and 14B) were performed using StereoInvestigator software (MicroBrightField). In every sixth coronal section, the entire neocortex was delineated along all axes by tracing its contour under a 4x objective (Nikon microscope). For each stereological measurement, an optical fractionator and a 100x objective was used to estimate cell numbers. When transplanted cells were counted, only labeled cells with morphologies characteristic of inhibitory neurons were counted; these comprised essentially all cells that were sampled. Sampling parameters varied between different experiments, but they were always set to sample sufficient numbers of cells such that the Gundersen Coefficient of Error was less than 0.10 for each measurement. Guard zones were set at approximately 10% of the section thickness, and the height of the optical dissector was at least 25

μm in size. The Cavalieri principle was applied to measure the volume of the neocortex.

When the population of interest was relatively small (< 4 x 10^4 cells; Chapter 3, Figures 12B and 13; Chapter 3), cells were directly counted, because the random systematic sampling of cells would not examine a sufficient number of objects to yield accurate stereological estimates. In Figures 12B and 13 of Chapter 3, transplanted cells were counted directly in every sixth coronal section. Sections spanned the entire rostro-caudal extent of the neocortex, and cells were counted along the entire dorso-ventral axis and throughout all depths of the neocortex in each coronal section. Again, only transplanted cells with inhibitory neuron morphologies were counted. The raw cell counts were multiplied by a factor of six to account for the section sampling frequency. An Abercrombie correction factor was not applied, since the diameters of transplanted inhibitory neurons were small (approximately 10 μ m) relative to the thickness of the sections (50 μm).

In Chapter 4, transplanted cell counts were made in the visual cortex of recipient animals that underwent monocular deprivation and optical imaging experiments. Transplanted cells were counted within the DiI-labeled boundaries of binocular primary visual cortex using a 20x objective (Olympus AX70 microscope). Total cell counts were made by counting transplanted cell bodies in all cortical layers of three 50 μ m coronal sections: the first and third sections included the rostral and caudal limits of the DiI-labeled visual cortex, respectively, while the second sampled section was equidistant from the first and third

sections (approximately 400 µ m separated each section). Cell counts were normalized to the area of the DiI labeled visual cortex, but were not scaled by any sampling factor.

Imaging of specimens by electron microscopy

Semi-thin 1.5 µ m sections were selected for ultrathin sectioning using a 40x objective (Nikon Eclipse microscope). Semi-thin sections were re-embedded in araldite, and then cut into ultra-thin 70 nm sections using an ultramicrotome (Leica). Photomicrographs of ultra-thin sections were obtained under a Fei microscope (Tecnai-Spirit) using a Morada digital camera (Olympus Soft Imaging Systems).

Production of digital images

All digital images were obtained using a confocal microscope (Leica SP5). Images were adjusted for brightness and contrast with Adobe Photoshop CS (Adobe Systems Inc.). In Chapter 3, Figures 1A, 7B, 9A, and 14B represent flattened Z-series of confocal slices (1A, 6 slices, 0.8 µm per slice; 7B, 10 slices, 1 µm per slice; 9A, 7 slices, 1.1 µm per slice; 14B, 9 slices, 1.2 µm per slice), and Figure 6A represents single confocal slices of 0.8 µm thickness. In Chapter 4, Figures 8A and 8B represent flattened Z-series of confocal slices (8B and 8C, 12 slices, 1.5 µm per slice), and Figure 8C represents single confocal slices of 1 µm thickness.

Section 7: Statistical analyses

All statistical analyses were performed using Prism 4.0 (Graphpad). In Chapter 3, a Student's t-test was used to compare differences between two groups, and an ANOVA was used to compare differences between three or more groups. In Chapter 4, the Mann-Whitney test was used to assess the significance of the differences in ODI values between experimental groups. A Student's t-test was used to compare cell counts between groups.

Chapter 3

Intrinsically determined developmental cell death of neocortical inhibitory neurons

Section 1: Introduction

Our understanding of neocortical inhibitory neuron development has expanded dramatically in the last decade. It is hard to believe that little more than ten years ago, the embryonic origins of this population were largely unknown (Anderson et al., 1997). Much of the field's research has since focused on the proliferative domains that produce inhibitory neurons, the patterning events that generate the diversity of inhibitory neuron subtypes, and the migration of inhibitory neurons from their ventral origins into the neocortex (Marin and Rubenstein, 2003; Campbell 2003; Wonders and Anderson, 2006). What has been missing, however, is a careful examination of the developmental cell death of neocortical inhibitory neurons.

Most studies of developmental neuronal cell death have focused on regions such as the brainstem and spinal cord (Buss et al., 2006). Although evidence for the developmental cell death of rodent neocortical neurons exists (Heumann and Leuba 1983; Finlay and Slattery, 1983; Ferrer et al., 1992), a thorough characterization of inhibitory neuron cell death has been missing, in part, because the marker identities of inhibitory neurons are not apparent until after the presumed period of inhibitory neuron developmental cell death (Del Rio et al., 1992, Huang et al., 1999).

Inhibitory neuron cell death has, however, been carefully described in another structure of the cerebral cortex, the olfactory bulb. Throughout postnatal life, persistent neurogenesis produces new inhibitory neurons that migrate into the olfactory bulb and integrate into extant olfactory circuits (Lois and Alvarez-

Buylla 1994; Carleton et al., 2003). During characteristic timepoints in their development, newborn olfactory bulb (OB) inhibitory neurons begin to undergo Bax-dependent programmed cell death (Petreanu and Alvarez-Buylla, 2002; Kim et al., 2007). The persistent integration of new OB inhibitory neurons is believed to maintain the adaptiveness of olfactory circuits, and the structural integrity of the OB (Cecchi et al., 2001; Imayoshi et al., 2008).

Inhibitory neuron transplantation may mimic olfactory bulb neurogenesis, in that transplanted cells – like adult-born olfactory bulb cells – must migrate, differentiate and integrate into existing neural circuits (Wichterle et al., 1999; Alvarez-Dolado et al., 2006). Given the therapeutic potential of inhibitory neuron transplantation (Alvarez-Dolado et al., 2006, Richardson et al., 2008), there is substantial interest in understanding the developmental processes that regulate the integration of transplanted cells into host brain circuits. Our understanding of OB neurogenesis suggests that cell death may prominently regulate the normal development of inhibitory neurons, as well as their engraftment into the postnatal brain.

I have thus characterized the pattern and basic mechanism of inhibitory neuron cell death, both during normal neocortical development and in the context of neocortical inhibitory neuron transplantation. My experimental approach has allowed me to compare the timing and extent of developmental cell death across endogenous and heterochronically transplanted populations of inhibitory neurons. My results indicate that developmental cell death eliminates large fractions of inhibitory neurons during a characteristic period of neocortical

development. Likewise, developmental cell death also eliminates large fractions of transplanted inhibitory neurons too. Surprisingly, the basic features of endogenous inhibitory neuron cell death are strikingly conserved in heterochronically translanted populations: endogenous and transplanted cells die at similar rates and at similar cell-intrinsic developmental ages. These findings indicate that the developmental cell death of inhibitory neurons may be intrinsically determined and largely uninfluenced by competitive interactions for limited environmentally derived resources. Instead, it appears that the postnatal developmental cell death of inhibitory neurons may reflect the execution of a fate that is determined during embryonic periods.

Section 2: Results

Temporal features of cleaved caspase-3 expression in the developing postnatal neocortex

I first characterized the temporal and spatial patterns of postnatal cell death in native cortical inhibitory neurons. To identify the inhibitory population, I used GAD67-GFP mice, which express GFP in essentially all cortical GABAergic inhibitory neurons (Tamamaki et al., 2003). I then quantified the expression of the apoptotic marker, cleaved caspase-3, across a range of postnatal ages. I measured cleaved caspase-3 expression in every sixth coronal section throughout the entire neocortex, and recorded the positions of caspase^{+} cells along three axes (rostro-caudal, medio-lateral, and superficial-deep).

Apoptotic GAD67-GFP neurons were primarily observed during the first two postnatal weeks of life (Figure 1A). Cleaved caspase-3 expression increased steadily across the GAD67-GFP population during postnatal days 1 to 5 (P1 to P5), peaked around P7, and then declined thereafter until approximately P15 (Figure 1B). A majority (75%) of GAD67-GFP apoptosis was observed between P7 and P11. From P15 into adulthood, cleaved caspase-3 expression remained essentially undetectable in GAD67-GFP neurons.

The temporal profile of GAD67-GFP cell death was generally quite similar to that of the entire cortical population (Figure 1C). Across the entire cortical population (GAD67-GFP$^+$ and GAD67-GFP$^-$ cells), cleaved caspase-3 expression increased between P1 and P5, and also reached a maximum at P7. The decline in cleaved caspase-3 expression, however, occurred more gradually in the entire population than in GAD67-GFP cells, reaching minimal levels between P20 and P60.

Generally, cell death exhibited a greater temporal restriction in the GAD67-GFP population: whereas 75% of GAD67-GFP cleaved caspase-3 expression occurred between P7 and P11, 75% of the total cleaved caspase-3 expression occurred between P3 and P11 (Figures 1B and 1C). Across the range of timepoints examined (P0 to P120), GAD67-GFP neurons constituted 25% of the total number of cleaved caspase-3$^+$ cells in the neocortex.

To determine whether the GAD67-GFP allele somehow altered the general timing and extent of developmental cell death, I also compared the numbers of neocortical cleaved caspase-3-expressing cells between GAD67-

GFP and wild-type mice (Figure 1D). I did not observe a significant difference in the total amount of cleaved caspase-3 cells at any of the three timepoints studied (P3, P7, and P11), indicating that cell death is not significantly altered in the GAD67-GFP background.

Spatial distribution of cleaved caspase-3 expression in the developing postnatal neocortex

I also examined the spatial distribution of cleaved caspase-3^+ cells throughout the developing neocortex. I quantified caspase expression along three divisions of the rostro-caudal axis of the neocortex, two medio-lateral divisions, and three superficial-deep divisions. The larger temporal profile of GAD67-GFP cell death (Figure 1B) was conserved within each division of the neocortex (Figure 2). As for the distribution of GAD67-GFP cell death, there was an even distribution of cell death across the rostro-caudal (Figure 2A) and medio-lateral axes (Figure 2B). However, GAD67-GFP cell death was less pronounced in deeper regions of cortex, and more prevalent in superficial ones (Figure 2C). Figure 2.

The spatial distribution of total cleaved caspase-3^+ cells (GAD67-GFP^+ and GAD67-GFP^- cells; Figure 1C) was generally similar to that of GAD67-GFP caspase expression (Figure 3). First, the temporal profile of caspase expression was conserved across various sub-divisions of neocortex. Second, cleaved caspse-3 expression was distributed fairly evenly along the rostro-caudal axis, consistent with results from previous studies in other rodent species (Ferrer et al,

1992; Figure 3A). Unlike GAD67-GFP cell death, which was distributed evenly along the medio-lateral axis, total cell death was distributed more medially (Figure 3B). Additionally, total cell death was more prevalent in superficial regions of the neocortex, as was observed for GAD67-GFP cell death (Figure 3C).

Over forty percent of developing inhibitory neurons are eliminated from the neocortex during the period of early postnatal cell death

I next examined the extent of GAD67-GFP cell death by measuring the size of the neocortical GAD67-GFP population across early postnatal life. Because both cell size and cortical volume change over the course of development, I used an optical fractionator method to obtain unbiased stereological estimates of GAD67-GFP population size.

The GAD67-GFP population reached a maximum size at P5 (1.65 ± 0.03 x 10^6 cells), and then declined dramatically during the next two weeks, as predicted by the temporal profile of GAD67-GFP cleaved caspase-3 expression (Figure 1B). Between P5 and P20, the population decreased by nearly 40%, reaching a stable size of 1.01 ± 0.02 x 10^6 cells by P20 (Figure 4A). Despite ongoing cleaved caspase-3 expression between P0 and P5 (Figure 1B), the GAD67-GFP population increased by 22% between P0 and P5 (from 1.36 ± 0.05 x 10^6 cells to 1.65 ± 0.03 x 10^6 cells, respectively), indicating that some level of perinatal inhibitory neurogenesis and migration may contribute inhibitory neurons to the neocortex until at least P5 (Inta et al., 2008).

I also measured the volume of the neocortex and calculated the density of neocortical GAD67-GFP neurons during postnatal life. Between birth and adulthood (P120), the volume of the GAD67-GFP neocortex expanded 5.6-fold, from 13.7 ± 0.5 mm^3 to 77.3 ± 3.1 mm^3 (Figure 4B). Together, the dramatic expansion of cortical volume, and the decrease in GAD67-GFP cell number, decreased the neocortical density of GAD67-GFP neurons by 87%, from 10.0 ± 1.6 x 10^4 cells/mm^3 at P0 to 1.3 ± 0.1 x 10^4 cells/mm^3 at P120 (Figure 4C).

The developmental cell death of native neocortical inhibitory neurons requires the pro-apoptotic function of *Bax*

While GAD67-GFP cells decreased in number around the period when cleaved caspase-3 expression was elevated, it remained possible that non-apoptotic mechanisms of cell death also mediated the elimination GAD67-GFP cells. I thus measured cleaved caspase-3 expression and GAD67-GFP cell numbers in $Bax^{-/-}$;GAD67-GFP mice (Knudson et al., 1995). I chose to measure cleaved caspase-3 expression at P7, when the number of neocortical cleaved caspase-3^+ cells reached a maximum (Figure 1). In $Bax^{-/-}$;GAD67-GFP mice, cleaved caspase-3 expression was essentially absent at P7 (Figure 5A), indicating that *Bax* is required for caspase-3 activation in developing neocortical inhibitory neurons.

To determine the extent by which *Bax*-dependent apoptotic mechanisms were responsible for the elimination of GAD67-GFP cells, I used stereology to count the GAD67-GFP population in $Bax^{-/-}$;GAD67-GFP mice. In *Bax* mutants,

the cortical GAD67-GFP population reached a maximum of 1.47 ± 0.04 x 10^6 cells at P5 and remained nearly identical in size thereafter (Figure 5B). At P120, the cortical GAD67-GFP population was 49% larger in *Bax*$^{-/-}$;GAD67-GFP mice than in wild type GAD67-GFP littermates (1.52 ± 0.08 x 10^6 versus 1.02 ± 0.04 x 10^6 cells. Thus, the developmental cell death of GAD67-GFP cells occurs through a *Bax*-dependent mechanism of programmed cell death.

Bax-dependent developmental cell death occurs uniformly across neurochemically defined populations of neocortical inhibitory neuron

While nearly 40% of the entire GAD67-GFP population was eliminated by developmental cell death (Figure 4), it remained unclear if developmental cell death selectively eliminated particular sub-populations of inhibitory neurons, or if it instead occurred uniformly across the entire GAD67-GFP population. This remained difficult to examine because the neurochemical identities of inhibitory neurons are not necessarily obvious until after cell death has occurred. For example, while the neurochemical maturation of PV expression proceeds into the fourth postnatal week of mouse life (Cavanagh and Parnavelas, 1989; Cavanagh and Parnavelas, 1990; Del Rio et al., 1994; Alcantara et al., 1996; Huang et al., 1999; Chattopaadhyaya, 2004), essentially all developmental cell death is complete by the end of the second postnatal week (Figures 1B and 4A).

The *Bax*$^{-/-}$;GAD67-GFP neocortex, however, contains inhibitory neurons cells that were spared from normal developmental cell death (Figure 5B). Provided that these cells can express their neurochemical identities, then it is

possible to identify those cells that would have normally been eliminated by cell death. To propose a simple case, if, cell death was restricted to immature cells of type "A," and the mature neocortical population (after cell death) is composed of 50% cell type "A" and 50% cell type "B," then the population in mature *Bax*$^{-/-}$ mice is expected to contain more than 50% of type "A" and less than 50% of type "B." This of course assumes that marker expression proceeds normally in those cells that were rescued from cell death, and it also assumes that non-cell autonomous mechanisms do not maintain the neurochemical composition of the population at 50% "A" and 50% "B."

I thus examined the expression of neurochemical markers in P120 *Bax*$^{-/-}$;GAD67-GFP mice, and compared it to that in wild type GAD67-GFP littermates. I performed immunohistochemistry for CB, CR, NPY, PV, and SOM, and compared the expression of these markers between the GAD67-GFP populations (Figure 6A). In terms of inhibitory neuron neurochemical marker expression, there was no significant difference in the composition of the P120 *Bax*$^{-/-}$;GAD67-GFP and wild type neocortex (Figure 6B). Thus, *Bax*-dependent developmental cell death appears equally affect all neurochemically defined types of inhibitory neurons, instead of being restricted to a particular subtype.

The timing of inhibitory neuron cell death is determined by the intrinsic age of the developing cells, not the developmental state of the brain

As described above, the developmental cell death of inhibitory neurons was restricted mainly to the second postnatal week (Figure 1B). Likewise, cell

death throughout the entire neocortical population was also most pronounced during the same period (Figure 1C). This suggested that cell death could be dependent on the maturational state of the brain. For example, neocortical cell death could be timed by a pro-apoptotic signal that is temporally restricted to a certain period of brain development.

To examine whether the timing inhibitory neuron cell death is determined by the maturational state of the brain, I used inhibitory neuron transplantation to examine the temporal features of cell death in transplanted cells. I dissected the MGE from E13.5 to E14.5 GFP^+ donor mice and transplanted 5 x 10^5 cells directly into the cortex of postnatal day 3 to 4 (P3 to P4) wild type recipient mice (Figure 7A). As a control injection, I also injected transplant vehicle (cell culture medium) into the contralateral hemisphere. Given that mouse gestation ends around E19, the transplantation of E13.5 to E14.5 cells into P3 to P4 recipients yielded a temporal difference of approximately 8 to 10 days between the ages of the transplanted cells and their native counterparts.

Heterochronic transplantation at P3 to P4 introduced newborn interneuron precursors into an environment where endogenous developmental cell death was occurring (Figures 1B and 1C). If the developmental cell death of inhibitory neurons was directed by signals present in the brain, I expected that the transplanted cells would express cleaved caspase-3 synchronously with the native, endogenous cells of the recipient. I thus quantified cleaved caspase-3 expression in GFP^+ transplanted cells, and also measured cleaved caspase-3

expression in native cells of the transplanted hemisphere, and in native cells of the contralateral control hemisphere.

As previously described, nearly all transplanted MGE cells dispersed throughout the recipient cortex and expressed the morphological features of GABAergic interneurons within 15 days after transplantation (15 DAT; Figure 7B; Wichterle et al., 1999; Alvarez-Dolado et al., 2006). Additionally, by 15 DAT some transplanted interneurons had received and made axo-dendritic and axo-somatic synaptic contacts with host neurons (Figure 8).

In the transplanted population, cleaved caspase-3 expression increased three-fold between 7 DAT and 15 DAT, and reached a maximum at 15 DAT (Figures 9A and 9B). Transplant cell death then decreased between 15 DAT and 25 DAT, reaching nearly undetectable levels by 45 DAT (Figure 9B). Conversely, the highest level of programmed cell death in endogenous cells was observed at 7 DAT (Figure 9C). Between 7 DAT and 15 DAT, cleaved caspase-3 expression declined approximately 80% in endogenous cells, consistent with the observations described in Figure 4A. The introduction of transplanted cells did not significantly alter the level of endogenous cell death at any of the timepoints studied (Figure 9C). Thus, transplanted interneuron cell death and endogenous cell death were largely asynchronous, with transplant cell death occurring after the majority of endogenous cell death.

Curiously, transplant cell death appeared to lag endogenous cell death by the temporal difference in the intrinsic ages of the transplanted and host cells: transplanted interneurons died when they reached a cellular age similar to that of

endogenous interneurons during the peak of normal developmental cell death (Figures 9A and 1B). These findings suggest that the timing of interneuron cell death is cell-intrinsically determined, and independent from the developmental state of brain.

Survival time-course of transplanted inhibitory neuron precursors

I complemented the quantification of transplant caspase expression by measuring the survival time-course of transplanted interneuron precursors. I injected 5 x 10^4 E13.5-E14.5 GFP-labeled MGE cells to P3 wild type mice and then counted the number of transplanted cells present at 4, 10, 20, 30, and 60 DAT. As previously described (Alvarez-Dolado et al., 2006), at 3 DAT to 4 DAT, around 35% of the transplanted cells survived in the recipient cortex (Figure 10A). I believe this initial cell death is inherent to the transplantation strategy, as cellular damage is likely to occur during the surgical procedure. Because transplanted cells are not widely dispersed between 0 DAT and 4 DAT, is difficult to determine if this initial cell death occurs through apoptosis, necrosis, or other forms of cellular destruction (Alvarez-Dolado et al., 2006). I have thus focused on the dynamics of the transplanted population size from 4 DAT onwards.

Between 4 DAT and 60 DAT, transplanted cells decreased in number by 46% (Figure 10A). The majority of the cells present at 4 DAT were eliminated between 10 DAT and 30 DAT, consistent with our observation that transplant caspase expression reached a maximum around 15 DAT (Figure 9B). Around 30 DAT to 60 DAT, the population stabilized in number, with 18.5 ± 0.1% surviving.

The survival fraction at 60 DAT (~18%) was similar to that previously described at 90 DAT[17], suggesting that a stable population size was reached by 60 DAT.

The transplant survival time-course was consistent with the characterization of cleaved caspase-3 expression in transplanted cells: the most significant reduction in transplant cell numbers occurred between 10 and 20 DAT (Figure 10A), which was the same period when cleaved caspase-3 expression was at a maximum (Figure 9B). Again, as I had observed for the expression of cleaved caspase-3 by transplanted and endogenous cells, the declines in the transplanted and endogenous inhibitory neuron population sizes were offset by the temporal difference in the intrinsic ages of the two populations (Figure 10B). This strengthens the notion that the death of developing inhibitory neurons is tightly related to their intrinsic cellular age.

The survival of transplanted inhibitory neurons is affected by the cell autonomous function of *Bax*

While the decline in transplanted inhibitory neurons was concurrent with the period of transplant cleaved caspase-3 expression (Figures 9 and 10), it remained possible that caspase-independent mechanisms could have accounted for at least some of transplant cell death. I thus transplanted $Bax^{-/-;}$GFP cells from the E13.5 MGE to P2 wild type recipients and counted the transplanted cells at 60 DAT. The $Bax^{-/-}$ transplant population was 110% larger than the $Bax^{+/-}$ and wild type transplant populations (Figure, 11A). In other words, the transplant population was reduced 53% when *Bax* function was eliminated in the

transplanted cells. This fraction was roughly equal to the extent of *Bax*-dependent cell death observed in endogenous GAD67-GFP neurons (Figures 4 and 5), and also similar to the extent of transplant cell death that was observed between 4 and 60 DAT (Figure 10). Together these data suggest that, between 0 and 4 DAT, transplant cell death is unlikely to be caused by a *Bax*-dependent mechanism of developmental cell death, as I have previously suggested. Most notably, these transplantation findings demonstrate that the developmental cell death of inhibitory neurons requires the cell-autonomous function of *Bax*.

TrkB signaling does not affect the migration or survival of transplanted inhibitory neurons

Given that neurotrophin signaling regulates the developmental cell death of neurons in other brain regions (Yuan et al., 2003; Buss et al., 2006), I examined whether it also regulates the cell death of inhibitory neurons. I decided to focus on the function of TrkB, a cell surface receptor that mediates neurotrophin signaling by BDNF, NT-3, and NT-4/5. I selected TrkB because it is expressed by inhibitory neuron precursors (Polleux et al., 2002), and moreover, previous studies have identified increased postnatal apoptosis of cortical inhibitory neurons in *TrkB* mutants, although it is not clear whether this is due to non-cell autonomous or cell autonomous mechanisms (Alcantara et al., 1997). *TrkB* mutant mice die very in the first few postnatal days of life, making it difficult to characterize postnatal developmental cell death in this background (Alcantara et al., 1997).

To examine the role of cell autonomous TrkB signaling in postnatal inhibitory neuron cell death, I chose to transplant *TrkB*$^{-/-}$ inhibitory neuron precursors from the E13.5 MGE to P2 wild-type recipients. To determine whether *TrkB* is required for the survival of developing inhibitory neurons, I counted transplanted cells at 60 DAT. Within 30 DAT, transplanted *TrkB*$^{-/-}$ cells had dispersed throughout the recipient cortex and attained a spatial distribution roughly similar to that of transplanted wild type cells (Figure 12A). Surprisingly, at 60 DAT, the survival of transplanted *TrkB*$^{-/-}$ inhibitory neurons was also similar to that of transplanted wild type inhibitory neurons at 60 DAT (Figure 12B). Thus, neurotrophin signaling through TrkB does not appear to cell autonomously regulate the migration or cell death of inhibitory neurons.

I also characterized neurochemical marker expression in transplanted *TrkB*$^{-/-}$ inhibitory neurons. I performed immunohistochemistry for CB, CR, NPY, PV and SOM at 60 DAT, and compared the expression levels between wild type and *TrkB*$^{-/-}$ transplanted cells (Figure 12C). At 60 DAT, equal fractions of CB, CR, NPY and SOM expressing cells were present in wild type and *TrkB*$^{-/-}$ transplants (CB, Student's t-test, $P = 0.56$; CR, $P = 0.23$; NPY, $P = 0.99$; SOM, $P = 0.50$). However, while $20.6 \pm 1.3\%$ of wild type transplanted cells expressed PV, only $8.8 \pm 0.7\%$ of *TrkB*$^{-/-}$ cells expressed PV. It remains unclear whether the loss of TrkB function causes the death of PV cells, whether it interferes with the expression of PV, or if it reduces the embryonic pool of interneuron precursors that eventually expresses PV.

Transplanted inhibitory neuron cell death remains constant in magnitude over a range of transplant sizes

When 5 x 10^4 inhibitory neuron precursors were transplanted to the postnatal cortex, approximately 40% of the transplanted population was eliminated between 4 and 60 DAT (Figure 10). Thus, it appeared that transplant cell death was nearly equal in magnitude to that of endogenous inhibitory neuron cell death during normal development (46%; Figure 4). These findings hinted that interneuron cell death could be restricted in both its timing and in its magnitude, and independent from competition-based mechanisms that adjust cell death to the number of developing cells present in the tissue.

I therefore investigated whether transplant cell death remained constant in magnitude across different transplant sizes. I counted transplanted cells at 60 DAT, when the transplanted population was stable in number (Figures 9 and 10), and I varied the initial transplant size over 4 orders of magnitude, from 5 x 10^3 to 2 x 10^6 cells. Surprisingly, across initial transplant sizes of 5 x 10^3, 5 x 10^4, 5 x 10^5, and 10^6 cells, relatively similar fractions (20.8 ± 2.4%, 22.3 ± 1.4%, 17.8 ± 0.1% and 15.3 ± 0.1%, respectively) of transplanted cells survived in the recipient brain (Figure 13; ANOVA, P = 0.12).

When the initial transplant size was increased to 2 x 10^6 cells, the survival fraction declined to 8.2 ± 0.1%, yielding a transplanted population equal to that observed when 10^6 cells were transplanted (10^6 = 1.53 ± 0.01 x 10^5; 2 x 10^6 = 1.65 ± 0.18 x 10^5; Student's t-test, P = 0.58). It thus appears that the host cortex

can support a very large but limited number of transplanted cells, and this limit is reached when approximately 10^6 cells are transplanted.

It nonetheless was surprising that transplant cell death remained constant across transplant sizes smaller than 2 x 10^6 cells. If the recipient neocortex possessed a cellular capacity that was approached when around 10^6 cells to 2 x 10^6 cells were transplanted, then we would expect that greater fractions of the smaller transplant sizes (from 5 x 10^3 cells to 5 x 10^5 cells) would have survived. But curiously, over a range of transplant sizes up to 10^6 cells, transplant cell death remained remarkably constant. These findings suggested that interneuron cell death could be intrinsically determined, rather than following from a population-wide mechanism in which the extent of cell death is determined solely by interactions between the developing cells and their environment.

The neocortex can support remarkable numbers of additional inhibitory neurons, with no effect on the endogenous population size

Transplantation introduced significant numbers of exogenous inhibitory neurons to the recipient brain. For example, the transplantation of 10^6 cells added nearly 1.5 x 10^5 exogenous inhibitory neurons to the recipient cortex (Figure 13). Considering that each cortical hemisphere normally contains approximately 5 x 10^5 inhibitory neurons (Figure 4), transplanted cells could augment the cortical inhibitory neuron population by over 30%. However, it remained possible that transplanted inhibitory neurons competitively affected the

survival of endogenous inhibitory neurons, such that the endogenous population was reduced because transplanted cells were present.

To determine whether endogenous inhibitory neuron survival was affected by the presence of transplanted inhibitory neurons, I counted endogenous inhibitory neurons at 60 days after the transplantation of 10^6 inhibitory neuron precursors. I transplanted 10^6 E13.5-E14.5 DsRed-labeled MGE cells to the neocortex of GAD67-GFP recipients, and made a control injection (containing the cell culture medium vehicle) to the contralateral neocortex (Figure 14A). As expected from the results presented in Figure 13, I observed an average of approximately 1.7×10^5 DsRed cells in the transplanted cortical hemisphere at 60 DAT (Figure 14B). Nonetheless, the endogenous GAD67-GFP populations were of similar sizes in the transplanted and the contralateral, control hemispheres (control = $5.04 \pm 0.15 \times 10^5$; mean, transplanted = $4.81 \pm 0.12 \times 10^5$; Figure 14B). Thus, the recipient cortical hemisphere was able to support approximately 35% additional inhibitory neurons, with no significant effect on the endogenous population size.

Section 3: Discussion

I have characterized the developmental cell death of neocortical inhibitory neurons, and compared the timing and extent of developmental cell death between endogenous and heterochronically transplanted inhibitory neurons. My findings demonstrate that programmed cell death is a significant determinant of neocortical inhibitory neuron population size in the neocortex. Additionally, I

have determined that two features of inhibitory neuron cell death – its timing and its extent – are remarkably conserved when inhibitory neurons are transplanted to the developing neocortex. Together, these findings provide evidence that the developmental cell death of neocortical inhibitory neurons is determined through an intrinsic mechanism that is insensitive to competitive interactions.

I first described programmed cell death in the developing postnatal neocortex of the mouse. Programmed cell death of developing inhibitory neurons occurred primarily during the first two postnatal weeks of life, with 75% of programmed cell death occurring between P7 and P11. Considering that the majority of neocortical inhibitory neurons are produced between E12 and E16 (Wonders and Anderson, 2006; Wonders et al., 2008), these findings indicate that the programmed cell death is most prevalent in this population when these cells are between 10 and 20 days old. While the developmental cell death of inhibitory neurons was temporally restricted, it occurred widely throughout the neocortex, and at a higher frequency in more superficial areas.

During the period of neocortical inhibitory neuron cell death, the population declined in size by 40% (from approximately 1.6×10^6 cells at P5 to 1.0×10^6 cells at P20). Between birth and P20, twenty-five percent of neocortical cleaved caspase-3+ cells were inhibitory neurons. Considering that 25% of the total cleaved caspase-3 expression was associated with the net elimination of 6×10^5 inhibitory neurons, I estimate that, between P0 and P20, programmed cell death eliminates at least 2.5×10^6 cells (GAD67-GFP$^+$ and GAD67-GFP$^-$ together) from the neocortex. It should of course be noted, that this estimate assumes GAD67-

GFP was detected in dying inhibitory neurons with high sensitivity and specificity, and that the durations of cleaved caspase-3 expression and the rate of cellular elimination are fairly constant across all neocortical populations.

The developmental cell death of neocortical inhibitory neurons required the function of the pro-apoptotic molecule, Bax. In *Bax*$^{-/-}$;GAD67-GFP mice, the inhibitory neuron population remained similar in size to that of P5 wild-type mice, indicating that a *Bax*-dependent apoptotic mechanism is responsible for the elimination of essentially all developing neocortical inhibitory neurons. This finding is consistent with other studies that have demonstrated an essential role for *Bax* in the developmental cell death of olfactory bulb inhibitory neurons (Kim 2007). The composition of the neocortical inhibitory population, in terms of neurochemically defined inhibitory neuron sub-populations, was not altered in *Bax*$^{-/-}$;GAD67-GFP mice, indicating that *Bax*-dependent developmental cell death is not normally restricted to a particular subset of developing inhibitory neurons.

After I characterized the timing, extent and basic mechanism of inhibitory neuron cell death, I began using a heterochronic transplantation strategy to examine how developmental cell death of inhibitory neurons is regulated. I used transplant to introduce E13.5-E14.5 inhibitory neuron precursors into the P2-P3 neocortex. This manipulation created a temporal difference of 8 to 10 days between the ages of the host and the transplanted inhibitory neurons. Additionally, it increased the number of young inhibitory neurons in the neocortex at the onset of cell death, which allowed me to study whether the extent of cell death was responsive to the number of cells present in the tissue.

Transplanted inhibitory neurons died in the recipient neocortex, but remarkably, they did not die synchronously with endogenous inhibitory neurons. Instead, transplant cell death (as indicated by cleaved caspase-3 expression levels and the transplanted cell survival time-course) lagged endogenous inhibitory cell death by roughly 8-10 days, a period that was roughly equal to the difference between the intrinsic ages of the two populations. This finding indicates that 1) developmental cell death of inhibitory neurons is not dependent on the developmental age of the brain, and 2) the timing of inhibitory neuron cell death is determined by the intrinsic developmental age of the cells themselves. While this phenomenon has not been studied in the developing brain, it has been observed in the posterior necrotic zone (PNZ) of the chick embryo, where heterochronically transplanted cells from the PNZ undergo developmental cell death at timepoints related to their intrinsic cellular age (Saunders, 1966).

The extent of inhibitory neuron cell death also appears to be intrinsically defined. Over a range of transplant sizes (from 5 x 10^3 to 10^6 cells), a remarkably consistent fraction of transplanted inhibitory neurons died in the recipient neocortex. As expected, however, transplanted cells could not be added to the recipient neocortex without limit. When 2 x 10^6 cells were transplanted, the surviving population similar in size to that observed when 1 x 10^6 cells were transplanted, indicating that a limit is reached when approximately 10^6 cells are transplanted. Perhaps competitive mechanisms serve to restrict the inhibitory neuron population size when very large numbers of cells are transplanted. However, it remains curious that transplant cell death occurred

when less than 10^6 cells were transplanted. Considering that transplant cell death remained remarkably constant – and similar to the extent of endogenous cell death - when anywhere from 5 x 10^3 to 10^6 cells were transplanted, it could be that developing inhibitory neurons are intrinsically determined to undergo a fixed rate of developmental cell death.

While transplant cell death does not adjust in magnitude until 2 x 10^6 cells are transplanted, other compensatory mechanisms may be initiated at lower thresholds. For example, the neocortex may maintain synapse number or inhibitory tone, instead of regulating cell survival. This has been observed in motor neurons of the spinal cord, where the disruption of developmental cell death did not necessarily increase the innervation of target muscles (Sun et al., 2003).

Transplanted inhibitory neurons do not compete with endogenous inhibitory neurons in order to survive in the host neocortex: the addition of transplanted inhibitory neurons did not affect the population size of endogenous inhibitory neurons, or the overall level of programmed cell death in the recipient neocortex. This further supports the hypothesis that inhibitory neuron cell death occurs through a non-competitive mechanism. However, we must be careful in excluding a competitive mechanism, for endogenous cells may have a competitive advantage over heterochronically transplanted cells. Or, competition may occur only between cells of similar developmental ages, but not between younger transplanted cells and older, endogenous cells. These possibilities

could be examined by homochronic transplantation of inhibitory neuron precursors into the embryonic brain.

Remarkably, the neocortex can support 35% additional inhibitory neurons, with no effect on the native inhibitory population size. Thus, the normal endogenous inhibitory population size (after age P20, and outside of a transplantation scenario) does not reflect the actual cellular capacity of the neocortex. If a competitive process of cell death normally tuned the endogenous inhibitory population towards a cellular capacity (which was, in turn, an intrinsic property of the brain itself), then it is puzzling that normal cell death should reduce the population to a size below this number. Perhaps this 'inaccuracy' actually reflects an advantageous feature that has evolved in the brain, such that it maintains a capacity for additional cells. Towards this end, it would be interesting to examine transplant survival in *Bax*$^{-/-}$ recipients, where the cellular capacity of the neocortex may already be stretched. Moreover, it would also be interesting to examine the function of the neocortex, and the behavior phenotypes of mice, when the neocortical inhibitory population has been increased to a maximum size.

If the developmental cell death of inhibitory neurons is not guided by competitive interactions for environmentally derived features, then how might it occur? I suggest two potential mechanisms. In the first, inhibitory neuron cell death may be intrinsically determined within the developing inhibitory population via homotypic interactions between inhibitory neurons. In this scenario, the survival of developing inhibitory neurons could be governed by the availability of

inhibitory neuron-derived features, which are produced in proportion to the number of isochronic inhibitory neurons present in the tissue. Developing inhibitory neurons may produce these survival-regulating features during cell-intrinsically defined periods, and in turn, they may also be sensitive to these features during a cell-intrinsically defined period. This would account for the lack of competition between endogenous and heterochronically transplanted inhibitory neurons. To consider a simple scenario, if 2×10^3 cells are initially present, then a given cell must compete with 2×10^3 other cells for a feature that is produced by, and present in proportion to, 2×10^3 cells. Given the balance of competitors and the level of trophic support produced by those same competitors, each cell has a 40% likelihood of failing to receive adequate survival signals. Likewise, when the number of transplanted cells is increased 200-fold, then each cell must compete with a larger number of cells, but it also competes for a larger supply of trophic signal, so its likelihood of dying remains at 40%. In this scenario, developmental cell death is competitive, but its timing and extent are intrinsically determined within the inhibitory neuron population. One could speculate that this mechanism may select for an inhibitory population that is appropriately coupled together, such that the surviving inhibitory neurons are those that successfully formed electrical or chemical synapses with fellow inhibitory neurons, for example.

A population-intrinsic mechanism, like the one I have just mentioned, is distinct from that proposed by the neurotrophin hypothesis, which states that developing neurons compete for externally produced features. It should be noted

that the neurotrophin hypothesis was developed largely through studies of spinal cord and brainstem neurons, which are populations that form afferent and efferent connections with distant structures (Oppenheim, 1991). Inhibitory neurons, by contrast, project locally. Perhaps, for this reason, inhibitory neuron cell death could be governed by local, homotypic interactions.

Alternatively, inhibitory neuron cell death may be intrinsically determined within individual embryonic interneuron precursors themselves, in a manner that is not governed by competition. For example, a certain ratio of defective inhibitory neuron precursors may be produced stochastically in the ventral forebrain, and those defective cells may become unable to survive in the postnatal cortex. Thus, transplant and endogenous cell death would occur in roughly equal magnitude, and at similar cell-intrinsic ages. As for the molecular nature of these fatal flaws, the defective cells could, for example, be aneuploid. In the developing placenta, for example, developmental cell death occurs in large sub-populations of cells that express gross chromosomal aberrations (Weier, 2005). In the developing telencephalon, aneuploid neuroblasts are observed at a rather high rate as well (approximately 30%; Rehen et al., 2001). Curiously, aneuploid neurons are much less frequently observed in the adult brain (Rehen et al.; 2001). Perhaps this implies that aneuploid neocortical neurons are eliminated by cell death during development. In considering this literature, it should be noted, however, that the methods for detecting aneuploid mitotic and post-mitotic cells are different, and of different sensitivities. Nonetheless, it would be informative to examine the genetic composition of the inhibitory neuron

population before and after developmental cell death occurs. Perhaps karyotypic aberrations, or less dramatic genetic defects, would be present in the inhibitory population before cell death occurred. The *Bax*$^{-/-}$ mice may prove quite useful for these experiments, since they contain an excess population that was rescued from developmental cell death.

On the other hand, inhibitory neuron cell death may not follow from random, accidental events in the ventral telencephalon. Perhaps a sub-population of embryonic inhibitory neuron precursors is instead programmed to die when it reaches a particular cellular age. For example, some inhibitory neurons may be fated to die after completing a transient role in cortical development. Here, again, it may be useful to compare the genetic composition and gene expression profiles of inhibitory neurons before and after developmental cell death occurs, and to compare these properties in *Bax*$^{-/-}$ and wild type inhibitory neurons.

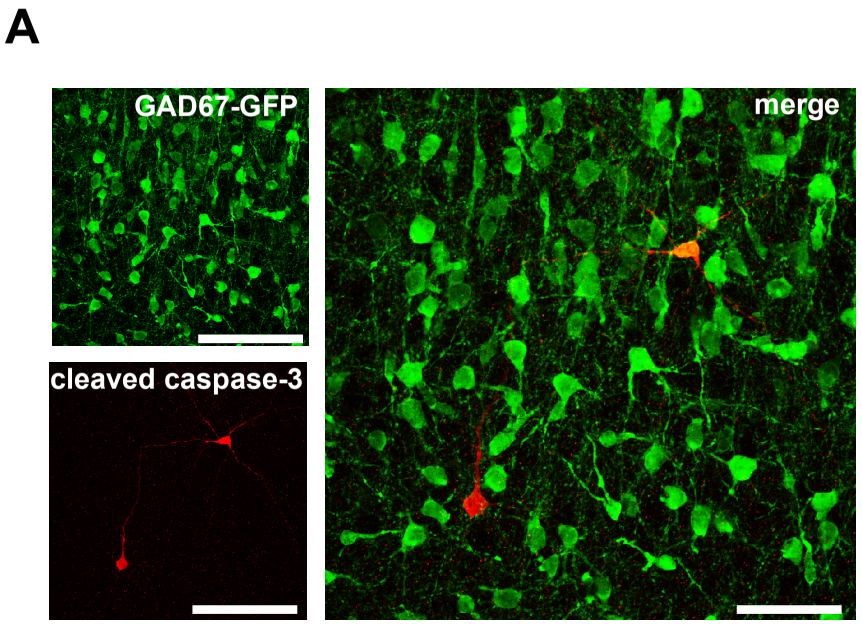
If the fates of inhibitory neuron precursors are determined in the ventral forebrain, and then expressed when these cells die some 10 to 20 days later, it would be particularly interesting to determine the nature of the cellular clock that establishes the timing of inhibitory neuron cell death. Moreover, it raises the intriguing question of how this fate is determined, and how the fleeting population contributes to cortical development and function. Perhaps short-lived inhibitory neurons serve as substrates for the migration of other cells, or they secrete guidance molecules that govern the migration of other neurons. Alternatively, this fleeting population may sculpt the proliferative activities of progenitor cells in

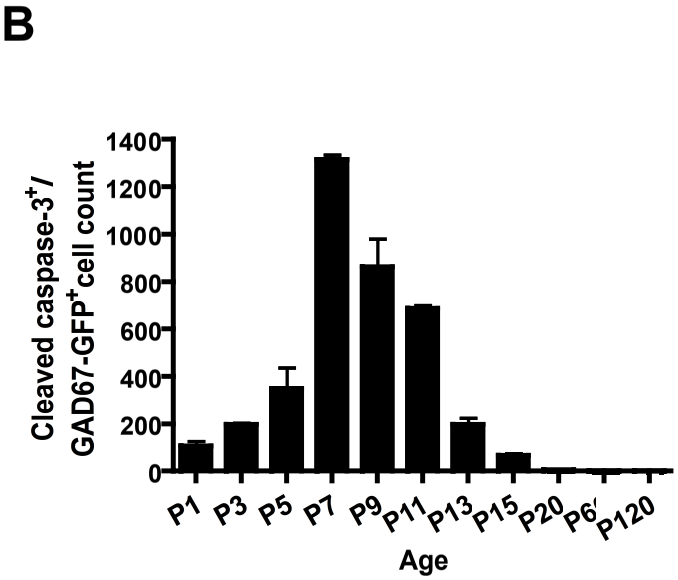
the dorsal telencephalon, as I have described in Chapter 1. Fleeting inhibitory neurons could also be designed to facilitate the formation of neural connections by other cells, or they could maintain the excitatory-inhibitory balance during early developmental periods, thereby guarding against seizures during epileptogenic periods.

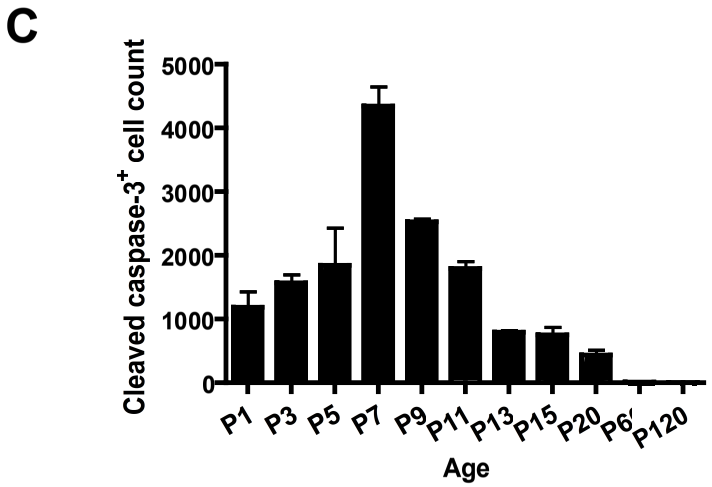
These experiments have contributed to our laboratory's development of inhibitory neuron transplantation strategies. While I have argued that many inhibitory neurons may be intrinsically determined to die in the neocortex, it is clear that others are destined to survive. I have determined when transplanted inhibitory neurons die, and I have determined the broad range over which the neocortical inhibitory population can be expanded. In the next chapter I will focus on those transplanted cells that survive in the recipient brain, and describe their impressive functional effects on the recipient neocortical circuitry.

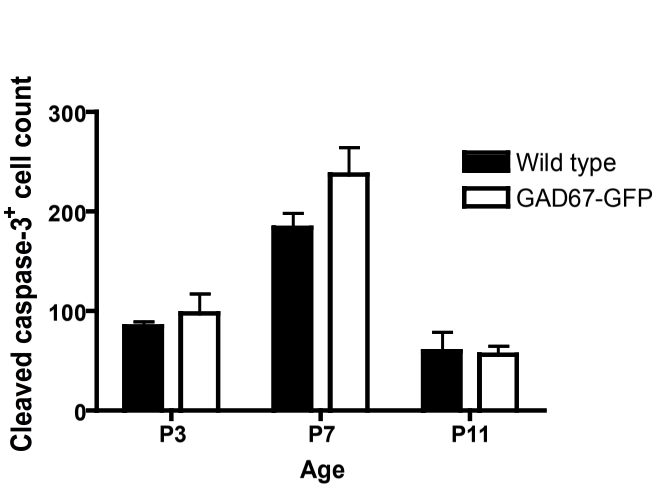
Figure 1. Quantification of cleaved caspase-3$^+$ cells in the postnatal neocortex.

(**A**) Fluorescence immunostaining for cleaved caspase-3 (red) and GAD67-GFP (green) in postnatal day 7 (P7) neocortex. Scale bar, 100 µm (left column) 50 µm (right column). (**B**) Temporal profile of cleaved caspase-3$^+$ cell counts in the neocortical GAD67-GFP population. Cleaved caspase-3$^+$ cells were most abundant at P7, but nearly undetectable by P15 (ANOVA, $P < 0.0001$). Seventy-five percent of the total cleaved caspase-3$^+$ GAD67-GFP cells were observed between P7 and P11. Error bars represent the standard error of the mean (s.e.m.). (**C**) Temporal profile of cleaved caspase-3$^+$ cells in the total neocortical population. Cleaved caspase-3$^+$ cells were also most abundant at P7, but declined in number through P20 (ANOVA, $P < 0.0001$). Seventy-five percent of the total cleaved caspase-3$^+$ cells were observed between P3 and P11. Error bars represent the s.e.m. (**D**) The temporal profile and extent of cleaved caspase-3 expression was similar between wild type and GAD67-GFP mice, indicating that developmental cell death was not significantly perturbed in the GAD67-GFP background (Student's t-test, $P = 0.57$ (P3); $P = 0.16$ (P7); $P = 0.89$ (P11). N = 3 per timepoint; error bars represent the s.e.m.


A
GAD67-GFP
cleaved caspase-3
merge


B
Cleaved caspase-3+/ GAD67-GFP+cell count
1400
1200
1000
800
600
400
200
0
P1 P3 P5 P7 P9 P11 P13 P15 P20 P6' P120
Age


C
Cleaved caspase-3+ cell count
5000
4000
3000
2000
1000
0
P1 P3 P5 P7 P9 P11 P13 P15 P20 P6' P120
Age


D
Cleaved caspase-3+ cell count
300
200
100
0
P3 P7 P11
Age
Wild type
GAD67-GFP

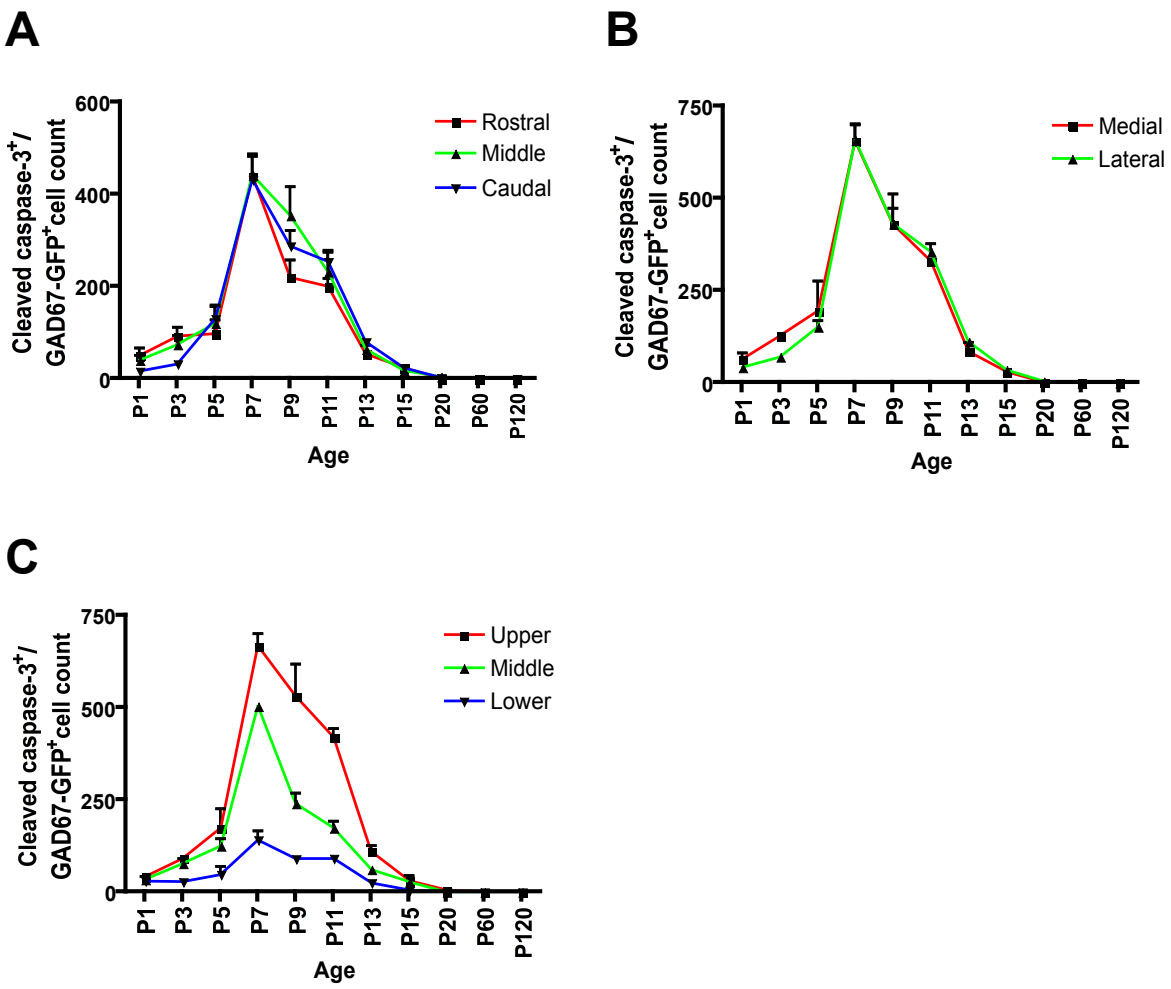


Figure 2. Spatial distribution of GAD67-GFP$^+$/cleaved caspase-3$^+$ cells in the postnatal neocortex.

Cleaved caspase-3$^+$ GAD67-GFP cells were evenly distributed throughout the rostro-caudal dimension of the neocortex (**A**) and the medio-lateral dimension (**B**). However, cleaved caspase-3$^+$ GAD67-GFP cells were more common in superficial regions of the cortex (**C**). N = 3 per timepoint; error bars represent the s.e.m.

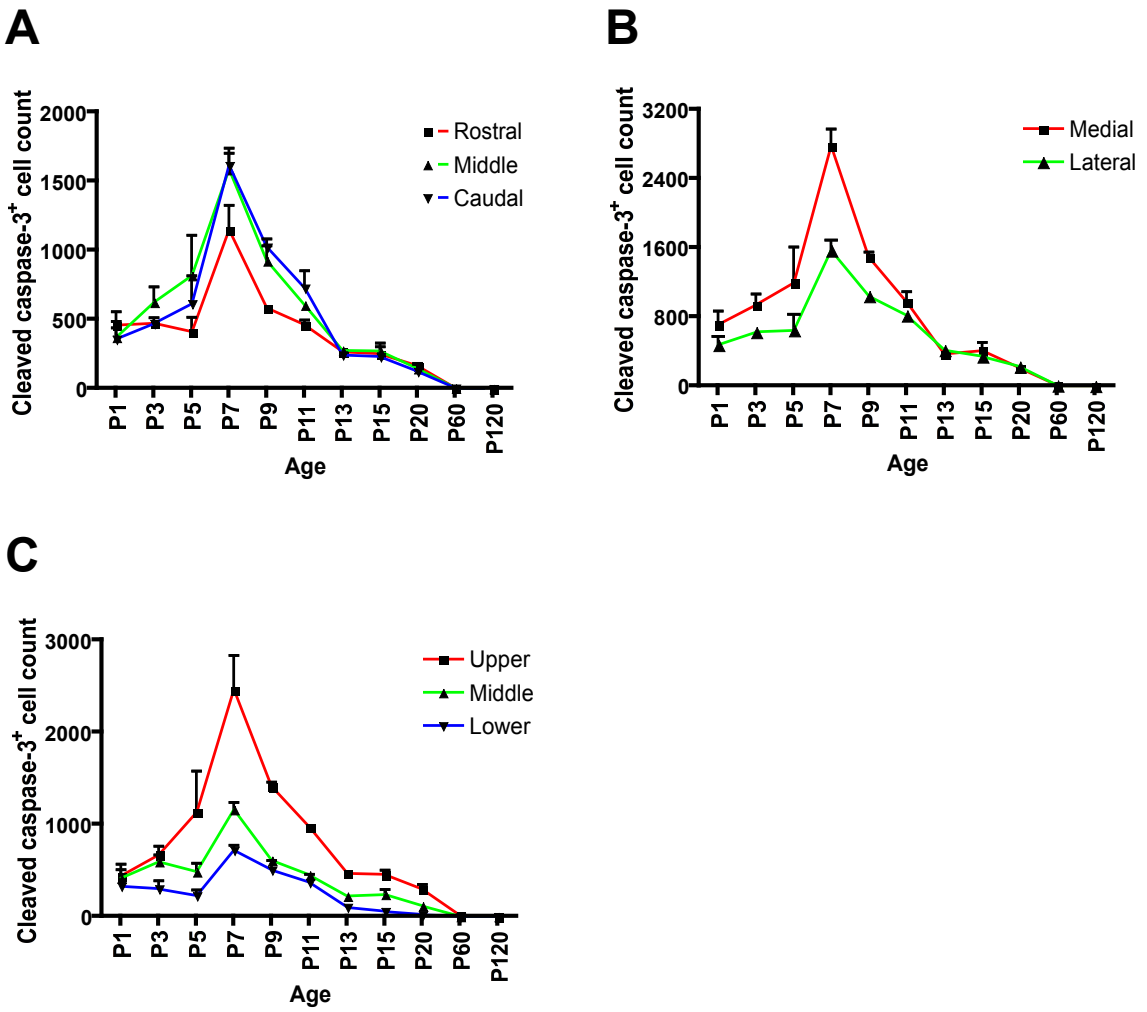


Figure 3. Spatial distribution of total (GAD67-GFP$^+$ and GAD67-GFP$^-$) cleaved caspase-3$^+$ cells in the postnatal neocortex.

Cleaved caspase-3$^+$ cells were evenly distributed throughout the rostro-caudal dimension of the neocortex (**A**). However, cleaved caspase-3$^+$ cells were more common medial (B) and superficial regions of the cortex (**C**). N = 3 per timepoint; error bars represent s.e.m.

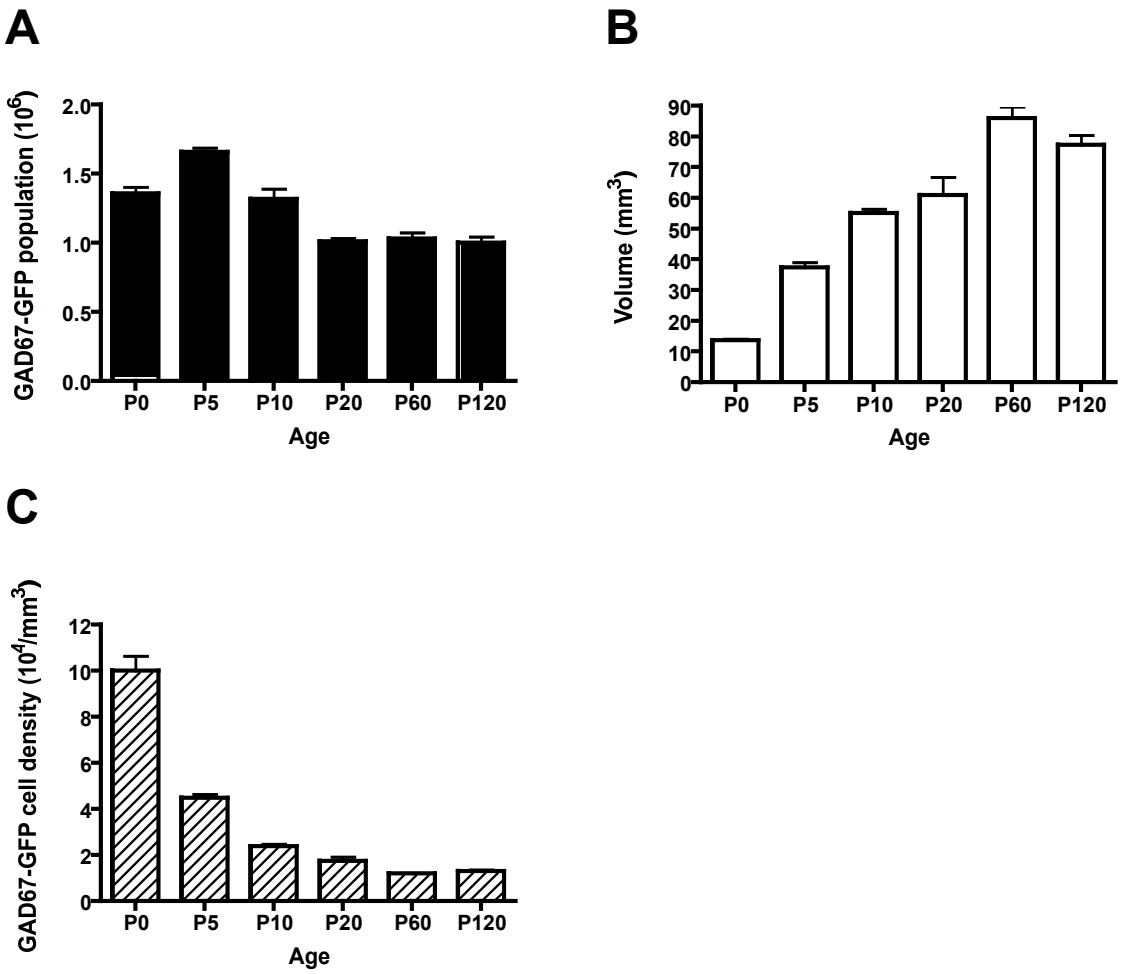


Figure 4. The neocortical GAD67-GFP population size decreases by 40% during early postnatal life.

(**A**) The neocortical GAD67-GFP population reaches a maximum around P5, and then declines by 40% between P5 and P20. Thereafter, the population remains stable in size until at least P120 (ANOVA, $P < 0.0001$). (**B**) The volume of the neocortex increases nearly 6-fold between P0 and P120 (ANOVA, $P < 0.0001$). (**C**) The density neocortical of GAD67-GFP neurons declines by 87% between P0 and P120 (ANOVA, $P < 0.0001$). N = 5 per timepoint; error bars represent s.e.m.

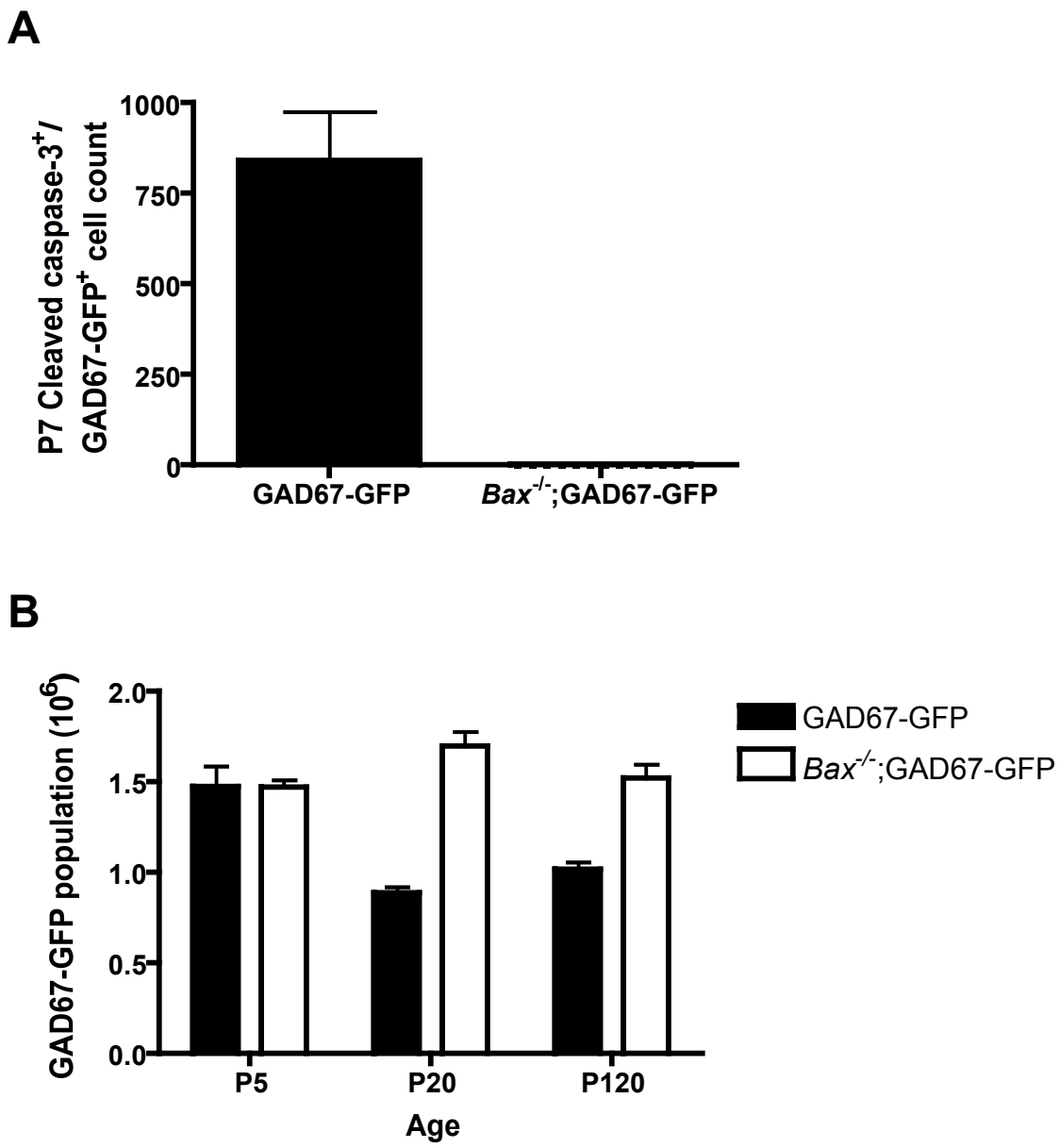


Figure 5. *Bax* is required for the developmental cell death of neocortical inhibitory neurons.

(**A**) Cleaved caspase-3 expression is essentially absent in the neocortex of P7 *Bax*$^{-/-}$;GAD67-GFP mice (Student's t-test, P = 0.0034). (**B**) The neocortical inhibitory population does not decline in *Bax*$^{-/-}$;GAD67-GFP mice, reaching a maximum size by P5 and remaining essentially stable in size thereafter (ANOVA, P = 0.12). N = 3 per timepoint; error bars represent s.e.m.

Figure 6. *Bax*-dependent developmental cell death is not restricted to a particular neurochemically defined sub-type of inhibitory neurons.

(A) Neurochemical marker expression in the P120 wild type and *Bax*$^{-/-}$;GAD67-GFP neocortex (CB = calbindin; CR = calretinin; NPY = neuropeptide y; PV = parvalbumin; SOM = somatostatin). (B) The composition of the neocortical inhibitory population, in terms of neurochemically defined inhibitory neuron sub-types, is not altered in the P120 *Bax*$^{-/-}$;GAD67-GFP neocortex, indicating that *Bax*-dependent cell death is not normally restricted to a particular neurochemically defined sub-type of cells (CB, Student's t-test, P = 0.51; ; CR, P = 0.48, NPY, P = 0.53, PV, P = 0.74, SOM, P = 0.18). N = 3 per timepoint; error bars represent s.e.m.

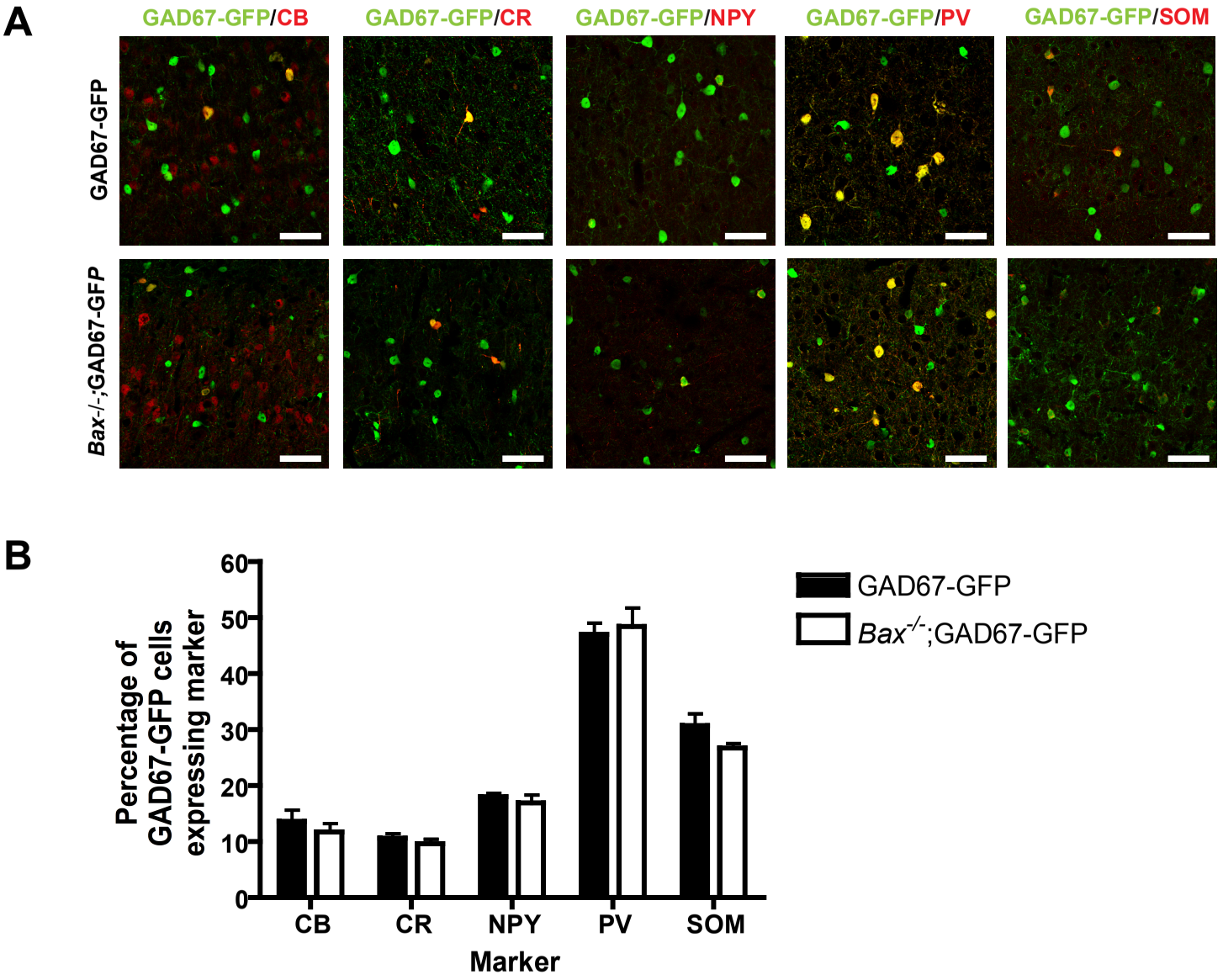

A
GAD67-GFP/CB
GAD67-GFP/CR
GAD67-GFP/NPY
GAD67-GFP/PV
GAD67-GFP/SOM
GAD67-GFP
Bax-/-;GAD67-GFP
B
Percentage of GAD67-GFP cells expressing marker
60
50
40
30
20
10
0
CB
CR
NPY
PV
SOM
Marker
GAD67-GFP
Bax-/-;GAD67-GFP

Figure 7. Heterochronically transplanted inhibitory neuron precursors disperse throughout the recipient neocortex and develop morphological characteristics of mature inhibitory neurons.

(**A**) Heterochronic transplantation of fluorescently labeled interneuron precursors into postnatal recipients. The medial ganglionic eminence was dissected from fluorescently labeled E13.5-E14.5 mice, triturated into a cell suspension, and injected into a single site (red) or eight sites (black and red) in the neonatal recipient neocortex. As described in the Methods, injections were made into a single site or multiple sites. (**B**) Transplanted GFP^+ MGE cells (initial transplant size, 5 x 10^5 cells) disperse throughout the recipient neocortex and develop the morphological properties of mature cortical interneurons by 15 days after transplantation (DAT). Scale bar, 80 μm.

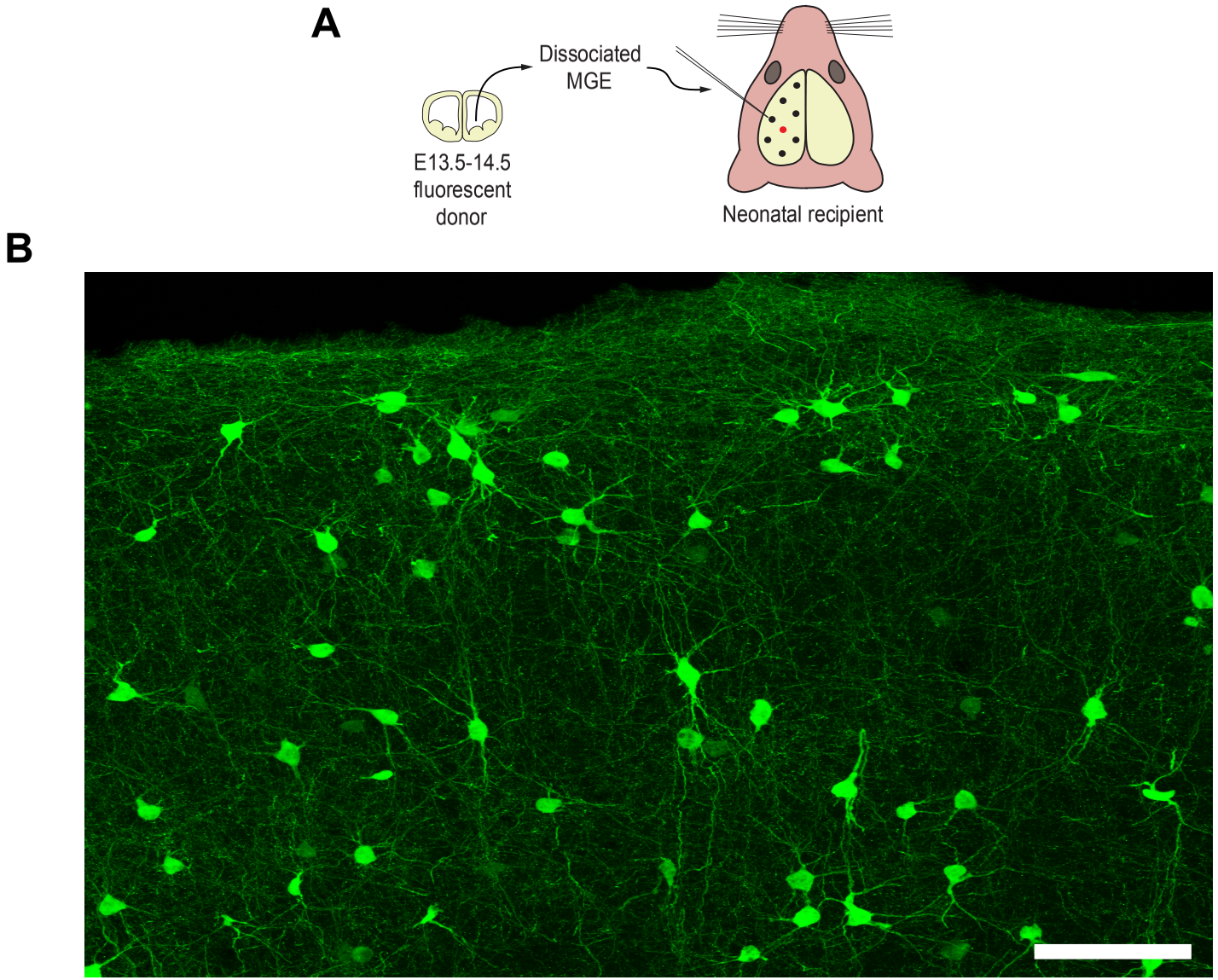

A
Dissociated
MGE
E13.5-14.5
fluorescent
donor
Neonatal recipient
B

Figure 8. Transplanted inhibitory neurons establish synaptic contacts with host neurons by 15 days after transplantation.

GFP+ transplanted inhibitory neurons are labeled by silver-enhanced black granules. (**A**) Low magnification electron micrograph of a transplanted, labeled inhibitory neuron. (**B**) Boxed area from (**A**), depicting axo-somatic synapses from an unlabeled cell onto the labeled cell body. (**C**) Labeled dendrite receiving a synaptic contact from an unlabeled terminal. (**D**) Low magnification electron micrograph of a labeled inhibitory neuron. (**E**) Boxed area (**D**), depicting axo-somatic synapses from the labeled cell onto an unlabeled cell body. (**F**) Labeled cell making a synaptic contact onto an unlabeled dendrite. Arrows indicate synaptic densities; Scale bars, 3μm (**A**), 1 μm (**D**), 500 μm (all others).

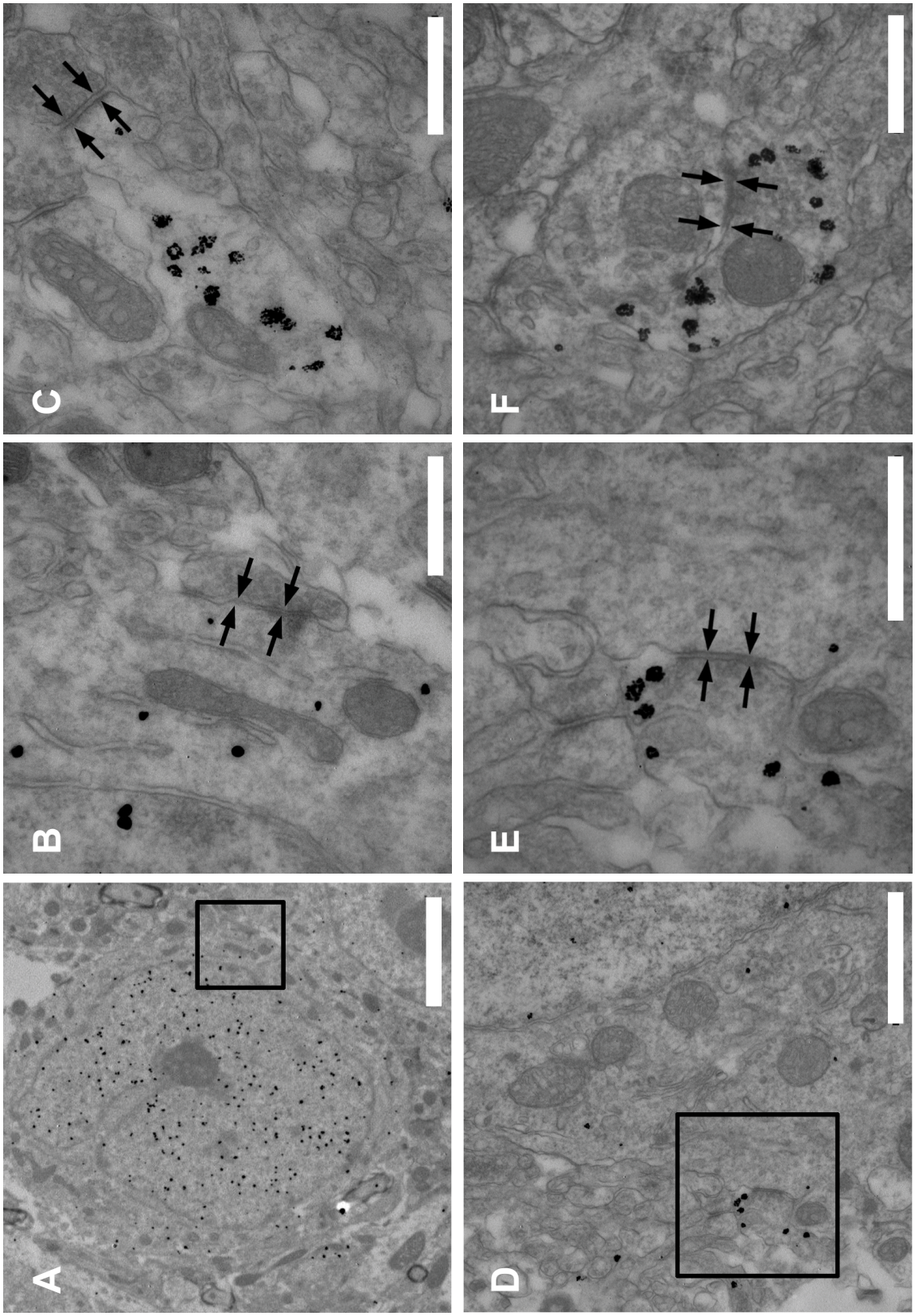
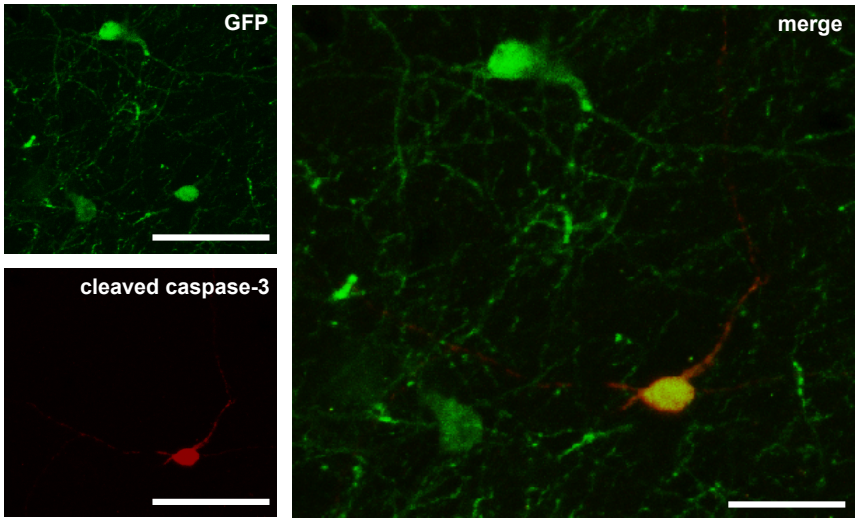

A
B
C
D
E
F

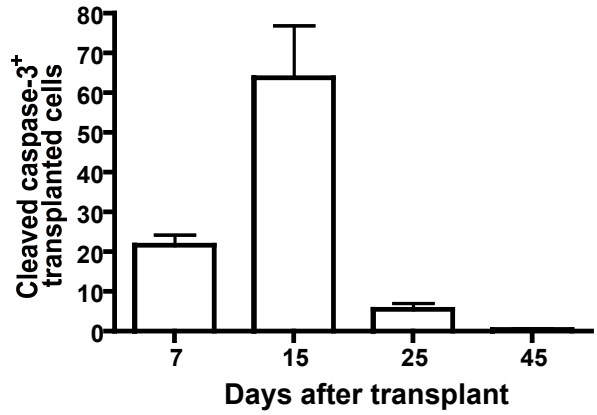
Figure 9. Quantification of cleaved caspase-3$^+$ transplanted inhibitory neurons.

(**A**) Fluorescence immunostaining for cleaved caspase-3 (red) and GFP (green) in transplanted inhibitory neurons at 15 days after transplantation (DAT). Scale bars, 50 µm (left) and 25 µm (right). (**B**) Cleaved caspase-3$^+$ transplanted cells peak in number at 15 DAT and declines to nearly undetectable numbers between 25 and 45 DAT (ANOVA, $P < 0.0001$). Peak numbers of cleaved caspase-3$^+$ transplanted cells are observed approximately 10 days after the peak of endogenous inhibitory neuron cell death (Figure 1B), when the transplanted population reaches same cellular age that endogenous inhibitory neurons had reached at the peak of endogenous cell death. (**C**) Quantificaiton of cleaved cleaved caspase-3$^+$ cells in the recipient neocortex after inhibitory neuron transplantation. Inhibitory neuron transplantation does not alter the extent of cell death in the neocortical hemisphere that receives the transplant, (Student's t-test, $P = 0.76$ (7 DAT), $P = 0.83$ (15 DAT), $P = 0.89$ (25 DAT), $P = 0.67$ (45 DAT)). N = 5 per timepoint; error bars represent the s.e.m.

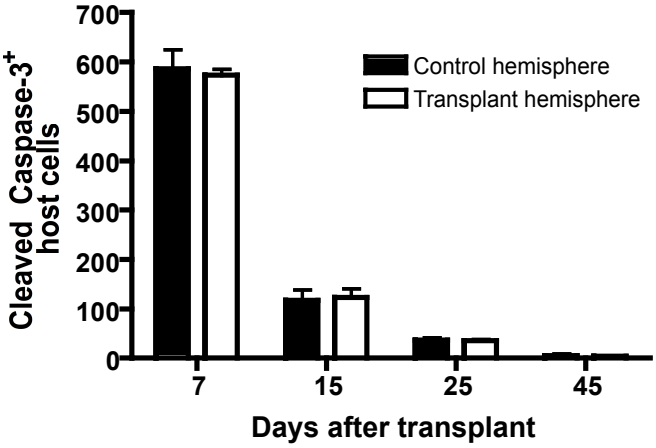
A


GFP
cleaved caspase-3
merge

B


Cleaved caspase-3+ transplanted cells
80
70
60
50
40
30
20
10
0
7
15
25
45
Days after transplant

C


Cleaved Caspase-3+ host cells
700
600
500
400
300
200
100
0
Control hemisphere
Transplant hemisphere
7
15
25
45
Days after transplant

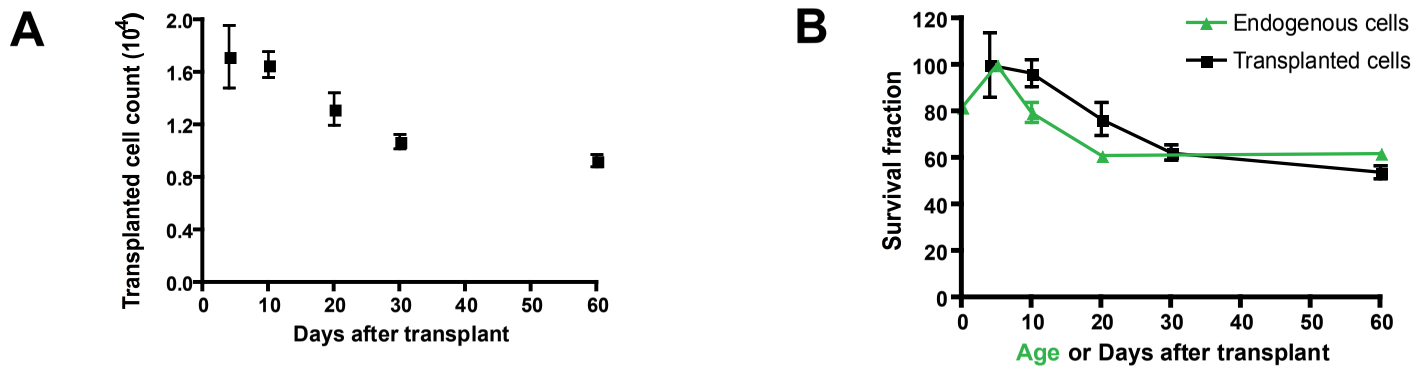


Figure 10. Nearly equal fractions of transplanted and endogenous inhibitory neurons undergo developmental cell death in the neocortex, at timepoints defined by their intrinsic cellular ages.

(**A**) Survival time-course of transplanted inhibitory neuron survival (initial transplant size, 5 x 10^4 cells). Between 4 and 60 days after transplantation (DAT), transplanted inhibitory neuronss decreased in number by 46% (ANOVA, P = 0.007). After 4 DAT, the majority of transplanted cells were eliminated between between 10 DAT and 30 DAT, consistent with the observation that caspase activation reached a maximum around 15 DAT (Figure 9B). Around 30 to 60 DAT, the population stabilized in number, with 18.5 ± 0.1% surviving. N = 6 (4 DAT); 5 (10 DAT); 8 (20 DAT); 9 (30 DAT); and 5 (60 DAT)); error bars represent the s.e.m. (**B**) Between 4 and 60 DAT, transplant cell death occurs at a rate that is similar to endogenous inhibitory neuron cell death (Figure 1B). The population sizes are represented as a percentage of their maximum size. Roughly equal fractions of transplanted and endogenous inhibitory neurons (40% and 46%, respectively) die during periods defined by their intrinsic cellular ages.

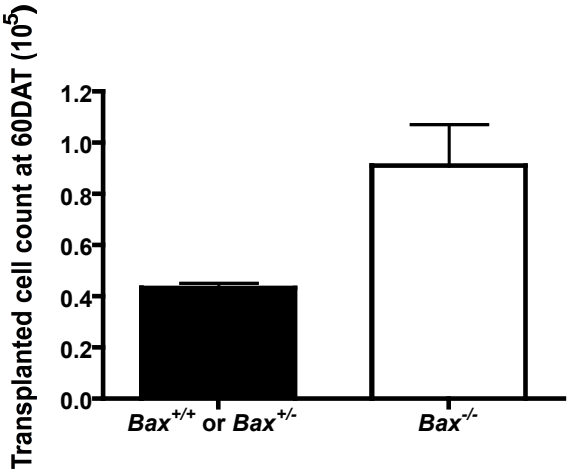


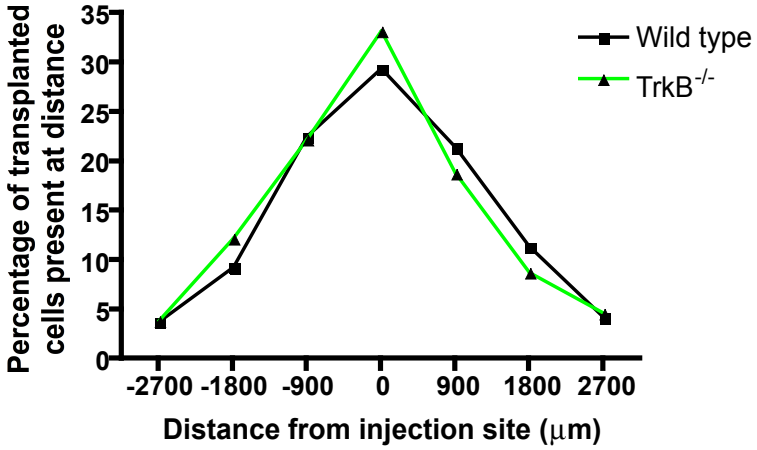
Figure 11. The developmental cell death of transplanted inhibitory neurons is regulated by the cell autonomous function of *Bax*

(**A**) Transplanted inhibitory neuron cell death is *Bax*-dependent. Greater numbers of transplanted $Bax^{-/-}$ inhibitory neurons survive in the recipient neocortex at 60 DAT, as compared to wild type and $Bax^{+/-}$ transplanted inhibitory neurons (Student's t-test, P = 0.03). N = 5 wild type and $Bax^{+/-}$ transplant recipients, and N = 6 $Bax^{-/-}$ transplant recipients; error bars represent the s.e.m.

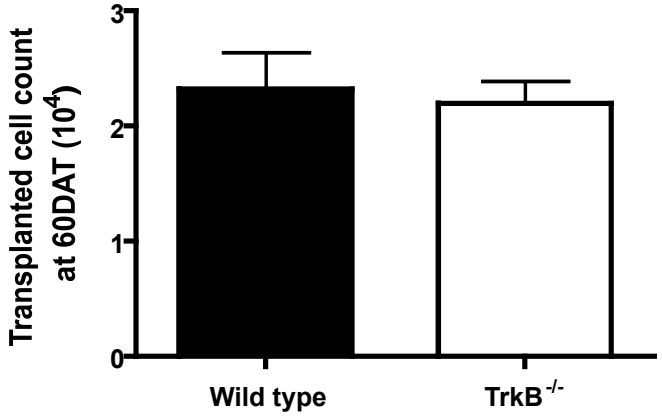
Figure 12. The developmental cell death of transplanted inhibitory neurons is not regulated by neurotrophin signaling through the TrkB receptor

(**A**) Transplanted *TrkB*$^{-/-}$ inhibitory neurons develop migrate throughout the wild-type recipient neocortex and develop a distributional pattern that is similar to that of wild type transplanted inhibitory neurons (30 DAT). N = 3 wild type transplant recipients; N = 4 *TrkB*$^{-/-}$ transplant recipients. (**B**) The loss of TrkB function does not affect the survival of transplanted inhibitory neurons at 60 DAT (P = 0.76). N = 5 per genotype; error bars represent the s.e.m. (**C**) Parvalbumin+ (PV) inhibitory neurons are reduced in *TrkB*$^{-/-}$ transplants (Student's t-test, P < 0.0001), while other neurochemically defined sub-populations are not reduced (CB = calbindin, P = 0.56; CR = calretinin, P = 0.23; NPY = neuropeptide y, P = 0.99; SOM = somatostatin, P = 0.50). N = 5 per genotype; error bars represent the s.e.m.

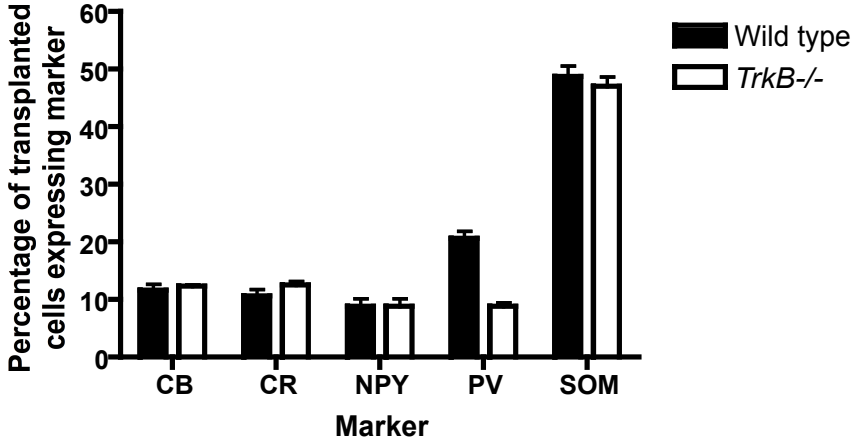
A


Percentage of transplanted cells present at distance
35
30
25
20
15
10
5
0
-2700 -1800 -900 0 900 1800 2700
Distance from injection site (μm)
Wild type
TrkB-/-

B


Transplanted cell count at 60DAT (10^4)
3
2
1
0
Wild type
TrkB-/-

C


Percentage of transplanted cells expressing marker
60
50
40
30
20
10
0
CB
CR
NPY
PV
SOM
Marker
Wild type
TrkB-/-

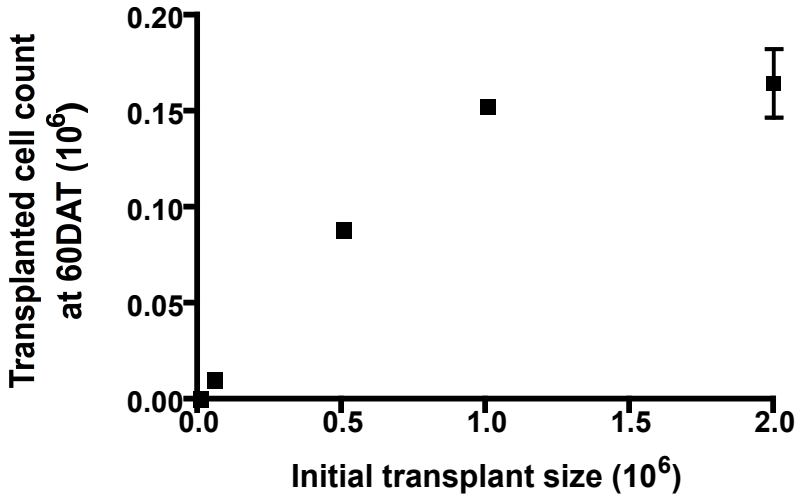


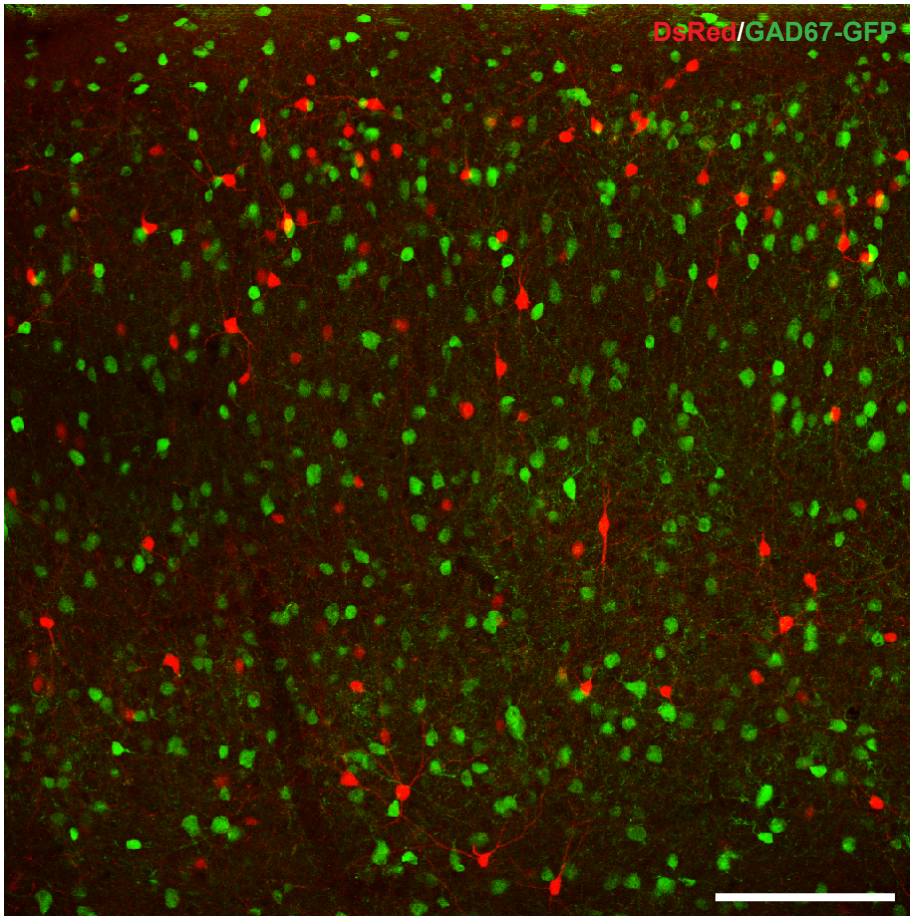
Figure 13. Transplanted inhibitory neuron cell death remains contant in magnitude over a range of transplant sizes.

Over initial transplant sizes ranging from 5 x 10^3 to 10^6 cells, the fraction of transplanted cells that survived at 60 DAT was relatively constant, ranging from 16-22% (ANOVA, P = 0.12). When an even larger number of inhibitory neurons was transplanted (initial transplant size = 2 x 10^6), a smaller fraction of transplanted cells survived in the host cortex (approximately 8%). N = 6 (initial transplant size = 5 x 10^3 cells), 7 (5 x 10^4), 3 (5 x 10^5), 3 (10^6), and 3 (2 x 10^6) per transplant size, 7, 3, 3 mice per transplant size, respectively). Error bars represent the s.e.m.

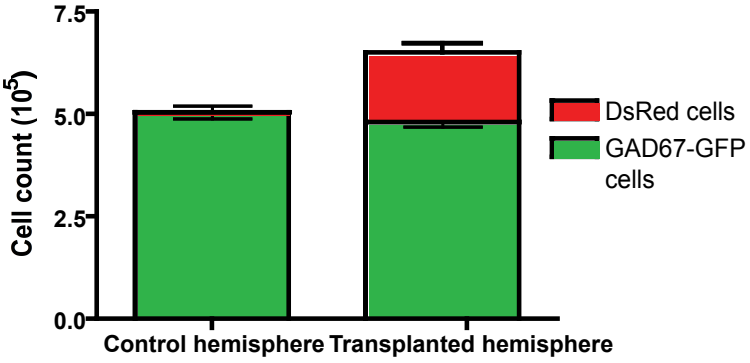
Figure 14. The neocortex can support 35% additional inhibitory neurons, with no effect on the endogenous inhibitory neuron population size.

(A) Fluorescence immunostaining for transplanted DsRed (red) inhibitory neurons and endogenous GAD67-GFP+ inhibitory neurons (green; 60 DAT). Scale bar, 150 μm. (B) The transplantation of 10^6 DsRed MGE cells added approximately 1.7 x 10^5 transplanted inhibitory neurons to the recipient neocortex (red). The neocortical hemisphere that received DsRed transplanted cells contained similar numbers of endogenous GAD67-GFP cells (Student's t-test, P = 0.28), indicating that the addition of transplanted inhibitory cells does not competitively affect the endogenous inhibitory population. N = 3 transplant recipients; error bars represent the s.e.m.

A


DsRed/GAD67-GFP

B


7.5
5.0
2.5
0.0
Cell count (10^5)
DsRed cells
GAD67-GFP cells
Control hemisphere
Transplanted hemisphere

Chapter 4

Cortical plasticity induced by inhibitory neuron transplantation

Section 1: Introduction

Brain plasticity is highest during specific periods of postnatal development. Such critical periods are essential to shaping sensory circuits, and they have been well studied in the neocortex of the mouse. In the mouse visual cortex, the critical period for cortical plasticity occurs around P22 to P32, reaching a peak of plasticity around P28 (Gordon and Stryker, 1996). If one eye is deprived of visual information during this critical period, a rapid rearrangement of neuronal responses occurs, such that neurons in the visual cortex become less responsive to the deprived eye, and more responsive to the non-deprived eye.

As reviewed in Chapter 1, critical period ocular dominance plasticity depends on the function of inhibitory GABAergic circuits (Hensch et al., 1998; Hensch, 2005). For example, the precocious enhancement of inhibitory transmission triggers early ocular dominance plasticity (Huang et al., 1999; Gordon and Stryker, 1999; Fagiolini and Hensch, 2000; Sugiyama et al., 2008), while the infusion of GABA receptor agonists restores ocular dominance plasticity in mutant mice that normally do not experience a critical period (Fagiolini and Hensch, 2000). It thus appears that a threshold level of GABAergic inhibition is required for the onset of ocular dominance plasticity. Once the critical period has occurred, plasticity cannot be restored by pharmacological agents that increase GABAergic inhibition (Fagiolini and Hensch, 2000). In fact, just a few manipulations have produced ocular dominance plasticity in rodents past the critical period, and these manipulations are ones that directly affect the structural arrangement of the cortex. For example, protetase infusion degrades peri-

neuronal nets and elicits ocular dominance plasticity in the adult visual cortex (Pizzorusso et al., 2002). Likewise, the genetic disruption of neurite-inhibiting neuron-myelin interactions also produces ocular dominance plasticity in adulthood (McGee et al., 2005). Thus, while the direct pharmacological augmentation of GABAergic signaling cannot induce ocular dominance plasticity after the critical period, ocular dominance plasticity is restored under conditions that favor cell structural rearrangements, possibly through the remodeling of existing GABAergic synapses, or by the formation of new ones (Sugiyama et al., 2008).

Given that transplanted inhibitory neuron precursors disperse throughout the host cortex (Wichterle et al., 1999), form new synapses with host neurons (Chapter 3), and alter inhibitory signaling in the host brain (Alvarez-Dolado et al., 2006), MGE cell transplantation may offer a cellular strategy for altering cortical plasticity in the recipient brain.

Here I present findings showing that transplanted inhibitory neuron precursors induce ocular dominance plasticity past the critical period. These results were produced through a close collaboration with, Sunil Gandhi, a post-doctoral researcher in the laboratory of Michael Stryker. Our experimental design was guided in part by the findings described in Chapter 3, which provided evidence that the timing of transplanted inhibitory neuron maturation is cell-intrinsically defined. We examined ocular dominance plasticity in mice that received transplants of embryonic MGE cells. Transplant recipients were examined when the transplanted population had reached a cell-intrinsic age that

was either equivalent to, or different from, the age of endogenous inhibitory neurons during the normal critical period. Surprisingly, transplanted inhibitory neurons induced ocular dominance plasticity when they reached the same age as endogenous inhibitory neurons during the normal critical period. Together our findings provide evidence that the critical period is regulated by the execution of a developmental program intrinsic to inhibitory neurons, and that transplanted inhibitory neurons retain the ability to execute this program in the recipient brain. These insights could prove valuable for therapeutic modification of brain plasticity in disease states, and for dissecting the normal mechanism by which the critical period is regulated.

Section 2: Results

Optical imaging of intrinsic signals in untreated GAD67-GFP mice at the peak of the critical period

During the normal critical period, MD causes a robust shift in neuronal responses in the binocular visual cortex away from the deprived eye and towards the non-deprived eye. We measured neuronal responses in the visual cortex using optical imaging of intrinsic signals, a rapid, repeated method for imaging neuronal activity through the intact skull (Figure 1B; Cang et al., 2005; Kaneko et al., 2008). Mice were presented with a visual stimulus designed to obtain unbiased and robust responses across the entire population of neurons in the binocular primary visual cortex (Niell and Stryker, 2008; Gandhi et al., 2008). Neuronal responses were gathered by reflecting light at wavelength of 610 nm

onto the brain and capturing the reflected 610 nm signal with a charge coupled device camera. To obtain a measure of the relative response to the two eyes, we took the peak value from the contralateral eye responses and the peak value from the ipsilateral eye responses and then computed an ocular dominance index (ODI). An ODI value of -1 represents responses dominated by ipsilateral eye stimulation, a value of 1 represents responses dominated by the contralateral eye, and a value of 0 represents equal responses to both eyes, or binocular responses.

We performed the majority of our experiments using GAD67-GFP mice. We originally chose the GAD67-GFP line because we wanted to perform simultaneous 2-photon *in vivo* imaging on transplanted DsRed^{+} inhibitory neurons and endogenous GAD67-GFP inhibitory neurons (Gandhi et al 2008). However, after we had completed several transplantation and optical imaging sessions, it became apparent that the intensity of the DsRed fluorescence emission was too low to visualize by 2-photon imaging. The 2-photon experiments were not continued, but we chose to complete the remaining intrinsic signal imaging experiments using the GAD67-GFP mice, given that we had gathered substantial data by the time we realized that we could not visualize DsRed cells *in vivo*.

We first used intrinsic imaging of optical signals to measure ocular dominance plasticity in untreated GAD67-GFP mice at the peak of the critical period. In P28 GAD67-GFP mice, the binocular visual cortex responded more strongly to the contralateral eye, yielding a mean ODI of approximately 0.23 ±

0.01 (mean ± s.d.; open black circles, Figure 2A). After four days of MD from P28 to P32, visual responses in the binocular visual cortex were shifted towards the ipsilateral eye and away from the contralateral eye, with a mean ODI value of 0.00 ± 0.03 (filled black circles, Figure 2A; Mann-Whitney, P = 0.03, U = 0). At these ages, the ODI values of GAD67-GFP mice were essentially identical to those of wild type C57Bl/6 mice (Cang et al., 2005). Thus, untreated GAD67-GFP mice exhibit normal ocular dominance plasticity during the critical period.

Transplantation of cells from the medial ganglionic eminence into P9-P11 recipients induces ocular dominance plasticity 33-35 days after transplantation

We first transplanted DsRed^{+} cells from the E13.5-E14.5 MGE into two sites flanking the primary visual cortex of P9-P11 GAD67-GFP recipient mice (Tamamaki et al., 2003) and then examined the effects of MD at 33-35 DAT (Figure 1A). At the time MD was initiated, recipient animals were P42-P46, more than two weeks past the peak of the normal critical period (Figure 3A). As described in Chapter 2, considerable cell death of transplanted MGE cells occurs in the first four weeks after transplantation. As a control for the effects of the transplantation procedure, and potential effects caused by the introduction of dead cells into the neocortex, we also transplanted freeze-thawed, dead E13.5-E14.5 MGE cells to a group of recipients.

Prior to MD, the binocular visual cortices of transplant recipients and age-matched, dead-cell control recipients responded more strongly to the

contralateral eye (Figure 3B; transplant recipient (open blue squares); mean ODI ± s.d. = 0.23 ± 0.02; dead-cell control recipient (open blue squares with red cross) mean ODI = 0.24 ± 0.01). Furthermore, the absolute magnitudes of cortical responses in transplant recipients and controls were similar (Figure 4). After MD, visual responses in transplant recipients were dramatically shifted towards the non-deprived eye (Figure 3B, closed blue squares; mean ODI = 0.04 ± 0.02). By contrast, visual responses were only modestly affected by MD in age-matched controls (Figure 3B, closed blue squares with red cross; mean ODI = 0.21 ± 0.02; Mann-Whitney test, P = 0.0012, U = 0). The lack of strong plasticity in the control animals was consistent with earlier descriptions of the decline of ocular dominance plasticity after the critical period. These findings demonstrated that MGE cell transplantation induced ocular dominance plasticity at P42-46, 15-20 days past the peak of the normal critical period.

To determine whether ocular dominance plasticity in the MGE transplant recipients was not an artifact of the recipient animals' genetic background (GAD67-GFP), we also made transplants to P10 wild-type recipients and examined the effects of MD 33-35 days later. Results in wild-type animals were similar to those in GAD67-GFP recipients, demonstrating that the effects of transplantation were not restricted to the recipient background (Figure 5, GAD67-GFP ODI = 0.05 ± 0.01; wild-type ODI = 0.04 ± 0.03; Mann-Whitney, P = 0.68, U = 30).

Transplanted cells from the medial ganglionic eminence do not induce ocular dominance plasticity 43-46 days after transplantation to P0-P2 recipients

Transplant recipients exhibited strong ocular dominance plasticity when they were P42-P46, 33-35 DAT. It remained unclear, however, whether the effects of transplantation were restricted in duration, restricted to certain recipient ages, or both. We examined these possibilities by transplanting E13.5-E14.5 $DsRed^{+}$ MGE cells to P0-P2 GAD67-GFP recipients and measuring the effects of MD at P43-46, 43-46 DAT (Figure 3A). Monocular deprivation at P43-P46 produced very little change in ocular dominance in animals transplanted at P0-P2 (Figure 3B, solid red diamonds; ODI= 0.16 ± 0.02) than in animals transplanted at P9-P11 (Figure 3B, solid blue squares; ODI = 0.04 ± 0.02; Mann-Whitney, P = 0.0018, U = 0).

Transplanted cell counts were nearly identical in these two recipient groups, suggesting that the number of transplanted cells did not account for the difference in cortical plasticity (P0-P2 recipient 43-46 DAT, mean ± s.e.m. = 183.8 ± 25.6 cells/mm^2; P9-P11 recipient 33-35 DAT, 182.9 ± 37.5 cells/mm^2; Student's t-test, p = 0.15). It thus appears that transplantation can induce ocular dominance plasticity in P9-P11 recipients when the transplanted cells are 33-35 days old, but not in P0-P2 recipients when the transplanted cells are 43-46 days old.

Transplanted cells from the medial ganglionic eminence induce ocular dominance plasticity 33-35 days after transplantation to P0-P2 recipients

In P42-P46 animals that received MGE cell transplants, ocular dominance plasticity was observed at 33-35 DAT, but not at 43-46 DAT. To determine whether transplant-induced plasticity was related to the age of the transplanted cells (33-35 DAT versus 43-46 DAT), or instead related to the age of the animal at the time of transplantation (P9-P11 versus P0-P2), we performed transplants to P0-P2 recipients and examined plasticity 33-35 days later (Figure 3A).

Thirty-three to thirty-five DAT to P0-P2 GAD67-GFP mice, MD had a strong effect on visual responses (Figue 3B, solid blue diamonds; ODI = 0.04 ± 0.02), compared to its much weaker effect at 43-46 DAT (Figure 3B; solid red squares; ODI= 0.16 ± 0.02; Mann-Whitney, P = 0.0025, U = 0). Thus, the effects of transplantation neither depended on the age of the recipient animal at the time of transplantation, nor on the age of the recipient animal at the induction of plasticity. Rather, the age of the transplanted cells seems to determine their effect on ocular dominance plasticity: transplantation induces plasticity when transplanted cells are 33-35 days old, and not when the cells are 43-46 days old.

Transplanted cells from the medial ganglionic eminence do not alter ocular dominance plasticity during the critical period

Transplanted MGE cells induced plasticity after the normal critical period, but it remained possible that transplantation may have disrupted the normal critical period of ocular dominance plasticity. To address this possibility, we

transplanted DsRed^{+} MGE cells to P11 GAD67-GFP recipients and examined the effects of MD 17 DAT (Figure 6). At this age, transplant recipients had reached the peak of the normal critical period. Monocular deprivation produced comparable effects in transplant recipients and untreated GAD67-GFP mice (17 DAT ODI = 0.04 ± 0.01; untreated P28 control ODI = 0.00 ± 0.01; Mann-Whitney, P = 0.057, U = 1), indicating that transplantation at P11 did not significantly alter ocular dominance plasticity during the normal critical period.

Transplantation induces cortical plasticity that is 77% as strong as that observed during the normal critical period

A majority of our optical imaging results were obtained by measuring visual responses in the same animal before and after monocular deprivation. This chronic procedure allowed us to quantify the effects of MD more precisely by calculating an ocular dominance shift (ODS), the difference between the ODIs before and after MD (Figure 7). Thirty-three to thirty-five days after transplantation into P9-11 recipients, MD produced an ODS that was more than five-fold larger than that observed in age-matched dead-cell control recipients, and more than double that produced 43-46 DAT into P0-2 recipients. Remarkably, the ODS observed 33-35 DAT into P9-11 recipients was 77% of that observed during the normal critical period in untreated animals. These findings indicate that transplantation had a potent effect on recipient ocular dominance plasticity at 33-35 DAT.

Transplanted cells from the medial ganglionic eminence populate the recipient visual cortex and develop into mature inhibitory neurons

At the end of the optical imaging experiments, electrodes coated with DiI were inserted to label the boundaries of binocular visual cortex, immediately after which the transplant recipients were perfused and prepared for histology. Transplanted cells were present in all layers of the recipient visual cortex (Figure 8A). We examined the morphologies of transplanted cells and observed that the vast majority (99.8 ± 0.2% of 3265 cells) had morphologies typical of mature inhibitory neurons (Figure 8B) while a very small fraction had glial morphologies (0.2 ± 0.2%). These observations demonstrate that transplanted inhibitory neuron precursors migrate into and survive in the visual cortex, consistent with results produced by transplantations into other brain regions (Wichterle et al., 1999; Alvarez-Dolado et al., 2006).

We characterized the molecular phenotypes of GFP^+ transplanted cells by immunostaining recipient brain sections (P9-11 wild type recipients, 33-35 DAT) for the calcium binding proteins calbindin (CB), calretinin (CR) and parvalbumin (PV); the neuropeptides somatostatin (SOM) and neuropeptide Y (NPY); as well as for GFP (Figure 8C). Nearly half of the transplanted cells studied (mean ± s.e.m., 49.5 ± 2.0%) expressed SOM, while approximately one-third expressed PV (33.9 ± 2.0%; Figure 8D). Smaller fractions of the transplanted neurons expressed CB (22.5 ± 1.2%), CR (17.5 ± 1.6%) and NPY (10.3 ± 1.7%). The distribution of inhibitory neuron subtypes within the transplanted population was similar to that observed when inhibitory neuron precursors are transplanted to

other regions of neonatal cortex (Chapter 2; Alvarez-Dolado 2006, Wonders et al., 2008). Together with the morphological phenotypes, the marker expression data indicated that the vast majority of transplanted MGE cells developed properties of mature inhibitory neurons.

Section 3: Discussion

We have discovered that transplanted MGE cells develop into mature inhibitory neurons in the visual cortex and induce potent ocular dominance plasticity outside the critical period. Thirty-three to thirty-five days after MGE cell transplantation into P9-P11 recipients, monocular deprivation produced a shift in visual responses comparable (77%) to that observed in untreated animals during the normal critical period. Dead-cell control recipients showed little plasticity in response to 4 days of MD at 33-35 DAT, which was similar to what has been described in untreated animals around this age (Gordon and Stryker, 1996; Taha et al., 2002). However, when transplanted cells reached 43-46 days of age, they did not induce strong ocular dominance plasticity. We examined ocular dominance plasticity during the normal critical period, at 17 DAT of MGE cells to P11 recipients, and determined that normal critical period plasticity remained intact, suggesting that transplantation did not merely delay normal ocular dominance plasticity.

A previous report found that the transplantation of cultured astrocytes enhanced ocular dominance plasticity (Muller and Best, 1989). In those experiments, transplanted cells were directly injected into binocular visual cortex,

where they remained in close proximity to the injection sites. By contrast, we transplanted MGE cells outside of the binocular visual cortex, and the transplanted cells then dispersed into this region. As mentioned, essentially every transplanted cell in the binocular visual cortex was identified as a mature inhibitory neuron, consistent with previous studies of MGE transplantation to other brain regions (Wichterle et al., 1999; Alvarez-Dolado et al., 2006). As some transplanted glial cells were also present at the injection sites in our experiments, we cannot completely exclude the possibility that transplanted glial cells enhance ocular dominance plasticity from outside the primary visual cortex.

The majority of mouse neocortical inhibitory neurons are born during E12-E16 (Wonders and Anderson, 2006; Wonders et al., 2008), which is approximately 30-35 days before critical period ocular dominance plasticity reaches a peak (Gordon and Stryker, 1996). Curiously, when we transplanted newborn inhibitory neuron precursors to P9-P11 or P0-P2 visual cortex, they induced potent ocular dominance plasticity 33-35 days later. Thus, transplanted inhibitory neurons induced ocular dominance plasticity when they reached a cellular age that was equivalent to that of endogenous inhibitory neurons at the peak of the normal critical period. This finding suggests that critical period plasticity could be regulated by the execution of a developmental program intrinsic to inhibitory neurons, and that transplanted inhibitory neurons maintain and execute this program in the recipient brain.

While GABA receptor agonists such as diazepam activate precocious ocular dominance plasticity before the critical period, they do not induce ocular

dominance plasticity after the critical period (Fagiolini and Hensch, 2000). Others have thus proposed that a threshold of inhibitory signaling sets off the critical period (Hensch et al., 1998; Fagiolini and Hensch, 2000), but once this threshold has been reached, ocular dominance plasticity is thereafter suppressed (Fagiolini and Hensch, 2000; Hensch, 2005). How, then, might transplanted inhibitory neurons induce ocular dominance plasticity after the critical period, when diazepam is no longer able to induce plasticity? Clearly transplanted inhibitory neurons must not be working simply by potentiating inhibition, as benzodiazepines do. Rather, it appears that, as transplanted inhibitory neurons emerge from an immature to mature state, they somehow induce ocular dominance plasticity (Sugiyama et al., 2008). Along these lines, two broad mechanisms are most consistent with the current literature (Hensch, et al., 1998; Huang et al., 1999; Fagiolini and Hensch, 2000; Pizzorusso et al., 2005; Sugiyama et al., 2008; Gandhi et al., 2008): 1) as transplanted inhibitory neurons mature, they may cell-autonomously introduce a dynamic, emerging state of new inhibition by forming perisomatic GABAergic efferents onto host neurons, or, 2) as transplanted inhibitory neurons mature, they may somehow unsettle the circuit mechanisms that terminate ocular dominance plasticity at the end of the critical period.

In discussing how the maturation of transplanted inhibitory neurons may induce ocular dominance plasticity, it is useful to first consider the maturation of a particular subset of endogenous inhibitory neurons, specifically, PV^+ cells. $Parvalbumin^+$ inhibitory neurons undergo a protracted neurochemical,

morphological, and electrophysiological maturation that suddenly accelerates during the critical period (Cavanagh and Parnavelas, 1989; Cavanagh and Parnavelas, 1990; Del Rio et al., 1994; Alcantara et al., 1996; Huang et al., 1999; Chattopaadhyaya, 2004). For example, around P24 to P28, PV^+ inhibitory neurons triple the densities of their perisomatic inputs onto excitatory neurons (Chattopadhyaya et al., 2004). Given that PV^+ cells are born around E12 to E16 (Wonders and Anderson, 2006; Wonders et al., 2008), they thus expand their peri-somatic innervation once they reach a cell-intrinsic age of approximately 30 to 35 days.

Notably, peri-somatic GABA signaling has been directly implicated in the regulation of ocular dominance plasticity (Fagiolini et al., 2004). Moreover, precocious ocular dominance plasticity can be induced by manipulations that accelerate the maturation of PV^+ inhibitory neurons (Huang et al., 1999; Sugiyama et al., 2008). Given that transplantation potently induces ocular dominance plasticity at 33-35 DAT, it is tempting to think that transplanted, PV^+ cells could induce ocular dominance plasticity by proceeding through a cell-intrinsic program for the late and rapid formation of peri-somatic innervation, as occurs in endogenous inhibitory neurons. In support of this interpretation, we determined that, at 33-35 DAT, a significant fraction of the transplanted population expressed PV (33%). Moreover, by ultrastructural analysis, we also determined that transplanted inhibitory neurons formed peri-somatic synapses, although we did not examine this feature at 33-35 DAT (Chapter 3).

To better elucidate whether the protracted maturation of PV^+ transplanted cells induces ocular dominance plasticity, it would be useful to characterize the morphological, neurochemical and electrophysiological maturation of transplanted inhibitory neurons. In particular, it would be informative to examine the maturational properties of transplanted PV^+ cells at 25 DAT (in addition to determining whether transplantation induces ocular dominance plasticity at 25 DAT). If transplantation did not induce ocular dominance plasticity at 25 DAT, and there was a significant difference in the PV^+ population between 25 DAT and 33-35 DAT, this would suggest that the maturation of transplant-derived peri-somatic inhibitory inputs could induce ocular dominance plasticity after the critical period. For further confirmation, one could also transplant a donor cell population that is enriched for or depleted of PV^+ inhibitory neuron precursors. To this end, the micro-dissection of donor tissue from sub-regions of the MGE may be useful (Fogarty et al., 2007; Wonders et al., 2008).

While I have speculated that transplantation-induced plasticity is mediated by the cell-intrinsic maturation of peri-somatic inhibition, it remains entirely possible that non-GABAergic mechanisms could instead be accountable for this effect. Thus, before testing for the particular role of PV^+ cells in transplantation-induced plasticity, it would be important to first examine whether transplanted cells mediate their effects through a GABAergic mechanism. To this end, it would be highly informative to transplant *Gad65*$^{-/-}$ inhibitory neuron precursors to wild-type recipients. As mentioned, *Gad65*$^{-/-}$ animals do not undergo normal critical period plasticity (Hensch et al., 1998). If the effects of transplantation

were mediated by the maturation of transplant-derived GABAergic inputs, then one would expect that *Gad65*$^{-/-}$ donor cells would not induce ocular dominance plasticity in transplant recipients.

If transplanted inhibitory neurons did not induce ocular dominance plasticity through a GABAergic mechanism, then how might they be working? A strong possibility is that transplanted MGE cells disrupt mechanisms that normally reduce the gross structural plasticity of neurons after the critical period. For example, it has been proposed that the structural plasticity of neurons, particularly that of PV^+ inhibitory neurons, is specifically restricted at the end of the critical period by the deposition of peri-neuronal nets (Piizzorusso et al., 2002; McGee et al., 2005). Notably, the degradation of peri-neuronal net components by chondroitinases (Pizzorusso et al., 2002), and the disruption of neurite-inhibiting Nogo receptor signaling (NgR; McGee et al., 2005), activates ocular dominance plasticity after the critical period. Perhaps transplanted MGE cells secrete proteases or otherwise disrupt the mechanisms that structurally restrict the structural rearrangements of endogenous inhibitory neurons, such that endogenous inhibitory neurons can again undergo cell structural changes that re-introduce a dynamic state to the morphologies of GABAergic neurons. To this end, it may be interesting to transplant MGE cells that cannot produce chondroitinases, or to infuse protease inhibitors after transplantation. Given that peri-neuronal nets are highly targeted to PV+ inhibitory neurons (McGee et al., 2005), and that peri-neuronal nets become abundant around the end of the critical period (Pizzorusso et al., 2002), it would also interesting to examine

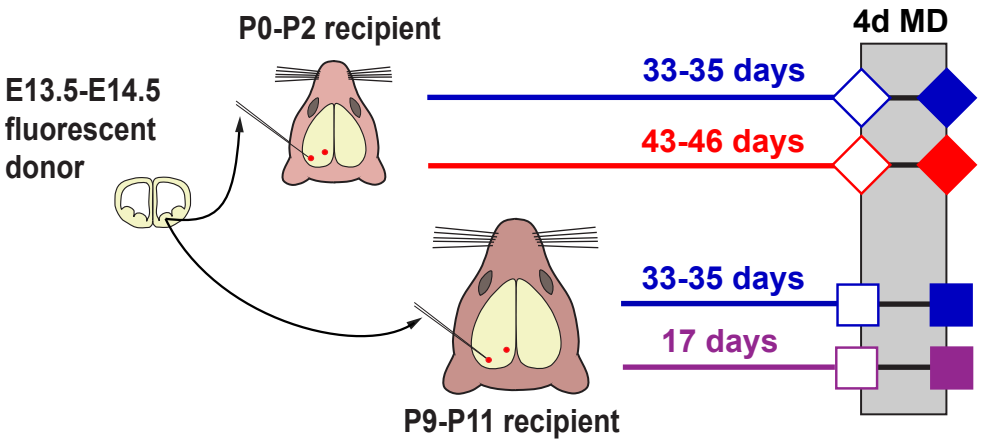
whether peri-neuronal nets are formed on transplanted inhibitory neurons. For example, peri-neuronal nets may be deposited on transplanted cells between 33-35 DAT and 43-46 DAT, leading to the cessation of transplant-induced plasticity. Finally, the ubiquitous disruption of NgR extends ocular dominance plasticity into adulthood (McGee et al., 2005). It is unknown, however, whether NgR signaling terminates plasticity through a mechanism that directly involves the inhibitory neuron population. It would thus be quite interesting to determine whether transplanted *NgR*$^{-/-}$ cells induce prolonged ocular dominance plasticity well past 33-35 DAT.

Inhibitory neuron transplantation may provide a means for inducing cortical plasticity with temporal and spatial precision. One could imagine trying to activate therapeutic circuit rearrangements by targeting inhibitory neurons to specific cortical regions, and then inducing plasticity by initiating relevant sensory and behavioral manipulations during a specific temporal window. This strategy could serve important therapeutic purposes, particularly if transplanted inhibitory neurons are able to induce cortical plasticity after transplantation to adult recipients, and across various cortical areas. In the visual cortex, for example, transplanted inhibitory neurons may correct visual impairments that arise from defective cortical circuits, such as amblyopia. Likewise, transplanted inhibitory neurons may facilitate the re-mapping of motor and sensory areas after stroke, one of the most common and devastating neurological injuries.

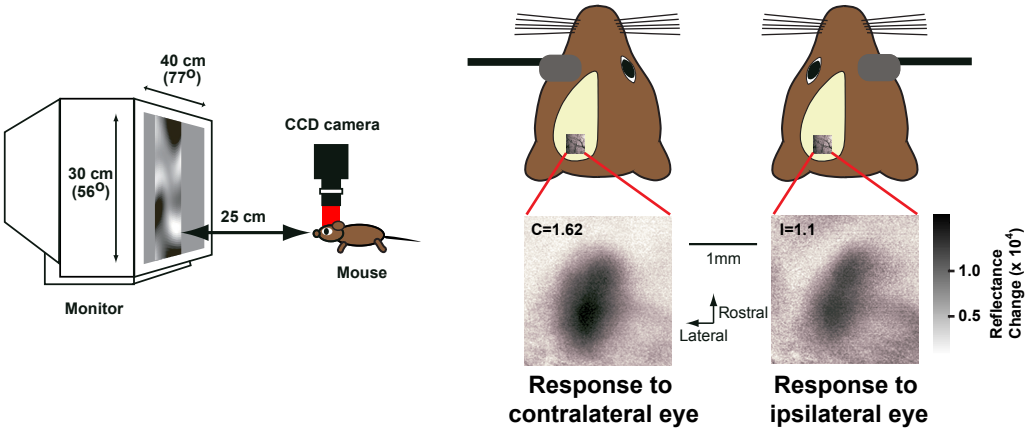
Figure 1. Experimental design: Inhibitory neuron precursor transplantation and optical measurements of visual responses.

(**A**) Inhibitory neuron precursors were transplanted from embryonic day 13.5-14.5 (E13.5-14.5) DsRed- or GFP-labeled donors to postnatal recipient mice. Primary cell suspensions were injected through a glass capillary needle into two sites (red circles) that flanked primary visual cortex. Embryonic cells were transplanted to postnatal day 0-2 (P0-2; diamonds) and P9-11 (squares) GAD67-GFP or wild type mice, and then left to develop in the recipient brain for 17, 33-35, or 43-46 days. Recipient animals then underwent 4 days of monocular visual deprivation (MD) contralateral to the transplanted hemisphere before cortical plasticity was assessed by optical imaging of intrinsic signals. Open symbols represent visual response measurements made immediately before MD, while solid symbols represent measurements made immediately after MD. (**B**) Visual responses were measured using optical imaging of intrinsic signals. A band-limited, contrast-modulated noise stimulus, designed to drive responses from nearly all neurons in primary visual cortex, was displayed within the binocular visual field (-5 to 15 deg). Reflected 610 nm light was imaged through the skull while the stimulus was viewed alternately through the contra- and ipsilateral eye every 5 minutes. Responses were extracted using Fourier analysis. The response amplitude for each eye was taken as the peak value of the smoothed Fourier map. An ocular dominance index (ODI) for each recording session was computed from the two responses.

A


P0-P2 recipient
4d MD
E13.5-E14.5
fluorescent
donor
33-35 days
43-46 days
33-35 days
17 days
P9-P11 recipient

B


40 cm
(77°)
30 cm
(56°)
CCD camera
25 cm
Mouse
Monitor
C=1.62
I=1.1
1mm
Rostral
Lateral
1.0
0.5
Reflectance
Change (x 10⁻⁴)
Response to
contralateral eye
Response to
ipsilateral eye

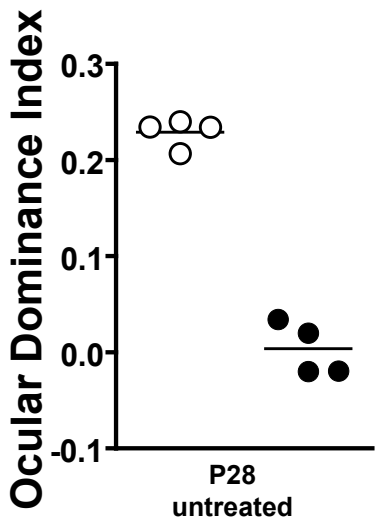


Figure 2. Untreated GAD67-GFP mice exhibit normal ocular dominance plasticity during the critical period

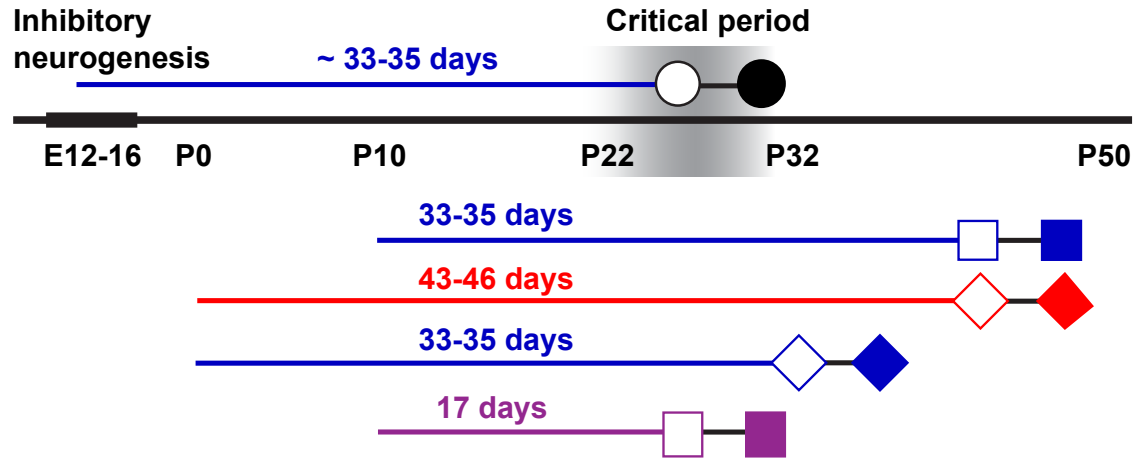
In GAD67-GFP mice at the peak of the normal critical period, the binocular visual cortex responded more strongly to the contralateral eye, yielding a mean ODI of approximately 0.22 (open black circles). After four days of MD of the contralateral eye from P28 to P32, visual responses in the binocular visual cortex of GAD67-GFP mice were shifted towards the ipsilateral eye, with a mean ODI value of 0.00 (filled black circles). At these ages, the ODI values of GAD67-GFP mice before and after 4 days of MD were essentially identical to those of wild type C57Bl/6 mice (Cang et al 2005).

Figure 3. Transplanted MGE cells induce ocular dominance plasticity 33-35 days after transplantation to P0-P2 and P9-P11 recipients, when they reach a cellular age equivalent to that of endogenous inhibitory neurons at the peak of the normal critical period.

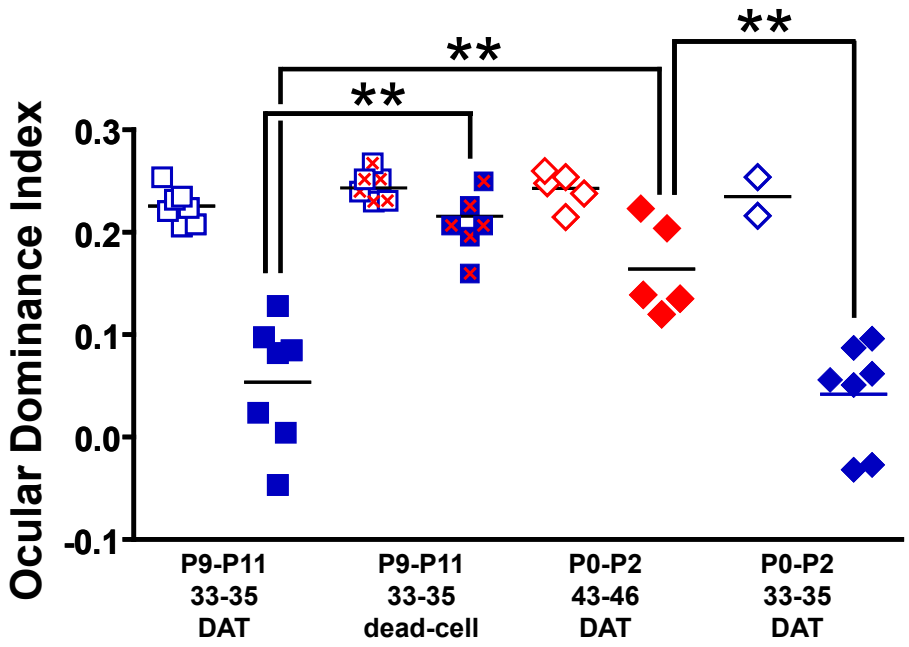
(**A**) Cortical inhibitory neurons are produced during embryonic days 12 to 16 (E12-16). Ocular dominance plasticity reaches a maximum during the normal critical period, around P26-P28, when cortical inhibitory neurons are approximately 33-35 days old (black circles). We first examined the effects of MD 33-35 days after transplantation (DAT) to P9-P11 recipients (blue squares), when transplanted cells reached the same age as native inhibitory neurons at the peak of the normal critical period. We also measured the effects of MD 43-46 DAT into P0-P2 recipients (red diamonds), 33-35 DAT into P0-P2 recipients (blue diamonds), and 17 DAT into P11 recipients (purple squares). Cortical plasticity was assessed by measuring visual responses immediately before (open symbols) and after (solid symbols) four days of MD. (**B**) Visual responses through the two eyes before MD were similar in transplant recipients and dead-cell control recipients (open blue squares with red crosses). Thirty-three to thirty-five DAT into P9-P11 recipients, 4 days of MD elicited a strong effect on visual responses in transplant recipients (solid blue squares), but not in dead-cell control recipients (solid blue squares with red crosses; Mann-Whitney test, $P = 0.006$, $U = 0$). In comparison to the effects of MD in P9-P11 recipients 33-35 DAT (solid blue squares), the effect of MD was considerably smaller in age-matched animals that received transplants at P0-P2 (43-46 DAT; solid red

diamonds; Mann-Whitney, P = 0.0018, U = 0). By contrast, monocular deprivation produced a stronger effect in P0-P2 recipients at 33-35 DAT (solid blue diamonds) than at 43-46 DAT (solid red diamonds; Mann-Whitney, P = 0.0025, U= 0).

A


Inhibitory
neurogenesis
~ 33-35 days
Critical period
E12-16
P0
P10
P22
P32
P50
33-35 days
43-46 days
33-35 days
17 days

B


Ocular Dominance Index
0.3
0.2
0.1
0.0
-0.1
**
**
**
P9-P11
33-35
DAT
P9-P11
33-35
dead-cell
P0-P2
43-46
DAT
P0-P2
33-35
DAT

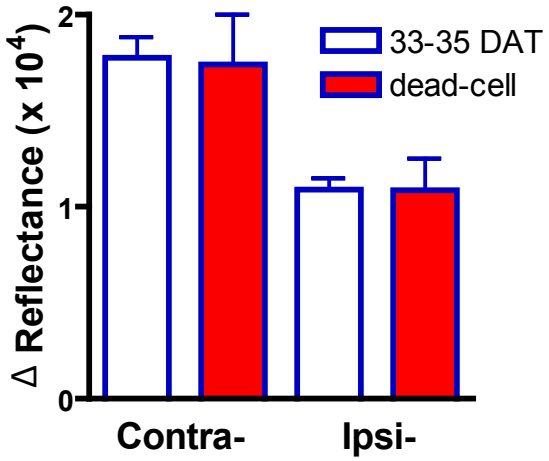


Figure 4. The absolute magnitudes of cortical responses are similar in MGE cell transplant recipients and dead-cell control recipients.

Comparison of visual responses to the contralateral and ipsilateral eye in MGE cell transplant recipients and dead-cell control recipients at 33-35 DAT. Animals received transplants at P9-P11. Visual responses are similar in MGE cell transplant recipients and dead-cell control recipients (comparison of contralateral responses: Mann-Whitney, P = 0.95, U = 17; ipsilateral: P = 0.95, U = 18; N = 6 MGE cell recipients and N = 4 dead-cell recipients).

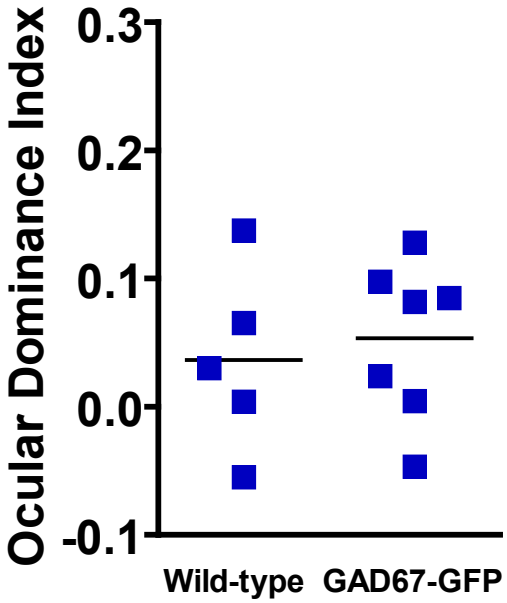


Figure 5. Ocular dominance plasticity is equally affected in wild type and GAD67-GFP mice at 33-35 days after transplantation.

Monocular deprivation was initiated 33-35 days after transplantation to P10 wild type and P9-P11 GAD67-GFP recipients. After four days of monocular deprivation, the ocular dominance indices of wild type and GAD67-GFP mice were similar, indicating that the effects of transplantation are not restricted to the GAD67-GFP background (wild-type ODI = 0.04 ± 0.03; GAD67-GFP ODI = 0.05 ± 0.03; Mann-Whitney, P = 0.68, U = 30).

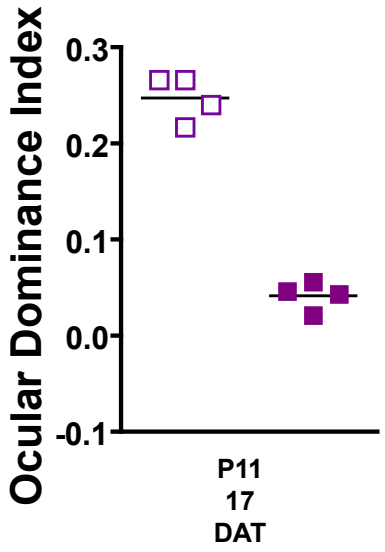


Figure 6. MGE cell transplantation does not alter ocular dominance plasticity during the critical period.

At 17 days after transplantation into P11 recipients, monocular deprivation produced strong ocular dominance plasticity, equal to that observed in untreated, age-matched mice at the peak of the critical period (Figure 2; Mann-Whitney, P = 0.057, U = 1).

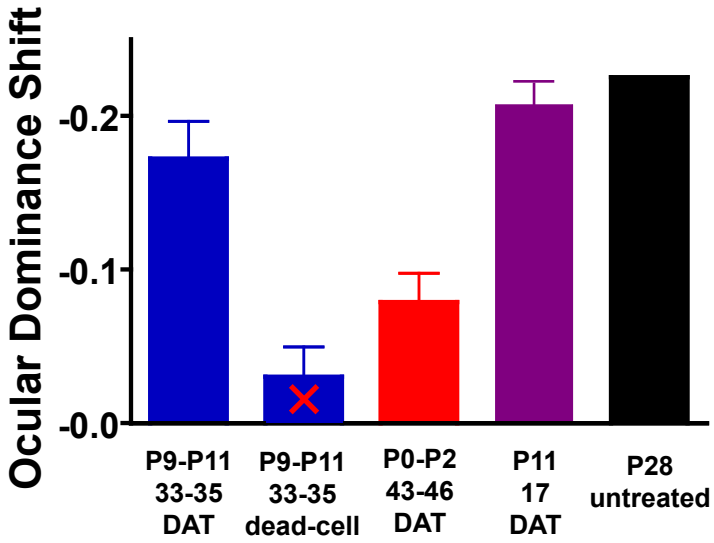
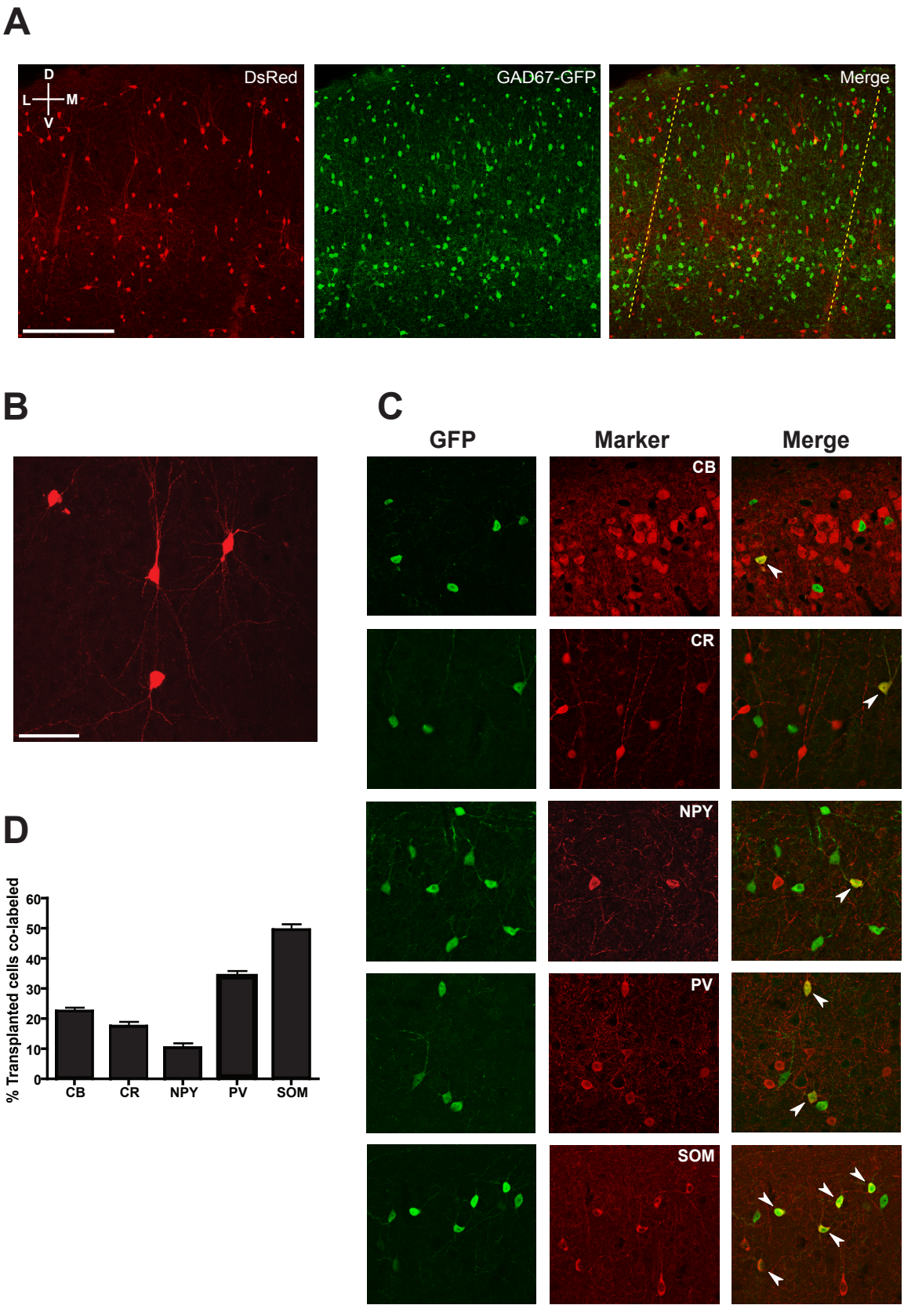


Figure 7. At 33-35 days after transplantation to P9-P11 recipients, ocular dominance plasticity is 77% the magnitude of that observed in untreated animals during the critical period.

An ocular dominance shift (ODS) was computed as the difference between ODI values before and after monocular deprivation. The ODS of P9-P11 recipients at 33-35 DAT (blue; N = 7) was 5.6 times that of P9-P11 dead-cell control recipients at 33-35 DAT (blue with red cross; N = 6) and 2.2 times that of P0-P2 recipients at 43-46 DAT (red; N = 5). The ODS of P9-P11 recipients at 33-35 DAT (blue) was 77% of that observed in untreated animals during the critical period (black; N = 4). Error bars represent s.e.m.

Figure 8. Transplanted MGE cells populate the recipient visual cortex and develop into mature inhibitory neurons.

(**A**) GAD67-GFP recipient cortex labeled for transplanted DsRed cells (red) and GAD67-GFP neurons (green). DiI injections (red; dotted yellow line for emphasis) label the binocular visual cortex, as identified by optical imaging of neural responses. Scale bar, 250 μm (**B**) Transplanted MGE cells develop morphologies of inhibitory neurons in the recipient visual cortex. Scale bar, 50 μm. (**C**) Transplanted GFP^+ inhibitory neurons (green) labeled for neurochemical markers of inhibitory neuron subtypes (red; CB = calbindin, CR = calretinin, NPY = neuropeptide y, PV = parvalbumin, SOM = somatostatin). White chevrons identify co-labeled cells. (**D**) Quantification of neurochemical marker expression in transplanted GFP^+ inhibitory neurons. The y-axis indicates the percentage of transplanted cells co-labeled by the marker; error bars represent the s.e.m. N = 6 animals. In all figures, recipient animals were assessed for plasticity at 33-35 DAT.


A
D
L
M
V
DsRed
GAD67-GFP
Merge
B
C
GFP
Marker
Merge
CB
CR
NPY
PV
SOM
D
% Transplanted cells co-labeled
60
50
40
30
20
10
0
CB
CR
NPY
PV
SOM

Chapter 5

Conclusions

My thesis research has focused on the developmental cell death and transplantation of neocortical inhibitory neurons, a cellular population with a unique potential to migrate and survive in the recipient brain after transplantation. Transplanted inhibitory neurons modify neural circuits in the brain, making them an attractive therapeutic candidate for treating neurological disorders and brain injuries, such as epilepsy, Parkinson's disease, Huntington's disease, and stroke (Richardson et al., 2008). As our laboratory has begun to explore the therapeutic applications of inhibitory neuron transplantation, we have maintained a basic focus on the developmental processes that regulate the integration of inhibitory neuron into brain circuits, both during normal development and in transplantation scenarios (Wichterle et al., 1999; Wichterle et al., 2003; Alvarez-Dolado et al., 2003). By better understanding the basic development of these cells, we hope to develop inhibitory neuron transplantation as a method for the safe and effective modification of brain circuits. By studying the fundamental processes through which the brain normally develops and assembles neural circuits, we also hope to elucidate the normal mechanisms of development, and to characterize developmental processes that could be affected in the pathophysiology of neurological diseases.

I began my research by focusing on the developmental cell death of inhibitory neurons. By studying the basic patterns of developmental cell death of inhibitory neurons, I have gained a fundamental insight into the behavior of transplanted inhibitory neurons: when isolated from the embryo and introduced into the postnatal brain, inhibitory neuron precursors develop as though they

remained in the embryo. Transplanted inhibitory neurons underwent a pattern of developmental cell death that was equal in magnitude to that of endogenous cell death, yet temporally distinct from endogenous cell death. The transplanted cells died when they reached an age equivalent to that of endogenous cells during the period of endogenous cell death. This finding suggested that the developmental cell death of inhibitory neurons could be intrinsically programmed within these cells, in a manner that is free from the developmental state of the brain, and free from competitive interactions. More generally, these results imply that transplanted inhibitory neurons could maintain and execute cell-intrinsic developmental programs in the recipient brain (Figure 1). This insight proved to be a guiding principle for my subsequent experiments, through which I studied the functional effects of inhibitory neuron transplantation.

In collaboration with Sunil Gandhi and Michael Stryker, I further explored the hypothesis that transplanted inhibitory neurons execute cell-intrinsic programs in the recipient brain. We transplanted embryonic inhibitory neuron precursors to the postnatal mouse visual cortex, and then studied their functional effects on ocular dominance plasticity in the recipient brain. In the mouse visual cortex, ocular dominance plasticity occurs during a critical period that is regulated by a threshold of GABAergic inhibitory signaling (Hensch et al., 1998; Fagiolini et al., 2000). We hypothesized that the developmental state of inhibitory neurons regulated ocular dominance plasticity, such that a transplanted cohort of developing inhibitory neurons could also induce plasticity during a particular stage of its development. The normal critical period for ocular dominance

plasticity occurs between P22 and P32 in the mouse (Gordon and Stryker, 1996), when endogenous inhibitory neurons are approximately 30-35 days old. Building on the basic insight that transplanted inhibitory neurons develop along intrinsically defined programs (Chapter 3), we transplanted newborn inhibitory neuron precursors to neonatal and young juvenile mice, and examined ocular dominance plasticity at 33-35 days after transplantation (DAT), 17 DAT, and 43-46 DAT. Surprisingly, transplanted inhibitory neurons induced strong ocular dominance plasticity at 33-35 DAT, but they did not affect ocular dominance plasticity at 17 or 43-46 DAT. Thus, transplanted inhibitory neurons induced profound ocular dominance plasticity outside the critical period, when they reached a cell-intrinsic age similar to that of endogenous inhibitory neurons during the peak of the normal critical period. These results imply that the cell-intrinsic maturation of inhibitory neurons regulates the critical period, and that transplanted inhibitory neurons maintain and execute a cell-intrinsic developmental program that can induce ocular dominance plasticity after the critical period (Figure 1).

Together, my findings suggest that transplanted inhibitory neurons possess cell-intrinsic programs that govern their developmental cell death, and induce ocular dominance plasticity in the recipient neocortex. Moreover, I have also suggested that endogenous inhibitory neuron cell death, and the normal critical period, also reflect the execution of these developmental programs. I do of course realize, however, that the whole of brain development does not simply reflect the individual behaviors of cells acting in isolation. At the very least,

inhibitory neurons must clearly interact with cellular and non-cellular features in their environment in order to migrate and induce plasticity. With respect to their developmental cell death, or the induction of ocular dominance plasticity, inhibitory neurons could moreover be directed via interactions with their environments that direct them to die, or direct them to induce plasticity. At the very minimum, however, inhibitory neurons must still reach a cell-intrinsically defined state in order to participate in, or respond to, such interactions. With respect to the notion of a cell-autonomous death program, it would be informative to examine the death of inhibitory neuron *in vitro*, where their environmental conditions can be controlled. Should their death *in vitro* resemble what I have observed *in vivo*, this would further imply that a cell-intrinsic program directs inhibitory neuron cell death.

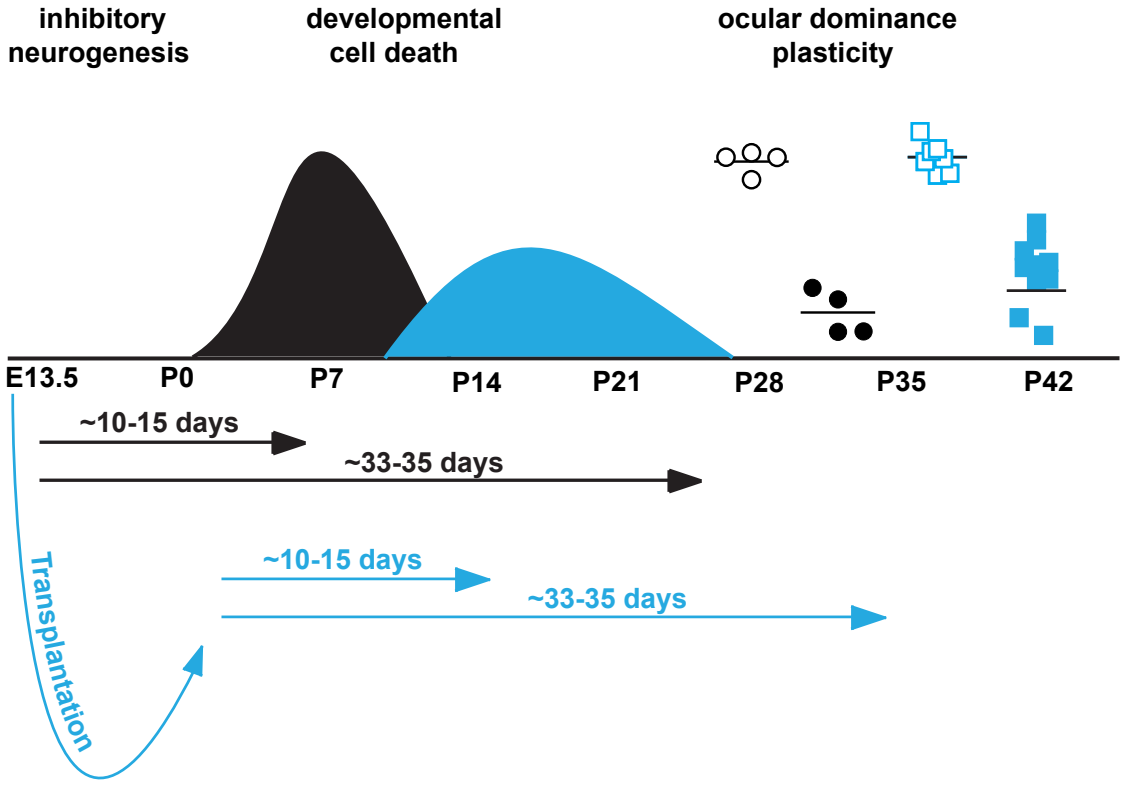
How might we determine which cell-intrinsic processes guide the developmental cell death of inhibitory neurons, and their effects on ocular dominance plasticity? I believe a comparison of gene expression in endogenous- and transplanted inhibitory neurons may be informative. Transplanted cells could be isolated at different timepoints (before, during, and after these cells die or induce plasticity) and their gene expression profiles and chromatin patterns could be analyzed. These experiments may identify signaling pathways and transcriptional events that govern the survival of inhibitory neurons and their functional effects on cortical plasticity. It would also be interesting to determine whether the temporal patterns of gene expression are conserved in transplanted inhibitory neurons, by comparing the expression profiles

transplanted cells to those of isochronic, endogenous inhibitory neurons. Again, if the gene expression profiles of heterochronically transplanted- and endogenous inhibitory neurons were similar when the cells are of the same intrinsic ages, it would suggest that the patterns of gene expression are highly programmed within the cells themselves, and free from extrinsic influences. This type of genomic approach may help elucidate the molecular clock by which inhibitory neuron-specific developmental events are timed. One should keep in mind, however, that the diversity of inhibitory neurons could be a complicating factor in this experiment. For example, the transcriptional profiles of different sub-types of inhibitory neurons may vary significantly (Sugino et al., 2006), so it might be necessary to identify and study particular sub-populations of these cells (Chapter 1; Discussion, Chapter 4).

Finally, the concept of cell-intrinsic developmental programs is highly relevant to regenerative medicine. Right now there is an enormous effort to treat various diseases by growing specialized cells *in vitro* and then transplanting these cells *in vivo*. Given the findings I have presented here, it will be crucial to better understand how cell culture conditions influence the intrinsic developmental programs of cultured cells. Only then will we be able to grow cells that safely and effectively integrate into diseased tissues.

Figure 1. Intrinsic developmental programs govern the cell death of inhibitory neurons and the critical period for ocular dominance plasticity. During normal development, inhibitory neurons begin to undergo significant cell death at P7, when they reach an intrinsic cellular age of approximately 10 to 15 days (black curve; Chapter 3). Later, when surviving inhibitory neurons reach approximately 33-35 days of age, they initiate a critical period for ocular dominance plasticity in the visual cortex (around P28, black circles; Chapter 4). When newborn inhibitory neurons are transplanted from the embryo into the postnatal brain (blue), they maintain and execute an intrinsic developmental program that results in significant transplanted cell death (blue curve; Chapter 3). However, significant numbers of transplanted cells also survive in the recipient brain, and those surviving cells later induce ocular dominance plasticity in the recipient, at ages beyond the normal critical period (blue squares; Chapter 4). The development of inhibitory neurons appears to follow an intrinsic cellular clock that is tightly conserved even when inhibitory neurons are transplanted: transplanted inhibitory neurons undergo developmental cell death and induce ocular dominance plasticity in the recipient brain when they reach intrinsic ages (approximately 10-15 days and 33-35 days, respectively) that are equivalent to the ages of endogenous inhibitory neurons at the peak of endogenous cell death and at the peak of the normal critical period, respectively. These results suggest that transplanted inhibitory neurons integrate into the recipient brain in a manner that reflects their normal endogenous development. In turn, this knowledge provides a rational basis for the design of inhibitory neuron transplantation

strategies, and it further underscores the need for *in vitro* cell culture systems that maintain and establish relevant cellular developmental programs.


inhibitory neurogenesis
developmental cell death
ocular dominance plasticity
E13.5
P0
P7
P14
P21
P28
P35
P42
~10-15 days
~33-35 days
Transplantation
~10-15 days
~33-35 days

Chapter 6

References

Abe-Dohmae, S., Harada, N., Yamada, K., & Tanaka, R. (1993). Bcl-2 gene is highly expressed during neurogenesis in the central nervous system. Biochemical and Biophysical Research Communications, 191 (3), 915-21.

Airaksinen, M., & Saarma, M. (2002). The GDNF family: Signalling, biological functions and therapeutic value. Nature Reviews Neuroscience, 3, 383-394.

Alcántara, S., Frisén, J., del Río, J., Soriano, E., Barbacid, M., & Silos-Santiago, I. (1997). TrkB signaling is required for postnatal survival of CNS neurons and protects hippocampal and motor neurons from axotomy-induced cell death. The Journal of Neuroscience, 17 (10), 3623-33.

Alvarez-Dolado, M., Calcagnotto, M., Karkar, K., Southwell, D., Jones-Davis, D., Estrada, R., et al. (2006). Cortical inhibition modified by embryonic neural precursors grafted into the postnatal brain. The Journal of Neuroscience, 26 (28), 7380-9.

Anderson, S., Eisenstat, D., Shi, L., & Rubenstein, J. (1997). Interneuron migration from basal forebrain to neocortex: dependence on Dlx genes. Science, 278 (5337), 474-6.

Ang, E., Haydar, T., Gluncic, V., & Rakic, P. (2003). Four-dimensional migratory coordinates of GABAergic interneurons in the developing mouse cortex. The Journal of Neuroscience, 23 (13), 5805-15.

Barbacid, M. (1994). The Trk family of neurotrophin receptors. Journal of Neurobiology, 25 (11), 1386-1403.

Behar, T., Schaffner, A., Scott, C., Greene, C., & Barker, J. (2000). GABA receptor antagonists modulate postmitotic cell migration in slice cultures of embryonic rat cortex. Cerebral Cortex, 10 (9), 899-909.

Boise, L., González-García, M., Postema, C., Ding, L., Lindsten, T., Turka, L., Mao, X., Nunez, G., & Thompson, C. (1993). Bcl-x, a Bcl-2-related gene that functions as a dominant regulator of apoptotic cell death. Cell, 74 (4), 597-608.

Bonni, A., Frank, D., Schindler, C., & Greenberg, M. (1993). Characterization of a pathway for ciliary neurotrophic factor signaling to the nucleus. Science, 262 (5139), 1575-9.

Born, D., & Rubel, E. (1985). Afferent influences on brain stem auditory nuclei of the chicken: Neuron number and size following cochlea removal. The Journal of Comparative Neurology, 231 (4), 435-45.

Buss, R., Sun, W., & Oppenheim, R. (2006). Adaptive roles of programmed cell death during nervous system development. Annual Review of Neuroscience, 29

(1), 1-35.

Butt, S., Fuccillo, M., Nery, S., Noctor, S., Kriegstein, A., Corbin, J., Fishell, G. (2005). The temporal and spatial origins of cortical interneurons predict their physiological subtype. Neuron, 48 (4), 591-604.

Buzsáki, G., Geisler, C., Henze, D., & Wang, X.-J. (2004). Interneuron Diversity series: Circuit complexity and axon wiring economy of cortical interneurons. Trends in Neurosciences, 27 (4), 186-93.

Buzsaki, G., Kaila, K., & Raichle, M. (2007). Inhibition and Brain Work. Neuron, 56 (5), 771-783.

Campbell, K. (2003). Dorsal-ventral patterning in the mammalian telencephalon. Current Opinion in Neurobiology, 13 (1), 50-6.

Cancedda, L., Fiumelli, H., Chen, K., & Poo, M.-M. (2007). Excitatory GABA action is essential for morphological maturation of cortical neurons in vivo. Journal of Neuroscience, 27 (19), 5224-5235.

Cang, J., Kalatsky, V., Löwel, S., & Stryker, M. (2005). Optical imaging of the intrinsic signal as a measure of cortical plasticity in the mouse. Visual neuroscience , 22 (5), 685-91.

Cardin, J., Carlén, M., Meletis, K., Knoblich, U., Zhang, F., Deisseroth, K., Tsai, L.-H., & Moore C. (2009). Driving fast-spiking cells induces gamma rhythm and controls sensory responses. Nature, ePub ahead of print.

Cardone, M., Roy, N., Stennicke, H., Salvesen, G., Franke, T., Stanbridge, E., Frisch, S., & Reed, J. (1998). Regulation of cell death protease caspase-9 by phosphorylation. Science, 282 (5392), 1318-21.

Carleton, A., Petreanu, L., Lansford, R., Alvarez-Buylla, A., & Lledo, P.-M. (2003). Becoming a new neuron in the adult olfactory bulb. Nature Neuroscience, 6 (5), 507-18.

Cavanagh, M., & Parnavelas, J. (1989). Development of vasoactive-intestinal-polypeptide-immunoreactive neurons in the rat occipital cortex: a combined immunohistochemical-autoradiographic study. The Journal of Comparative Neurology, 284 (4), 637-45.

Cecchi, G., Petreanu, L., Alvarez-Buylla, A., & Magnasco, M. (2001). Unsupervised learning and adaptation in a model of adult neurogenesis. Journal of Computational Neuroscience, 11 (2), 175-82.

Chattopadhyaya, B., Di Cristo, G., Higashiyama, H., Knott, G., Kuhlman, S.,

Welker, E., Huang, J. (2004). Experience and activity-dependent maturation of peri-somatic GABAergic innervation in primary visual cortex during a postnatal critical period. The Journal of Neuroscience, 24 (43), 9598-611.

Chattopadhyaya, B., Dicristo, G., Wu, C., Knott, G., Kuhlman, S., Fu, Y., Palmiter, R., & Huang, J. (2007). GAD67-Mediated GABA Synthesis and Signaling Regulate Inhibitory Synaptic Innervation in the Visual Cortex. Neuron, 54 (6), 889-903.

Chinnaiyan, A., O'Rourke, K., Tewari, M., & Dixit, V. (1995). FADD, a novel death domain-containing protein, interacts with the death domain of Fas and initiates apoptosis. Cell, 81 (4), 505-12.

Cobos, I., Calcagnotto, M., Vilaythong, A., Thwin, M., Noebels, J., Baraban, S., Rubenstein, J. (2005). Mice lacking Dlx1 show subtype-specific loss of interneurons, reduced inhibition and epilepsy. Nature Neuroscience, 8 (8), 1059-1068.

Cobos, I., Long, J., Thwin, M., & Rubenstein, J. (2006). Cellular patterns of transcription factor expression in developing cortical interneurons. Cerebral Cortex 16(1), 82-8.

Cohen, S., & Levi-Montalcini, R. (1956). A nerve growth-stimulating factor isolated from snake venom. Proceedings of the National Academy of Sciences, 42 (9), 571-574.

Cowan, W., Fawcett, J., O'Leary, D., & Stanfield, B. (1984). Regressive events in neurogenesis. Science, 225 (4668), 1258-65.

Cuzon, V., Yeh, P., Cheng, Q., & Yeh, H. (2006). Ambient GABA promotes cortical entry of tangentially migrating cells derived from the medial ganglionic eminence. Cerebral Cortex, 16 (10), 1377-88.

Datta, S., Ranger, A., Lin, M., Sturgill, J., & Ma, Y. (2002). Survival factor-mediated BAD phosphorylation raises the mitochondrial threshold for apoptosis. Developmental Cell, 3 (5), 631-43.

Dayer, A., Cleaver, K., Abouantoun, T., Cameron, H. (2005). New GABAergic interneurons in the adult neocortex and striatum are generated from different precursors. The Journal of Cell Biology, 168 (3), 415-427.

Del Rio, J., Soriano, E., & Ferrer, I. (1992). Development of GABA-immunoreactivity in the neocortex of the mouse. The Journal of Comparative Neurology, 326 (4), 501-26.

Denaxa, M., Chan, C., Schachner, M., & Parnavelas, J. (2001). The adhesion

molecule TAG-1 mediates the migration of cortical interneurons from the ganglionic eminence along the corticofugal fiber system. Development, 128 (22), 4635-44.

Denaxa, M., Kyriakopoulou, K., Theodorakis, K., Trichas, G., Vidaki, M., Takeda, Y., et al. (2005). The adhesion molecule TAG-1 is required for proper migration of the superficial migratory stream in the medulla but not of cortical interneurons. Developmental Biology , 288 (1), 87-99.

Deng, Y., Lin, Y., & Wu, X. (2002). TRAIL-induced apoptosis requires Bax-dependent mitochondrial release of Smac/DIABLO. Genes & Development, 16 (1), 33-45.

Drager, U. (1978). Observations on monocular deprivation in mice. Journal of Neurophysiology, 41 (1), 28-42.

Drager, U. (1975). Receptive fields of single cells and topography in mouse visual cortex. The Journal of Comparative Neurology, 160 (3), 269-90.

Du, C., Fang, M., Li, Y., Li, L., & Wang, X. (2000). Smac, a mitochondrial protein that promotes cytochrome c-dependent caspase activation by eliminating IAP inhibition. Cell , 102 (1), 33-42.

Du, T., Xu, Q., Ocbina, P., & Anderson, S. (2008). Nkx2.1 specifies cortical interneuron fate by activating Lhx6. Development, 135 (8), 1559-67.

Ebens, A., Brose, K., Leonardo, E., Hanson, M., Bladt, F., Birchmeier, C., Barres, B., Tessier-Lavigne, M. (1996). Hepatocyte growth factor/scatter factor is an axonal chemoattractant and a neurotrophic factor for spinal motor neurons. Neuron, 17 (6), 1157-72.

Enari, M., Sakahira, H., Yokoyama, H., Okawa, K., Iwamatsu, A., & Nagata, S. (1998). A caspase-activated DNase that degrades DNA during apoptosis, and its inhibitor ICAD. Nature, 391 (6662), 43-50.

Erbel-Sieler, C., Dudley, C., Zhou, Y., Wu, X., & Estill, S. (2004). Behavioral and regulatory abnormalities in mice deficient in the NPAS1 and NPAS3 transcription factors. Proceedings of the National Academy of Sciences, 101 (37), 13648-53.

Fagiolini, M., & Hensch, T. (2000). Inhibitory threshold for critical-period activation in primary visual cortex. Nature, 404 (6774), 183-6.

Fagiolini, M., Fritschy, J.-M., Löw, K., Möhler, H., Rudolph, U., & Hensch, T. (2004). Specific GABAA circuits for visual cortical plasticity. Science, 303 (5664), 1681-3.

Ferrer, I., Bernet, E., Soriano, E., del Rio, T., & Fonseca, M. (1990). Naturally occurring cell death in the cerebral cortex of the rat and removal of dead cells by transitory phagocytes. Neuroscience, 39 (2), 451-8.

Finlay, B., & Slattery, M. (1983). Local differences in the amount of early cell death in neocortex predict adult local specializations. Science, 219 (4590), 1349-51.

Flames, N., Long, J., Garratt, A., Fischer, T., Gassmann, M., Birchmeier, C., Lai, C., Rubenstein, J., Marin, O. (2004). Short- and long-range attraction of cortical GABAergic interneurons by neuregulin-1. Neuron, 44 (2), 251-61.

Fogarty, M., Grist, M., Gelman, D., Marin, O., Pachnis, V., & Kessaris, N. (2007). Spatial genetic patterning of the embryonic neuroepithelium generates GABAergic interneuron diversity in the adult cortex. Journal of Neuroscience, 27 (41), 10935-10946.

French, L., Hahne, M., Viard, I., Radlgruber, G., Zanone, R., Becker, K., Muller, C., Tschopp, J. (1996). Fas and Fas ligand in embryos and adult mice: ligand expression in several immune-privileged tissues and coexpression in adult tissues characterized by apoptotic cell turnover. The Journal of Cell Biology, 133 (2), 335-43.

Freund, T. (2003). Interneuron Diversity series: Rhythm and mood in peri-somatic inhibition. Trends in Neurosciences, 26 (9), 489-495.

Galvao, R., Garcia-Verdugo, J., & Alvarez-Buylla, A. (2008). Brain-derived neurotrophic factor signaling does not stimulate subventricular zone neurogenesis in adult mice and rats. Journal of Neuroscience, 28 (50), 13368-13383.

Gandhi, S., Yanagawa, Y., & Stryker, M. (2008). Delayed plasticity of inhibitory neurons in developing visual cortex. Proceedings of the National Academy of Sciences, 105 (43), 16797-802.

Gonchar, Y., Wang, Q., Burkhalter, A. (2008). Multiple distinct subtypes of GABAergic neurons in mouse visual cortex identified by triple immunostaining. Frontiers in Neuroanatomy, 1 (3), 1-11.

Gordon, J., & Stryker, M. (1996). Experience-dependent plasticity of binocular responses in the primary visual cortex of the mouse. The Journal of Neuroscience, 16 (10), 3274-
86.

Gorski, J., Talley, T., Qiu, M., Puelles, L., Rubenstein, J., & Jones, K. (2002). Cortical excitatory neurons and glia, but not GABAergic neurons, are produced in

the Emx1-expressing lineage. The Journal of Neuroscience, 22 (15), 6309-14.

Gross, A., McDonnell, J., & Korsmeyer, S. (1999). Bcl-2 family members and the mitochondria in apoptosis. Genes & Development, 13 (15), 1899-911.

Haase, G., Pettmann, B., Raoul, C., & Henderson, C. (2008). Signaling by death receptors in the nervous system. Current Opinion in Neurobiology, 18 (3), 284-91.

Hadjantonakis, A., Gertsenstein, M., Ikawa, M., Okabe, M., & Nagy, A. (1998). Generating green fluorescent mice by germline transmission of green fluorescent ES cells. Mechanisms of Development, 76 (1-2), 79-90.

Hakem, R., Hakem, A., Duncan, G., Henderson, J., Woo, M., Soengas, M., Elia, A., de la Pompa, J., Kagi, D., Khoo, W., Potter, J., Yoshida, R., Kaufman, S., Lowe, S., Penninger, J., Mak, T. (1998). Differential requirement for caspase 9 in apoptotic pathways in vivo. Cell, 94 (3), 339-52.

Hamburger, V., & Levi-Montalcini, R. (1949). Proliferation, differentiation and degeneration in the spinal ganglia of the chick embryo under normal and experimental conditions. The Journal of Experimental Zoology, 111 (3), 457-501.

Hamburger, V., Brunso-Bechtold, J., & Yip, J. (1981). Neuronal death in the spinal ganglia of the chick embryo and its reduction by nerve growth factor. The Journal of Neuroscience, 1 (1), 60-71.

Hanover, J., Huang, Z., Tonegawa, S., & Stryker, M. (1999). Brain-derived neurotrophic factor overexpression induces precocious critical period in mouse visual cortex. The Journal of Neuroscience, 19 (22), 1-5.

Hensch, T. (2005). Critical period plasticity in local cortical circuits. Nature Reviews Neuroscience, 6 (11), 877-888.

Hensch, T. (2004). Critical period regulation. Annual Review of Neuroscience, 27 (1), 549-579.

Hensch, T., Fagiolini, M., Mataga, N., Stryker, M., Baekkeskov, S., & Kash, S. (1998). Local GABA circuit control of experience-dependent plasticity in developing visual cortex. Science, 282 (5393), 1504-8.

Heumann, D., & Leuba, G. (1983). Neuronal death in the development and aging of the cerebral cortex of the mouse. Neuropathology and Applied Neurobiology, 9 (4), 297-311.

Hu, Y., Benedict, M., Wu, D., Inohara, N., & Núñez, G. (1998). Bcl-X_L interacts with Apaf-1 and inhibits Apaf-1-dependent caspase-9 activation. Proceedings of

the National Academy of Sciences, 95 (8), 4386-91.

Huang, Z., Di Cristo, G., & Ango, F. (2007). Development of GABA innervation in the cerebral and cerebellar cortices. Nature Reviews Neuroscience, 8 (9), 673-686.

Huang, Z., Kirkwood, A., Pizzorusso, T., Porciatti, V., Morales, B., Bear, Maffei, L., Tonegawa, S. (1999). BDNF regulates the maturation of inhibition and the critical period of plasticity in mouse visual cortex. Cell, 98 (6), 739-55.

Imayoshi, I., Sakamoto, M., Ohtsuka, T., Takao, K., Miyakawa, T., Yamaguchi, M., Mori, K., Ikeda, T., Itohara, S., Kageyama, R. (2008). Roles of continuous neurogenesis in the structural and functional integrity of the adult forebrain. Nature Neuroscience, 11 (10), 1153-61.

Inta, D., Alfonso, J., von Engelhardt, J., Kreuzberg, M., Meyer, A., van Hooft, J., Monyer, H. (2008). Neurogenesis and widespread forebrain migration of distinct GABAergic neurons from the postnatal subventricular zone. Proceedings of the National Academy of Sciences, 105 (52), 20994-9.

Johnson, E., Taniuchi, M., & DiStefano, P. (1988). Expression and possible function of nerve growth factor receptors on Schwann cells. Trends in Neurosciences, 11 (7), 299-304.

Joza, N., Susin, S., Daugas, E., Stanford, W., Cho, S., Li, C., Sasaki, T., Elia, A., Cheng, H., Ravagnan, L., Ferri, K., Zamzami, N., Wakeham, A., Hakem, R., Yoshida, H., Kong, Y., Mak, T., Zuniga-Pflucker, J., Kroemer, G., Penninger, J. (2001). Essential role of the mitochondrial apoptosis-inducing factor in programmed cell death. Nature, 410 (6828), 549-54.

Kalatsky, V., & Stryker, M. (2003). New paradigm for optical imaging: temporally encoded maps of intrinsic signal. Neuron, 38 (4), 529-45.

Kamnasaran, D., Muir, W., Ferguson-Smith, M., & Cox, D. (2003). Disruption of the neuronal PAS3 gene in a family affected with schizophrenia. Journal of Medical Genetics, 40 (5), 325-32.

Kaneko, M., Hanover, J., England, P., & Stryker, M. (2008). TrkB kinase is required for recovery, but not loss, of cortical responses following monocular deprivation. Nature Neuroscience, 11 (4), 497-504.

Kang, T.-B., Ben-Moshe, T., Varfolomeev, E., Pewzner-Jung, Y., Yogev, N., Jurewicz, A., Waisman, A., Brenner, O., Haffner, R., Gustafsson, E., Ramakrishnan, P., Lapidot, T., Wallach, D. (2004). Caspase-8 serves both apoptotic and nonapoptotic roles. Journal of Immunology, 173 (5), 2976-84.

Kaplan, D., Martin-Zanca, D., & Parada, L. (1991). Tyrosine phosphorylation and tyrosine kinase activity of the trk proto-oncogene product induced by NGF. Nature, 350 (6314), 158-60.

Kato, M., & Dobyns, W. (2005). X-linked lissencephaly with abnormal genitalia as a tangential migration disorder causing intractable epilepsy: Proposal for a new term, “interneuronopathy.” Journal of Child Neurology, 20 (4), 392-7.

Kawaguchi, Y., & Kubota, Y. (1997). GABAergic cell subtypes and their synaptic connections in rat frontal cortex. Cerebral Cortex, 7 (6), 476-86.

Kim, W., Kim, Y., Eun, B., Park, O.-H., Kim, H., Kim, K., Park, C.-H., Vinsant, S., Oppenheim, R., Sun, W. (2007). Impaired migration in the rostral migratory stream but spared olfactory function after the elimination of programmed cell death in Bax knock-out Mice. Journal of Neuroscience, 27 (52), 14392-14403.

Kitamura, K., Yanazawa, M., Sugiyama, N., & Miura, H. (2002). Mutation of ARX causes abnormal development of forebrain and testes in mice and X-linked lissencephaly with abnormal genitalia in humans. Nature Genetics, 32 (3), 359-69.

Kluck, R., Bossy-Wetzel, E., Green, D., & Newmeyer, D. (1997). The release of cytochrome-c from mitochondria: A primary site for Bcl-2 regulation of apoptosis. Science, 275 (5303), 1132-6.

Knudson, C., Tung, K., Tourtellotte, W., Brown, G., & Korsmeyer, S. (1995). Bax-deficient mice with lymphoid hyperplasia and male germ cell death. Science, 270 (5233), 96-9.

Krajewska, M., Mai, J., Zapata, J., Ashwell, K., Schendel, S., Reed, J., Krajewski, S. (2002). Dynamics of expression of apoptosis-regulatory proteins Bid, Bcl-2, Bcl- X, Bax and Bak during development of murine nervous system. Cell Death and Differentiation, 9 (2), 145-57.

Kriegstein, A., & Noctor, S. (2004). Patterns of neuronal migration in the embryonic cortex. Trends in Neurosciences , 27 (7), 392-9.

Kuida, K., Haydar, T., Kuan, C., Gu, Y., Taya, C., Karasuyama, H., Su, M., Rakic, P., Flavell, R. (1998). Reduced apoptosis and cytochrome c-mediated caspase activation in mice lacking caspase-9. Cell, 94 (3), 325-37.

Kuida, K., Zheng, T., Na, S., Kuan, C., Yang, D., Karasuyama, H., Rakic, P., Flavell, R. (1996). Decreased apoptosis in the brain and premature lethality in CPP32-deficient mice. Nature, 384 (6607), 368-72.

Lavdas, A., Grigoriou, M., Pachnis, V., & Parnavelas, J. (1999). The medial ganglionic eminence gives rise to a population of early neurons in the developing cerebral cortex. The Journal of Neuroscience, 19 (18), 7881-8.

Lehmann, K., Butz, M., & Teuchert-Noodt, G. (2005). Offer and demand: Proliferation and survival of neurons in the dentate gyrus. European Journal of Neuroscience, 21 (12), 3205-3216.

Letinic, K., Zoncu, R., & Rakic, P. (2002). Origin of GABAergic neurons in the human neocortex. Nature, 417 (6889), 645-9.

Levi-Montalcini, R. (1949). The development to the acoustico-vestibular centers in the chick embryo in the absence of the afferent root fibers and of descending fiber tracts. The Journal of Comparative Neurology, 91 (2), 209-41.

Levi-Montalcini, R., & Cohen, S. (1956). In vitro and in vivo effects of a nerve growth-stimulating agent isolated from snake venom. Proceedings of the National Academy of Sciences, 42 (9), 695-9.

Lewis, D., Hashimoto, T., & Volk, D. (2005). Cortical inhibitory neurons and schizophrenia. Nature Reviews Neuroscience, 6 (4), 312-24.

Lewis, P., Patel, A., Johnson, A., & Balázs, R. (1976). Effect of thyroid deficiency on cell acquistion in the postnatal rat brain: a quantitative histological study. Brain Research, 104 (1), 49-62.

Li, G., Adesnik, H., Li, J., Long, J., Nicoll, R., Rubenstein, J., Pleasure, S. (2008). Regional distribution of cortical interneurons and development of inhibitory tone are regulated by Cxcl12/Cxcr4 signaling. Journal of Neuroscience, 28 (5), 1085-98.

Li, P., Nijhawan, D., Budihardjo, I., Srinivasula, S., Ahmad, M., Alnemri, E., et al. (1997). Cytochrome c and dATP-dependent formation of Apaf-1/Caspase-9 complex initiates an apoptotic protease cascade. Cell, 91 (4), 479-89.

Lin, L., Doherty, D., Lile, J., Bektesh, S., & Collins, F. (1993). GDNF: A glial cell line-derived neurotrophic factor for midbrain dopaminergic neurons. Science, 260 (5111), 1130-2.

Lois, C., & Alvarez-Buylla, A. (1994). Long-distance neuronal migration in the adult mammalian brain. Science, 264 (5162), 1145-8.

Lopez-Bendito, G., Lujan, R., Shigemoto, R., & Ganter, P. (2003). Blockade of GABA(B) receptors alters the tangential migration of cortical neurons. Cerebral Cortex, 13 (9), 932-42.

LoTurco, J., Owens, D., Heath, M., Davis, M., & Kriegstein, A. (1995). GABA and glutamate depolarize cortical progenitor cells and inhibit DNA synthesis. Neuron, 15 (6), 1287-98.

Luo, X., Budihardjo, I., Zou, H., Slaughter, C., & Wang, X. (1998). Bid, a Bcl2 interacting protein, mediates cytochrome c release from mitochondria in response to activation of cell surface death receptors. Cell, 94 (4), 481-90.

Maric, D., Liu, Q., Maric, I., Chaudry, S., & Chang, Y. (2001). GABA expression dominates neuronal lineage progression in the embryonic rat neocortex and facilitates neurite outgrowth via GABA(A) autoreceptor/Cl- chnnels. Journal of Neuroscience, 21 (7), 2343-60.

Marin, O., & Rubenstein, J. (2003). Cell migration in the forebrain. Annual Review of Neuroscience, 26 (1), 441-483.

Marín, O., Yaron, A., Bagri, A., Tessier-Lavigne, M., & Rubenstein, J. (2001). Sorting of striatal and cortical interneurons regulated by semaphorin-neuropilin interactions. Science, 293 (5531), 872-5.

Markram, H., Toledo-Rodriguez, M., Wang, Y., Gupta, A., Silberberg, G., & Wu, C. (2004). Interneurons of the neocortical inhibitory system. Nature Reviews Neuroscience, 5 (10), 793-807.

Martinou, J., Dubois-Dauphin, M., Staple, J., Rodriguez, I., Frankowski, H., Missotten, M., Albertini, P., Talabot, D., Catsicas, S., Pietra, C. (1994). Overexpression of Bcl-2 in transgenic mice protects neurons from naturally occurring cell death and experimental ischemia. Neuron, 13 (4), 1017-30.

McGee, A., Yang, Y., Fischer, Q., Daw, N., & Strittmatter, S. (2005). Experience-driven plasticity of visual cortex limited by myelin and Nogo receptor. Science, 309 (5744), 2222-6.

Metin, C., Baudoin, J.-P., Rakic, S., & Parnavelas, J. (2006). Cell and molecular mechanisms involved in the migration of cortical interneurons. European Journal of Neuroscience, 23 (4), 894-900.

Michaelidis, T., Sendtner, M., Cooper, J., Airaksinen, M., Holtmann, B., Meyer, M., Thoenen, H. (1996). Inactivation of Bcl-2 results in progressive degeneration of motoneurons, sympathetic and sensory neurons during early postnatal development. Neuron, 17 (1), 75-89.

Miyoshi, G., Butt, S., Takebayashi, H., & Fishell, G. (2007). Physiologically distinct temporal cohorts of cortical interneurons arise from telencephalic Olig2-expressing precursors. Journal of Neuroscience, 27 (29), 7786-7798.

Morales, B., Choi, S.-Y., & Kirkwood, A. (2002). Dark rearing alters the development of GABAergic transmission in visual cortex. The Journal of Neuroscience, 22 (18), 8084-90.

Motoyama, N., Wang, F., Roth, K., Sawa, H., Nakayama, K., Nakayama, K., Negishi, I., Senju, S., Zhang, Q., Fujii, S. (1995). Massive cell death of immature hematopoietic cells and neurons in Bcl-X_L-deficient mice. Science, 267 (5203), 1506-10.

Mueller, C., & Best, J. (1989). Ocular dominance plasticity in adult cat visual cortex after transplantation of cultured astrocytes. Nature, 342 (6248), 427-30.

Muzio, M., Chinnaiyan, A., Kischkel, F., O'Rourke, K., Shevchenko, A., Ni, J., Scaffidi, C., Bretz, J., Zhang, M., Gentz, R., Mann, M., Krammer, P., Peter, M., Dixit, V. (1996). FLICE, a novel FADD-homologous ICE/CED-3-like protease, is recruited to the CD95 (Fas/APO-1) death-inducing signaling complex. Cell, 85 (6), 817-27.

Nadarajah, B., Alifragis, P., Wong, R., & Parnavelas, J. (2002). Ventricle-directed migration in the developing cerebral cortex. Nature Neuroscience, 5 (3), 218-24.

Nagata, S. (1997). Apoptosis by death factor. Cell, 88 (3), 355-65.

Nakajima, K. (2007). Control of tangential/non-radial migration of neurons in the developing cerebral cortex. Neurochemistry International, 51 (2-4), 121-131.

Nery, S., Fishell, G., & Corbin, J. (2002). The caudal ganglionic eminence is a source of distinct cortical and subcortical cell populations. Nature Neuroscience, 5 (12), 1279-1287.

Niell, C., & Stryker, M. (2008). Highly selective receptive fields in mouse visual cortex. The Journal of Neuroscience, 28 (30), 7520-36.

Nieuwenhys, R. (1994). The neocortex. Anatomy and Embryology, 190, 307-337.

Nikolaev, A., McLaughlin, T., O'Leary, D., & Tessier-Lavigne, M. (2009). APP binds DR6 to trigger axon pruning and neuron death via distinct caspases. Nature, 457 (7232), 981-9.

Noctor, S., Martínez-Cerdeño, V., Ivic, L., & Kriegstein, A. (2004). Cortical neurons arise in symmetric and asymmetric division zones and migrate through specific phases. Nature Neuroscience, 7 (2), 136-44.

Nordeen, E., Nordeen, K., Sengelaub, D., & Arnold, A. (1985). Androgens

prevent normally occurring cell death in a sexually dimorphic spinal nucleus. Science, 229 (4714), 671-3.

Nóbrega-Pereira, S., Kessaris, N., Du, T., Kimura, S., Anderson, S., & Marín, O. (2008). Postmitotic Nkx2.1 controls the migration of telencephalic interneurons by direct repression of guidance receptors. Neuron, 59 (5), 733-45.

Oppenheim, R. (1991). Cell death during development of the nervous system. Annual Review of Neuroscience, 14, 453-501.

Owens, D., & Kriegstein, A. (2002). Is there more to GABA than synaptic inhibition? Nature Reviews Neuroscience, 3 (9), 715-727.

Parks, T. (1979). Afferent influences on the development of the brain stem auditory nuclei of the chicken: Otocyst ablation. The Journal of Comparative Neurology, 183 (3), 665-77.

Parnavelas, J. (2000). The origin and migration of cortical neurones: new vistas. Trends in Neurosciences, 23 (3), 126-31.

Petreanu, L., & Alvarez-Buylla, A. (2002). Maturation and death of adult-born olfactory bulb granule neurons: role of olfaction. The Journal of Neuroscience, 22 (14), 6106-13.

Pizzorusso, T., Medini, P., Berardi, N., Chierzi, S., Fawcett, J., & Maffei, L. (2002). Reactivation of ocular dominance plasticity in the adult visual cortex. Science, 298 (5596), 1248-51.

Polleux, F., Whitford, K., Dijkhuizen, P., Vitalis, T., & Ghosh, A. (2002). Control of cortical interneuron migration by neurotrophins and PI3-kinase signaling. Development, 129 (13), 3147-60.

Powell, E., Mars, W., & Levitt, P. (2001). Hepatocyte growth factor/scatter factor is a motogen for interneurons migrating from the ventral to dorsal telencephalon. Neuron, 30 (1), 79-89.

Pozas, E., & Ibanez, C. (2005). GDNF and GFR-1 Promote Differentiation and Tangential Migration of Cortical GABAergic Neurons. Neuron, 45 (5), 701-713.

Putcha, G., Moulder, K., Golden, J., & Bouillet, P. (2001). Induction of BIM, a proapoptotic BH3-only BCL-2 family member, is critical for neuronal apoptosis. Neuron, 29 (3), 615-28.

Raff, M., Barres, B., Burne, J., Coles, H., Ishizaki, Y., & Jacobson, M. (1994). Programmed cell death and the control of cell survival. Philosophical Transactions of the Royal Society of London Series B, Biological Sciences, 345

(1313), 265-8.

Raoul, C., Henderson, C., & Pettmann, B. (1999). Programmed cell death of embryonic motoneurons triggered through the Fas death receptor. The Journal of Cell Biology, 147 (5), 1049-62.

Rehen, S.-K., McConnell, M.-J., Kaushal, D., Kingsbury, M., Yang, A., & Chun, J. (2001). Chromosomal variation in neurons of the developing and adult mammalian nervous system. The Proceedings of the National Academy of Science, 98 (23), 13361-6.

Riccio, A., Ahn, S., Davenport, C., Blendy, J., & Ginty, D. (1999). Mediation by a CREB family transcription factor of NGF-dependent survival of sympathetic neurons. Science, 286 (5448), 2358-61.

Richardson, R., Barbaro, N., Alvarez-Buylla, A., & Baraban, S. (2008). Developing cell transplantation for temporal lobe epilepsy. Neurosurgical Focus, 24 (3-4), E16.

Sakamaki, K., Inoue, T., Asano, M., Sudo, K., Kazama, H., Sakagami, J., Sakata, S., Ozaki, M., Nakamura, S., Toyokuni, S., Osumi, N., Iwakura, Y., Yonehara, S. (2002). Ex vivo whole-embryo culture of caspase-8-deficient embryos normalize their aberrant phenotypes in the developing neural tube and heart. Cell Death and Differentiation, 9 (11), 1196-206.

Sanes, D., Reh, T., & Harris, W. (2006). Development of the Nervous System. Elsevier.

Sarkisian, M., Frenkel, M., Li, W., Oborski, J., & LoTurco, J. (2001). Altered interneuron development in the cerebral cortex of the flathead mutant. Cerebral Cortex, 11 (8), 734-43.

Sato, M., & Stryker, M. (2008). Distinctive features of adult ocular dominance plasticity. Journal of Neuroscience, 28 (41), 10278-10286.

Saunders, J. (1966). Death in embryonic systems. Science, 154 (749), 604-12.

Scaffidi, C., Fulda, S., Srinivasan, A., Friesen, C., Li, F., Tomaselli, K., Debatin, K., Krammer, P., Peter, M. (1998). Two CD95 (APO-1/Fas) signaling pathways. The EMBO Journal, 17 (6), 1675-87.

Shimizu, S., Narita, M., & Tsujimoto, Y. (1999). Bcl-2 family proteins regulate the release of apoptogenic cytochrome c by the mitochondrial channel VDAC. Nature, 399 (6735), 483-7.

Sohal, V., Zhang, F., Yizhar, O., & Deisseroth, K. (2009). Parvalbumin neurons

and gamma rhythms enhance cortical circuit performance. Nature, ePub ahead of print.

Stumm, R., Zhou, C., Ara, T., Lazarini, F., Dubois-Dalcq, M., Nagasawa, T., et al. (2003). CXCR4 regulates interneuron migration in the developing neocortex. The Journal of Neuroscience, 23 (12), 5123-30.

Sugino, K., Hempel, C., Miller, M., Hattox, A., Shapiro, P., Wu, C., Huang, Z.-J., & Nelson, S. (2006). Molecular taxonomy of major neuronal classes in the adult mouse forebrain. Nature Neuroscience, 9 (1), 99-107.

Sugiyama, S., Di Nardo, A., Aizawa, S., Matsuo, I., Volovitch, M., Prochiantz, A., Hensch, T. (2008). Experience-dependent transfer of Otx2 homeoprotein into the visual cortex activates postnatal plasticity. Cell, 134 (3), 508-20.

Sun, W., Gould, T., Vinsant, S., Prevette, D., & Oppenheim, R. (2003). Neuromuscular development after the prevention of naturally occurring neuronal death by Bax deletion. Journal of Neuroscience, 23 (19), 7298-310.

Sun, W., Winseck, A., Vinsant, S., Park, O.-h., Kim, H., & Oppenheim, R. (2004). Programmed cell death of adult-generated hippocampal neurons is mediated by the proapoptotic gene Bax. Journal of Neuroscience, 24 (49), 11205-13.

Sussel, L., Marin, O., Kimura, S., & Rubenstein, J. (1999). Loss of Nkx2.1 homeobox gene function results in a ventral to dorsal molecular respecification within the basal telencephalon: evidence for a transformation of the pallidum into the striatum. Development, 126 (15), 3359-70.

Taha, S., Hanover, J., Silva, A., & Stryker, M. (2002). Autophosphorylation of CaMKII is required for ocular dominance plasticity. Neuron, 36 (3), 483-91.

Tamamaki, N., Yanagawa, Y., Tomioka, R., Miyazaki, J.-I., Obata, K., & Kaneko, T. (2003). Green fluorescent protein expression and colocalization with calretinin, parvalbumin, and somatostatin in the GAD67-GFP knock-in mouse. The Journal of Comparative Neurology, 467 (1), 60-79.

Tanaka, D., Yanagida, M., Zhu, Y., Mikami, S., Nagasawa, T., Miyazaki, J.-I., Yanagawa, Y., Obata, K., Murakami, F. (2009). Random walk behavior of migrating cortical interneurons in the marginal zone: Time-lapse analysis in flat-mount cortex. The Journal of Neuroscience, 29 (5), 1300-11.

Tiveron, M.-C., Rossel, M., Moepps, B., Zhang, Y., Seidenfaden, R., Favor, J., Konig, N., Cremer, H. (2006). Molecular interaction between projection neuron precursors and invading interneurons via stromal-derived factor 1 (CXCL12)/CXCR4 signaling in the cortical subventricular zone/intermediate zone. Journal of Neuroscience, 26 (51), 13273-13278.

Trune, D. (1982). Influence of neonatal cochlear removal on the development of mouse cochlear nucleus: I. Number, size, and density of its neurons. The Journal of Comparative Neurology, 209 (4), 409-24.

Trune, D. (1982). Influence of neonatal cochlear removal on the development of mouse cochlear nucleus: II. Dendritic morphometry of its neurons. The Journal of Comparative Neurology, 209 (4), 425-34.

Valcanis, H., & Tan, S.-S. (2003). Layer specification of transplanted interneurons in developing mouse neocortex. The Journal of Neuroscience, 23 (12), 5113-22.

Varfolomeev, E., Schuchmann, M., Luria, V., Chiannilkulchai, N., Beckmann, J., Mett, I., Rebrikov, D., Brodianski, V., Kemper, O., Kollet, O., Lapidot, T., Soffer, D., Sobe, T., Avrham, K., Goncharov, T., Holtmann, H., Lonai, P., Wallach, D. (1998). Targeted disruption of the mouse Caspase 8 gene ablates cell death induction by the TNF receptors, Fas/Apo1, and DR3 and is lethal prenatally. Immunity, 9 (2), 267-76.

Vawter, M. (2000). Dysregulation of the neural cell adhesion molecule and neuropsychiatric disorders. European Journal of Pharmacology, 405 (1-3), 385-95.

Veis, D., Sorenson, C., Shutter, J., & Korsmeyer, S. (1993). Bcl-2-deficient mice demonstrate fulminant lymphoid apoptosis, polycystic kidneys, and hypopigmented hair. Cell, 75 (2), 229-40.

Vekrellis, K., McCarthy, M., Watson, A., Whitfield, J., Rubin, L., & Ham, J. (1997). Bax promotes neuronal cell death and is downregulated during the development of the nervous system. Development, 124 (6), 1239-49.

Verhagen, A., & Vaux, D. (2002). Cell death regulation by the mammalian IAP antagonist Diablo/Smac. Apoptosis, 7 (2), 163-6.

Vetencourt, J., Sale, A., Viegi, A., Baroncelli, L., De Pasquale, R., F. O'leary, O., Castren, E., Maffei, L. (2008). The Antidepressant Fluoxetine Restores Plasticity in the Adult Visual Cortex. Science, 320 (5874), 385-388.

Vintersten, K., Monetti, C., Gertsenstein, M., Zhang, P., Laszlo, L., Biechele, S., et al. (2004). Mouse in red: Red fluorescent protein expression in mouse ES cells, embryos, and adult animals. Genesis, 40 (4), 241-246.

Wang, X., Tegner, J., Constantinidis, C., & Goldman-Rakic P. (2004). Division of labor among distinct subtypes of inhibitory neurons in a cortical microcircuit of inhibitory neurons in a cortical microcircuit of working memory. Proceedings of

the National Academy of Sciences, 101 (5), 1368-73.

Weier, J., Weier, H.-U., Jung, C., Gormley, M., Zhou, Y., Chu, L., Genbacev, O., Wright, A., Fisher, S. (2005). Human cytotrophoblasts acquire aneuploidies as they differentiate to an invasive phenotype. Developmental Biology, 279 (2), 420-32.

Wichterle, H., Alvarez-Dolado, M., Erskine, L., & Alvarez-Buylla, A. (2003). Permissive corridor and diffusible gradients direct medial ganglionic eminence cell migration to the neocortex. Proceedings of the National Academy of Sciences, 100 (2), 727-32.

Wichterle, H., Turnbull, D., Nery, S., Fishell, G., & Alvarez-Buylla, A. (2001). In utero fate mapping reveals distinct migratory pathways and fates of neurons born in the mammalian basal forebrain. Development, 128 (19), 3759-71.

Wiesel, T., & Hubel, D. (1963). Single-cell responses in striate cortex of kittens deprived of vision in one eye. Journal of Neurophysiology, 26, 1003-17.

Wonders, C., & Anderson, S. (2006). The origin and specification of cortical interneurons. Nature Reviews Neuroscience, 7 (9), 687-696.

Wonders, C., Taylor, L., Welagen, J., Mbata, I., Xiang, J., & Anderson, S. (2008). A spatial bias for the origins of interneuron subgroups within the medial ganglionic eminence. Developmental Biology, 314 (1), 127-136.

Wonders, C., Taylor, L., Welagen, J., Mbata, I., Xiang, J., & Anderson, S. (2008). A spatial bias for the origins of interneuron subgroups within the medial ganglionic eminence. Developmental Biology, 314 (1), 127-136.

Xu, Q., Cobos, I., De La Cruz, E., Rubenstein, J., & Anderson, S. (2004). Origins of cortical interneuron subtypes. The Journal of Neuroscience, 24 (11), 2612-22.

Yamamoto, Y., Livet, J., Pollock, R., Garces, A., Arce, V., de Lapeyrière, O., Henderson, C. (1997). Hepatocyte growth factor (HGF/SF) is a muscle-derived survival factor for a subpopulation of embryonic motoneurons. Development, 124 (15), 2903-13.

Yang, J., Liu, X., Bhalla, K., Kim, C., Ibrado, A., Cai, J., Pent, T., Jones, D., Wang, X. (1997). Prevention of apoptosis by Bcl-2: Release of cytochrome c from mitochondria blocked. Science, 275 (5303), 1129-32.

Yeh, W., Pompa, J., McCurrach, M., Shu, H., & Elia, A. (1998). FADD: Essential for embryo development and signaling from some, but not all, inducers of apoptosis. Science, 279 (5358), 1954-8.

Yuan, J., & Yankner, B. (2000). Apoptosis in the nervous system. Nature, 407 (6805), 802-9.

Yuan, J., Lipinski, M., & Degterev, A. (2003). Diversity in the mechanisms of neuronal cell death. Neuron, 40 (2), 401-13.

Zha, J., Harada, H., Yang, E., Jockel, J., & Korsmeyer, S. (1996). Serine phosphorylation of death agonist BAD in response to survival factor results in binding to 14-3-3 not BCL-X_L. Cell, 87 (4), 619-28.

Zuliani, C., Kleber, S., Klussmann, S., & Wenger, T. (2005). Control of neuronal branching by the death receptor CD95 (Fas/Apo-1). Cell Death & Differentiation, 13 (1), 31-40.

Publishing Agreement

I hereby grant permission to the Graduate Division of the University of California, San Francisco to release copies of my thesis, dissertation, or manuscript to the Campus Library to provide access and preservation, in whole or in part, in perpetuity.



Author Signature

6-12-9

Date